Evaluation of a Novel β-cyclodextrin Functionalized Nano Adsorbent for Removal of Pharmaceuticals

by

Ezgi Demircan Ozelcaglayan

A thesis
presented to the University of Waterloo
in fulfillment of the
thesis requirement for the degree of
Doctor of Philosophy
in
Civil Engineering - Water

Waterloo, Ontario, Canada, 2022

Examining Committee Membership

The following served on the Examining Committee for this thesis. The decision of the Examining Committee is by majority vote.

External Examiner	Banu Ormeci Professor Department of Civil and Environmental Engineering Carleton University
Supervisor	Wayne J. Parker Professor Department of Civil and Environmental Engineering University of Waterloo
Internal Member(s)	Neil Thomson Professor Department of Civil and Environmental Engineering University of Waterloo
	Anh Pham Assistant Professor Department of Civil and Environmental Engineering University of Waterloo
Internal-External Member	Michael Tam Professor Department of Chemical Engineering University of Waterloo

Author's Declaration

I hereby declare that I am the sole author of this thesis. This is a true copy of the thesis, including any final revisions, as accepted by my examiners.

I understand that my thesis may be made electronically available to the public.

Abstract

β-CD functionalized adsorbents have increasingly been reported for the removal of organic micropollutants. They have been considered attractive due to the hydrophobic cavity of β-CD which provides non-covalent interactions with small organic molecules described as host-guest complexation. The reversible non-covalent interactions allow the desorption of organic micropollutants, therefore, making them promising for reuse in adsorption. Despite the literature on host-guest complexation of pharmaceuticals with β-CD and β-CD derivatives, their adsorption via β-CD functionalized adsorbents has received little attention. The adsorption mechanism has usually depended on the physicochemical properties of the organic micropollutant. However, there has been insufficient information on the adsorption of target pollutants as a mixture and at an environmentally relevant concentration. Further, the capture and recovery of the β-CD functionalized adsorbents need to be quantified to provide insights into their reuse potential. The goal of this study was to address these gaps by evaluating a novel β-CD functionalized magnetic nano adsorbent that was developed for the adsorption of pharmaceuticals.

The adsorption of a target list of pharmaceuticals that span a range of physicochemical properties was investigated. Solid phase concentration of ibuprofen was elevated when the solution pH was lower than the pKa of ibuprofen as the hydrophobicity was increased. The presence of calcium ions enhanced the adsorption of ibuprofen as the surface charge of the model adsorbent was reduced. Hence, it was revealed that the surface characteristics of the adsorbent significantly impact the adsorption and the modifications on β-CD needs further investigation at the molecular level.

The adsorption of the target pharmaceuticals was assessed as a mixture and at an environmentally relevant concentration to gain insight into the partitioning. It was found that the molecular geometry of the pharmaceuticals altered the partitioning when they are present as a mixture. Naproxen with a planar molecular geometry provided the highest partitioning (0.4 mg/g) while sulfamethoxazole yielded the lowest partitioning with a bent geometry (0.1 mg/g). However, no trend was observed with respect to the hydrophobicities of the target pharmaceuticals. The results suggested that partitioning should be investigated at the molecular level to gain insight into the adsorption mechanism.

The partitioning of the target pharmaceuticals onto the β-CD functionalized nano adsorbent was investigated at the molecular level to understand the impact of modifications on β-CD on the host-

guest interactions. This approach has been rarely employed in the investigation of β-CD functionalized nano adsorbents. The reactivity of the selected β-CD derivatives was investigated via molecular electrostatic surface potential mapping. It was shown that the reactivity of the β-CD derivatives was altered when the substitution degree of the modified β-CD or the type of grafting agent was changed. Further investigation of the average substitution degree of β-CD via molecular simulations revealed the presence of free carboxyl (-COOH) groups that changed the reactivity and hence resulted in repulsive interactions with ibuprofen around neutral pH. The results assisted in explaining the effect of pH and cations on adsorption obtained in the experimental study. This study also showed that the effect of cations on adsorption will depend on the type of grafting agent employed in the development of the β-CD functionalized nanocomposites.

The impact of the physicochemical properties of the adsorbates was investigated via molecular dynamics of selected-host guest complexes. The molecular dynamics simulation showed that the positively charged target compound yielded the most stable complex (-75.9 kcal/mol) which was in agreement with the electrostatic molecular surface potential mapping. The grafting agents that have aromatic rings have been shown to provide additional electrostatic interactions where π- π were demonstrated by the distance between the aromatic rings of the host and the guest. Hence, this method provided insights into specific non-covalent interactions between the adsorption site and the target pharmaceutical. Further, the complexation of fulvic acid with the selected β-CD derivatives was demonstrated for the first time which helped to understand the competition with the target pharmaceuticals for the adsorption site. Overall, this study employed a molecular-level investigation for the first time to investigate the impact of the physicochemical properties of target organic micropollutants on adsorption.

The magnetic properties of the β-CD functionalized adsorbent provide ease of separation and in this study, a high gradient magnetic separator was evaluated for the capture and recovery of the novel β-CD functionalized adsorbent. Turbidity was introduced as a method that is fast and reliable to track the mass of nanoparticles with R^2 values of at least 0.99 for the low and high concentration ranges. This relationship was employed to quantify the performance of the system with respect to capture and recovery efficiency. A multi-layer steel wool placement provided 98% capture efficiency when compared to a typical placement that yielded 30% capture efficiency. It was also found that flow velocity was the significant factor impacting the capture and recovery of the adsorbent. Overall, 90% capture and 60 % recovery efficiencies were achieved at 2T and 0.22 ml/s. Further, the impact of

HGMS on the size distribution of the particles showed that large-size particles were selectively captured and recovered. Preferential capture might be a limitation in the long-term utilization of the particles as the adsorption capacity can be reduced, yet it can be advantageous for lab-scale method development for preconcentrating the pharmaceuticals.

Acknowledgements

I'm extremely grateful to my supervisor Dr. Wayne Parker for his endless patience and guidance in the completion of this thesis and for all the support he provided during my graduate studies.

I'd like to thank the members of the committee, Dr. Banu Ormeci, Dr. Neil Thomson, Dr. Anh Pham, and Dr. Michael Tam for reviewing my thesis and providing valuable feedback.

I would like to extend my sincere thanks to Dr. Mark Servos and Leslie Bragg for their kindness and support during my experimental work.

I am also thankful to Dr. John Honek for his valuable discussions during my studies.

To Ali, I could not have undertaken this journey without you.

To my family, thank you for accepting my decisions and supporting me in my journey.

To my friends, thank you for the endless support, encouragement, and good times we had during this journey.

To our dog, Loki, who joined our family last year, thank you for all the hugs whenever I needed them.

Table of Contents

List of Figures

List of Tables

List of Abbreviations

β-CD, β-Cyclodextrin;

β-CD FMNP, β-Cyclodextrin functionalized magnetic nanoadsorbent;

$CaCl_2$, calcium chloride;

DES, diethylstilbestrol;

DFS, 4,4′-difluorodiphenylsulfone,

DFB, decafluorobiphenyl;

DFB-β-CD, decafluorobiphenyl-β-CD;

DMF, dimethyl formamide;

E1, estrone;

E2, estradiol;

E3, estriol;

EE2, ethinylestradiol;

EPI, epiclorohydrin;

EtOH, Ethanol;

Fe_3O_4, iron oxide;

EDTA, ethylenediaminetetraacetic acid;

HCl, hydrochloric acid;

HGMS, high gradient magnetic separator;

MDE- β-CD,Mono-6-Deoxy-6-ethylenediamine-β-CD;

MeOH, methanol;

MESP, molecular electrostatic surface potential;

MCPA, 2-methyl-4-chlorophenoxyacetic acid;

NaOH, sodium hydroxide;

NOM, natural organic material;

OMP, organic micropollutant;

PEG, polyethylene glycol;

PFASs, per- and polyfluoroalkyl substances;

PFBS, perfluorobutanesulfonic acid;

PFHxA, perfluorohexanoic acid;

PFOA, perflorooctanoic acid;

PFBA, pentafluorobenzoic acid;

PFDA, perfluorodecanoic acid;

PFHpA, perfluoroheptanoic acid;

PFHxS, perfluorohexanesulphonic acid;

PFNA, perfluorononanoic acid;

PFOS, perfluorooctanesulfonic acid;

sd, substitution degree

SiO_2, silicon dioxide;

TFTPN, 2,3,5,6-tetrafluoroterephthalonitrile;

TiO_2, titanium dioxide;

TTSBI,5,5′,6,6′-tetrahydroxy-3,3,3′,3′-tetra-methylspirobisindan;

Chapter 1

Introduction

1.1. Problem statement

The occurrence of pharmaceuticals in water has become a significant concern over the last decade as their potential risk to living organisms has not been fully revealed [1]. Pharmaceuticals are a class of organic micropollutants (OMPs) that include nonsteroidal anti-inflammatory drugs, antidepressants, antibiotics, antiepileptics, beta-blockers and, lipid-lowering drugs [1]-[4]. They have been continuously introduced into the water, and have been found in surface waters, groundwaters, finished drinking water and wastewater effluents at very low concentrations (ng/L to µg/L) [5]-[9]. A number of pharmaceuticals have been listed as priority OMPs (i.e., sulfamethoxazole-antibiotic) based on their frequency of occurrence in water systems and impact on the environment and human health (i.e., development of bacterial resistance to the antibiotics) [10]. Thus, their removal from water via existing and novel technologies has drawn great attention.

The removal of pharmaceuticals from water with current physicochemical and biological treatment technologies has been reported [11]. However, these technologies are not specific to OMPs and their performance for the removal of pharmaceuticals varied [3], [11]. In addition, the cost-effectiveness, reuse potential, and ease of integration with existing treatment processes have differed [8], [9], [12]. Furthermore, there have been concerns over more toxic products that are generated from the target pharmaceuticals in these processes (i.e., biological processes, UV irradiation) [10], [12]-[14]. Therefore, simple and cost-effective technologies for the removal of pharmaceuticals from water are needed.

The use of adsorption-based technologies provides cost-effective and flexible designs hence they are often employed for the removal of OMPs [11]. In this regard, adsorbents derived from clays, minerals, carbonaceous materials, and engineered nanomaterials have been reported [15], [16]. Among these, engineered nanomaterials are considered attractive due to their high surface area, tunable surface characteristics, and potential to be modified to gain selectivity toward target contaminants [17]. Trends in the literature reveal that the development of novel adsorbents for the removal of OMPs from water is ongoing.

β-cyclodextrin (β-CD) functionalized nano adsorbents have increasingly been reported in this regard as β-CD provides an adsorption site for OMPs [18]. β-CD is commercially available and nontoxic cyclic oligosaccharide that has a hydrophobic cavity. The hydrophobic cavity allows noncovalent interactions with OMPs, described as host-guest complexation, where the β-CD is the host and the OMP is the guest [19]-[22]. This complexation enables the adsorption of OMPs when the β-CD is integrated into polymers or nanocomposite adsorbent structures [23], [24]. The reversible nature of interactions between the target OMPs and the β-CD functionalized adsorbent allows desorption of the adsorbed OMPs that makes β-CD functionalized adsorbents promising for reuse applications [20], [22], [25], [26]. In this regard, a number of knowledge gaps that need further investigation have been identified.

β-CD functionalized nano adsorbents have been investigated for adsorption of various types of OMPs (i.e., Bisphenol-A, PFOA, Methylene Blue) [27]-[31]. However, pharmaceuticals have received little attention, although extensive literature describing pharmaceutical-β-CD host-guest complexes is available [23], [24], [32]-[35]. While the adsorption has been reported to depend on physiochemical properties of OMPs (i.e., hydrophobicity) [18], [36]-[38], a limited number of studies have investigated the competitive adsorption that can occur when they are present as a mixture [24],[32],[39]. Furthermore, adsorption has usually been assessed at a high concentration range (mg/L) to gain insight into the adsorption models at equilibrium. Because of this, there has been limited information on adsorption at concentrations that reflects actual systems [28], [40]-[42]. Therefore, further investigation on partitioning at environmentally relevant concentrations of contaminants that span a range of physicochemical properties is needed.

The affinity of OMPs towards the β-CD adsorption site depends on the noncovalent interactions taking place during host-guest complexation. In this regard, the modification of β-CD for integration into polymer or nanocomposites and the surface characteristics of the adsorbents have been found to play an important role in the adsorption of OMPs [28], [32]. In addition, functional groups on OMPs that determine their physicochemical properties have been reported to affect their adsorption [24], [30]. However, the impact of these factors on the noncovalent interactions has not been examined in detail due to time-consuming experimental methods and the complex nature of nano adsorbents [85] [88]. To understand the adsorption mechanism, characterization and quantification of the non-covalent interactions are required. Therefore, a systematic investigation of the noncovalent interactions with respect to the changes in these supramolecular systems at the molecular level is needed. It is

hypothesized that molecular simulations may be employed to provide meaningful insights in this regard.

A number of β-CD functionalized nano adsorbents with magnetic properties that provide relatively easy capture and recovery after the adsorption and the desorption of the OMPs have been reported for reuse purposes [24], [36], [41], [43], [44]. This has typically been achieved via magnetic decantation techniques however, the capture and recovery efficiencies have not been quantified [24], [36]. In addition, the separation technique has been reported to impact adsorbent integrity and hence the adsorption capacity in reuse [44]. Hence, efficient techniques that allow sequential capture and recovery are needed for β-CD functionalized magnetic nano adsorbents.

In this study, a novel β-CD functionalized magnetic nano adsorbent (β-CD FMNP) developed for the adsorption of pharmaceuticals was investigated to address these gaps. The β-CD FMNP is a spherical core-shell nanoparticle developed from a nanogel scaffold that was embedded with Fe_3O_4 and coated with a silica shell to prevent oxidation. β-CDs are grafted onto the structure as carboxymethylated β-CDs [45].

1.2. Objectives and scope

The goal of this research was to evaluate a novel β-CD functionalized magnetic nanoadsorbent that was designed for the removal of pharmaceuticals from water. This was achieved through;

- investigating the adsorption of a model pharmaceutical (ibuprofen) and the impact of water chemistry on its adsorption and assessing the adsorption of a list of pharmaceuticals as a mixture at environmentally relevant concentrations via batch adsorption tests,
- evaluating the reactivity of selected β-CD derivatives through molecular electrostatic surface potentials via molecular simulation,
- investigating the stability of the host-guest complexation of target OMPs with selected β-CD derivatives via molecular simulation,
- evaluating the capture and recovery of the model adsorbent via a bench scale high gradient magnetic separator (HGMS) and,
- assessing turbidity as a method to track the mass of the model adsorbent in the HGMS system.

1.3. Significance

The knowledge acquired in this body of research improves our understanding of the use of β-CD functionalized nano adsorbents for the removal of pharmaceuticals. The results provide insight into the driving mechanisms for the adsorption of a range of pharmaceuticals. The results also provide insight into the factors that impact the host-guest complexation which has not been investigated systematically by conducting molecular simulations. Hence, the molecular modelling study revealed potential strategies to enhance the development of β-CD functionalized adsorbents. The use of a high gradient magnetic separator for the capture and recovery of a novel β-CD functionalized adsorbent was tested for the first time which provides insight into the reuse potential of the magnetic nanoadsorbent. Ultimately, this research contributes to the development of novel adsorbents for use in water treatment applications.

1.4. Thesis structure

This thesis consists of 6 chapters including an introduction chapter. The second chapter includes a critical review of β-CD functionalized adsorbents reported in the literature for the adsorption of organic micropollutants. Chapter 3 presents an experimental study of the adsorption of a target list of pharmaceuticals at environmentally relevant concentrations with a model adsorbent and includes an investigation of the impact of water chemistry on adsorption. Chapter 4 presents a molecular simulation study that investigated the impact of β-CD modifications on the surface characteristics of the adsorbent. The competition between the pharmaceuticals during adsorption was also assessed via molecular dynamics simulation. Chapter 5 presents the results of a study of the use of HGMS for the capture and recovery of the model adsorbent. The use of turbidity as an analytical tool to track the mass of β-CD FMNPs in HGMS systems is also evaluated. Finally, the conclusions and recommendations for future work are presented in Chapter 6.

Chapter 2

Literature review

2. β-Cyclodextrin functionalized adsorbents for removal of organic micropollutants from water

2.1. Introduction

Organic micropollutants (OMPs) are increasingly being reported in low concentrations (ng/L to μg/L) in waste, surface, and groundwaters [1]-[8]. A number of them have been defined as pseudo-persistent pollutants as they enter water systems continuously, yet their potential harm to aquatic life or human health is not known well [46]. While their fate and removal in treatment processes are an ongoing issue, regulations typically do not address these contaminants.

While the risks associated with OMPs are generally unclear, the ability of technologies including advanced oxidation, photolysis, biological processes, coagulation-flocculation, ozonation, chlorination, membranes, nanofiltration, reverse osmosis, and adsorption to remove them from water have been reported [11]. Some of these technologies can transform OMPs into other forms, which raises concerns over the toxicity of the transformation products [10]-[14]. Further, the technologies differ in terms of cost-effectiveness, the potential to recover/reuse components, and the feasibility of integration with existing treatment processes [3], [8], [12]. Therefore, there a motivation to develop novel, simple, selective, and cost-effective techniques for the removal of OMPs from water.

Adsorption-based technologies are often employed for OMP treatment because of their potential to provide cost-effective and flexible designs and adsorbents derived from clays, minerals, carbonaceous materials, or synthesized as polymers and nanocomposite materials have been reported [11], [15], [16]. β-Cyclodextrin (β-CD) has received attention because of its unique hydrophobic cavity that creates a convenient adsorption site for small organic molecules (Figure 2-1) [19]-[22]. It is non-toxic and commercially available and can be polymerized or grafted onto nanoparticles that become insoluble in water hence, can be employed as an adsorbent.

The interactions between small organic molecules and β-CD have been described as a host-guest complexation, where β-CD behaves as the host and the organic molecule is the guest [18]. These noncovalent interactions are reversible which allows for the desorption of organic molecules from β-

CD [20], [22], [25], [26]. Therefore, β-Cyclodextrin (β-CD) adsorbents are being actively developed as they have been deemed to be efficient, selective, and reusable.

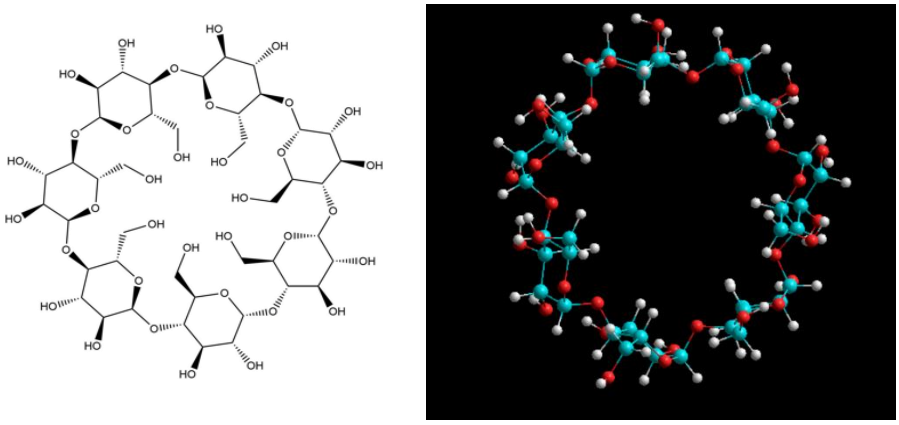

Figure 2-1: a) Chemical structure of β-CD, b) representation of β-CD cavity in 3D (white: hydrogen, red: oxygen, green: carbon)

Given the growing body of literature on β-CD functionalized adsorbents and the role that they may play in controlling OMP removal, it was deemed important to synthesize the current knowledge base to highlight opportunities for their application and to identify gaps that may act as barriers to their use. This critical review establishes the current state of knowledge and application of β-CD functionalized adsorbents for OMP removal and provides analysis to set the course for new research. An inventory of OMPs that have been employed in studies has been gathered to provide a baseline for future studies. The adsorption properties of β-CD functionalized adsorbents and the impact of water chemistry on the adsorption of OMPs have been reviewed. Significant findings to help the development of β-CD functionalized adsorbents have been summarized. The potential for recovery and reuse was investigated in detail and recommendations for additional studies in this area are presented.

2.2. Adsorption of OMPs with β-CD functionalized adsorbents

2.2.1. β-CD functionalized adsorbents

β-CD functionalized adsorbents have been developed with a variety of configurations to provide desired features such as fast adsorption, high adsorption capacity, and reusability. The configurations have been categorized as either cross-linked polymer-based or nanocomposite structures (Table 2-1) and the studies that addressed their application to OMPs were reviewed. The β-CD has been modified

via one or more -OH linkages for its integration into the polymer or nanocomposite configurations [37], [45]. It was recognized that the size of the β-CD functionalized adsorbents has a range between nanometer and micrometer. The dry size of the adsorbents obtained by XRD and the hydrodynamic size obtained by DLS can result in differences in size. Hence, the β-CD functionalized adsorbents are addressed as nano adsorbents in the subsequent discussion. Each adsorbent has unique physicochemical properties that lead to different adsorption characteristics which are discussed subsequently.

Table 2-1: β-CD functionalized adsorbent configurations

Reference	Polymers	Reference	Nanocomposites
[37]	Cross-linked	[23]	Microcrystalline cellulose
[32]	Cross-linked	[47]	Cellulose bead
[48]	Cross-linked	[24]	Magnetic (Fe_3O_4) nanoparticle
[49]	Cross-linked	[36]	Magnetic (Fe_3O_4) graphene sheet
[33]	Cross-linked	[43]	Magnetic (Fe_3O_4) nanoparticle
[28]	Cross-linked	[50]	Nanofiber membrane
[51]	Cross-linked	[44]	Magnetic (Fe_3O_4) graphene oxide sheet
[52]	Cross-linked	[29]	Magnetic (Fe_3O_4) nanoparticle
[53]	Cross-linked	[41]	Magnetic (Fe_3O_4) bifunctional nanoparticle
[54]	Cross-linked	[42]	Macroporous membrane
[40]	(Hierarchically) crosslinked	[30]	Magnetic (Fe_3O_4) nanoparticles
[39]	(Hyper) cross-linked	[55]	Multiwalled carbon nanotubes
[56]	(Hierarchically) cross-linked	[57]	TiO_2 nanoparticles
[58]	(Hydrogel) cross-linked	[31]	Magnetic (Fe_3O_4) micelles
[27]	Cross-linked	[59]	Nanofiber
[60]	Cross-linked	[34]	Magnetic (Fe_3O_4) nanoparticle
[35]	Cross-linked polymer bead		-

Crosslinked polymer adsorbents consist of β-CD molecules that are linked to each other via crosslinking agents which provide unique characteristics of the assemblage. Linear or cyclic crosslinkers such as polyethylene glycol (PEG) [51], citric acid [37], epichlorohydrin (EPI) [21], chitosan/ ethylenediaminetetraacetic acid (EDTA) [33] have been reported to provide a high density of adsorption sites. Aromatic (rigid) crosslinkers such as 4,4′-difluorodiphenylsulfone (DFS) [60], 2,3,5,6-tetrafluoroterephthalonitrile (TFTPN) [32], [48], [49] or decafluorobiphenyl (DFB) [28] have been found to provide further enhanced adsorption properties compared to other types of crosslinkers. Furthermore, modifications on these aromatic crosslinkers have been found to provide excellent adsorption properties with respect to per- and polyfluoroalkyl substances (PFAS) that have a moderate affinity for the hydrophobic cavity of β-CD [27], [28]. Recent reports describe the use of a combination

of different aromatic crosslinkers to generate micro-meso porous structures that result in fast adsorption kinetics [39], [40], [56]. These studies have shown that an appropriate selection of crosslinkers and associated functional groups can be employed to design adsorbents for specific applications. The high adsorption capacities and rapid adsorption of OMPs make cross-linked polymer configurations attractive for water treatment applications.

Nanocomposite structures are typically created by grafting β-CD molecules onto a backbone structure (i.e., nanoparticles, nanotubes, nanobeads) to provide adsorption properties to the assemblage. The most commonly reported nanocomposites consist of core-shell nanoparticles (TiO_2, Fe_3O_4, SiO_2) with a surface-coating (i.e.; silica, thiodiglycolic acid) to provide mechanical stability [24], [29]-[31], [41], [43], [57]. The grafting of β-CD is achieved by modification of the β-CD and/or functionalization of the surface of the nanocomposite [24]. The adsorption properties (i.e., maximum adsorption capacity) reported for these nanocomposites have typically been less than those reported for crosslinked polymers or other types of nanocomposite structures that are discussed subsequently.

Other nanocomposite adsorbents have β-CD molecules incorporated into (nano) beads [23], [35], [47], nanotubes/nanosheets and membranes [36], [42], [44], [50], [55], [59]. Superior adsorption relative to core-shell nanoparticles and cross-linked polymers has been reported with extremely fast kinetics and high adsorption capacities. Nanocomposites are deemed desirable because of their extraordinary properties such as large surface area, tunable size, surface chemistry [23], and the potential to design them to possess desired properties (i.e., magnetic, selectivity to target contaminants, physical and chemical stability) that can enhance their application.

2.2.2. Target organic micropollutants

Prior studies of the application of β-CD adsorbents have targeted contaminants on the basis of their frequency of occurrence and persistence in water systems as well as their harmful impacts on the environment [23], [28], [37], [48]. On this basis, the classes of OMPs examined have included pharmaceuticals, hormones, endocrine disruptors, organic dyes, short-chain phenols, herbicides, and PFAS (Table 2-2). Although this type of classification does not directly provide insights into adsorption properties, at least 70% removal efficiency has been reported for all contaminants regardless of their class and across the range of adsorbents tested. These results indicate that β-CD functionalized adsorbents can be employed for the treatment of a broad range of OMPs that exist in water.

Table 2-2: Organic micropollutants tested in adsorption studies

Pharmaceuticals	**Reference**	**Organic Dyes**	**Reference**	**Alkyl and Benzyl Phenols***	**Reference**	**Hormones**	**Reference**	**PFAS**	**Reference**
Diazepam	[34]	Aniline	[51]	Octyl phenol Nonyl phenol	[48]	E2 EE2	[48] [35]	PFOA	[28]
Procaine Imipramine Ciprofloxacin	[33]	Eosin Phloxine	[30]	2,4-dichlorophenol 2-naphthol Propranolol (HCl)	[40]	Cholesterol	[35]	PFBA PFNA PFHpA PFDA PFHxA PFBS PFHxS GenX PFOS	[27]
Ketoprofen, Diclofenac Ibuprofen	[35]	Congo red	[43]	1-naphthol	[29]	DES E1	[48]		
Atenolol Atrazine Gabapentin Valsartan	[23]	Disperse red 1 Acid blue Methyl orange	[55] [57]	Propranolol (HCl) Bisphenol-S	[23]	Estriol	[35] [36] [32] [44]		
Naproxen	[24][35]	Methyl orange	[61]	p-nitrophenol 4-chlorophenol 3-phenylphenol 2-naphthol	[39]			**Herbicides**	**Reference**
Carbamazepine	[24] [32]	Methylene blue	[37] [55] [57] [58] [61]	3-phenylphenol 2,4,6-trichlorophenol Bisphenol-S	[53]			MCPA Metolachlor	[23]
				Bisphenol-F Bisphenol-S	[36]				
				Bisphenol-S	[33]				
				Chloroxylenol	[32]				

*BPA: See Appendix A Table 1 and Table 2 for references

Bisphenol-A has been the most commonly studied OMP as the hydrophobic cavity of β-CD can potentially accommodate the phenol groups. Similarly, with the exception of atrazine, gabapentin, cholesterol, and PFAS, all of the OMPs in Table 2 have at least one aromatic ring. Hence, the success in the adsorption of these compounds is consistent with the β-CD host-guest complexation with small aromatic compounds due to the inclusion mechanism [18], [21].

Relatively large (i.e.; estriol, eosin, and phloxine) and relatively hydrophilic compounds (i.e.; PFAO) have also been reported to have high removal efficiencies with β-CD adsorbents [24] [27], [28], [30], [35]. The effective removal of these compounds suggests that electrostatic interactions with the functional moieties (i.e., crosslinkers) on β-CD adsorbent could combine with partial or full inclusion in the β-CD cavity to provide adsorption. Hence, while small aromatic compounds appear to be well suited for the application of β-CD adsorbents, the literature suggests that β-CD adsorbents may also be employed for the removal of different sizes and shapes of OMPs.

It was noted that while the cited studies have examined the removal of a range of OMPs with β-CD adsorbents, few studies have quantified adsorption kinetics or developed adsorption isotherms for the targeted compounds [23], [36], [42], [48], [49], [50], [60]. Therefore, although the number of OMPs evaluated appears large, only a fraction of the studies has developed information that would allow for extension to other applications. The subsequent sections discuss studies that have examined adsorption properties in detail.

2.2.3. Adsorption Kinetics

The kinetics of OMP adsorption onto β-CD adsorbents have been investigated in selected studies (Appendix A Table 1) since contact time is a key parameter for determining when equilibrium is established in isotherm studies and as part of the design of adsorption processes. The literature was examined to identify the kinetic models that have been employed for OMP adsorption by β-CD functionalized adsorbents (Appendix A Table 1). Most studies have evaluated Pseudo First Order and Pseudo Second Order models and found PSO to better describe the kinetics. Hence the subsequent discussion focuses on the results obtained with the PSO model (Equation 2-1);

$$\frac{dq_t}{dt} = k_2(q_e - q_t)^2 \qquad (2\text{-}1)$$

where t (min) is the contact time, k_2 (g mg^{-1} min^{-1}) is the adsorption rate constant, q_t (mg/g) and q_e (mg/g) are the mass of adsorbate adsorbed onto adsorbent at time t and equilibrium respectively.

It was anticipated that adsorbent morphology may impact adsorption kinetics due to the potential for diffusion-limited mass transfer within porous adsorbents. In one study, after an initial rapid adsorption phase where many available sites on the surface were present, adsorption slowed due to diffusion into pores imposing a mass transfer resistance [60]. To investigate the literature further in this regard, the rates of Bisphenol-A adsorption, as indicated by the rate constants with different adsorbent types were compared. It was found that the rate constants (Appendix A Table 1) varied between the adsorbent types (0.057-2.05(g/mg.min)) [23], [40], [42], [60]. Non-morphological properties of adsorbents such as the presence of additional functional groups that allow nonspecific interactions and pore size [37] have been reported to impact the adsorption kinetics. However, there was no pattern observed between the morphology and the fitted rate constants to link the adsorption kinetics to adsorbent morphology and functionality.

As the noncovalent interactions are unique to each β-CD-OMP system, the rate of adsorption could be affected by the characteristics of the OMP. In studies that employed multiple OMPs (Appendix A Table 1), the rate constants were found to differ substantially between compounds [24], [32], [37], [55], [57]. This observation was consistent for both polymer and nano-composite type β-CD adsorbents. The varied rate constants have been attributed to differences in OMP physicochemical properties including water-octanol partition coefficient [32], size [24], [37], and planarity [24] that impact the interactions between the OMP and β-CD. These results indicate that the OMP type might be as significant as the adsorbent type in determining the kinetics of adsorption. However, the significance of these factors has not been fully elucidated and more research on this would assist with future applications of β-CD adsorbents.

Rapid attainment of equilibrium in batch tests is considered a desirable characteristic of an adsorbent. Equilibrium times (Appendix A Table 1) describe the contact time after which no additional uptake is observed and can provide insight into the rate of adsorption. Although equilibrium times (Appendix A Table 1) have varied greatly, most studies have reported that adsorption was rapid at the beginning of batch tests and subsequent adsorbate uptake was more gradual as equilibrium was approached regardless of the β-CD adsorbent configuration [24], [28], [29], [33], [37], [40], [44], [47], [48], [53], [54], [56], [60]. Polymer type β-CD adsorbents where crosslinkers provide micro or mesoporous structures and membrane type β-CD nanocomposites have been found to provide ultrafast

adsorption where equilibrium was reached in minutes [23], [24], [32], [37], [50], [55]. In this regard, β-CD functionalized adsorbents have been found to be superior to conventional adsorbents such as activated carbon that require longer contact times to reach equilibrium.

While OMPs are typically present in actual waters at very low concentrations (μg/L or ng/L) most of the studies reviewed (Appendix A Table 1) were conducted at concentrations in the mg/L range. Only a limited number of studies have investigated kinetics over a wider range of OMP concentrations [28], [40]-[42], [62]. The limited number of results available for environmentally representative concentrations suggests that there is a need for studies that examine the kinetics of adsorption of OMPs by β-CD adsorbents to support the design of treatment processes.

2.2.4. Adsorption isotherms

Adsorption isotherms describe the relationship between the concentration of the adsorbate on the sorbent and the concentration in the solution at equilibrium and are key for the adsorption process design [63]-[65]. The literature was examined to identify the isotherm models that have been employed to describe the equilibrium partitioning of OMPs to β-CD adsorbents. Langmuir and Freundlich isotherms have most frequently been employed while Temkin and Sips isotherms have only occasionally been identified as the best fit model (Appendix A Table 2) and hence the subsequent discussion focuses on the former two models [33], [37]. It should be noted that for a large number of studies the quality of fit of Langmuir and Freundlich isotherms was found to be similar.

The Langmuir isotherm is described by Equation 2-2;

$$Q_e = \frac{Q_{max} \times K_L \times C_e}{1 + K_L \times C_e} \qquad (2\text{-}2)$$

where Q_e is the equilibrium mass of adsorbed contaminant on the adsorbent (mg/g), C_e is the equilibrium concentration of contaminant (mg/L) in the solution, Q_{max} is the maximum adsorption capacity, (mg/g) and K_L is the affinity parameter or Langmuir constant (L/mg) [63]. Langmuir adsorption assumes a fixed number of accessible sites are available on the adsorbent surface, all active sites have the same energy, adsorption is reversible, adsorption is monolayer and there is no interaction between adsorbate species.

The Freundlich isotherm is an empirical relationship given in Equation 2-3;

$$Q_e = K_f . C_e^n \qquad (2\text{-}3)$$

where K_F is the Freundlich constant ((mg/g) $(L/mg)^{1/n}$), n is the Freundlich exponent and Q_e is the adsorbed adsorbate mass per unit mass of adsorbent, (mg/g), C_e is the equilibrium concentration of adsorbate in solution after adsorption (mg/L) and 1/n is the Freundlich intensity parameter which is an indicator of the diversity of free energies associated with different adsorption sites on a heterogeneous sorbent.

The inclusion model for the adsorption of small OMPs onto β-CD adsorbents usually involves a 1:1 correspondence between the host and the guest suggesting that adsorption should follow Langmuir-type adsorption. To gain insight into this, the effect of adsorbent type on the isotherm model was examined. Bisphenol-A was selected for this purpose (Appendix A Table 2) as it has been the most commonly employed OMP and has been described as a good fit for the β-CD cavity due to the presence of phenol groups that participate in the inclusion mechanism. It was found that Langmuir type adsorption of bisphenol-A has been most commonly reported for both crosslinked polymers and nanocomposites (Appendix A Table 2). It should be noted that a number of these adsorbents had rigid aromatic crosslinkers in their structure which might accommodate non-covalent interactions with bisphenol-A [48], [49], [60] however Langmuir type isotherms still fit the data well.

A limited number of studies have reported bisphenol-A adsorption to be a better fit by a Freundlich type isotherm (Appendix A Table 2) [24], [50], [53] and this has been attributed to the contributions of either heterogeneous or multilayer adsorption. While the heterogeneity of sites has not been fully elucidated, it was observed that these latter adsorbents had crosslinkers or grafting agents which could be protonated or deprotonated based on pH. These features could provide electrostatic interactions with the functional groups of OMPs in addition to those with the β-CD moieties and contribute to the heterogeneity of the sites. The improved fit of the Freundlich model to data obtained for small OMPs other than bisphenol-A shows that the non-cavity interactions can impact the adsorption behavior of a range of compounds [24], [32], [33], [39]. In summary, the type of crosslinker and grafting agent influence the isotherm model for small OMPs.

The literature was also examined to assess the isotherm models that have been found to best fit the adsorption of larger or non-aromatic OMPs such as PFAO (Appendix A Table 2). Freundlich isotherm models were found to be consistently employed in these cases [28], [39], [43], [53], [57], and this was consistent with the presence of more heterogenous adsorption mechanisms. The successful adsorption of these OMPs shows that electrostatic interactions are active as their size or shape is not conducive

for inclusion in the β-CD cavity. However, the underlying mechanisms responsible for the heterogenous adsorption of large or nonaromatic OMPs remain to be identified.

Studies that examined multiple OMPs with relatively different sizes were further investigated to evaluate the roles of cavity versus non-cavity interactions in adsorption (Appendix A Table 2). Studies that employed bisphenol-A, methylene blue and methyl orange reported Langmuir type adsorption for bisphenol-A, whereas the Sips isotherm best described methylene blue, and methyl orange adsorption [37], [61]. This was attributed to the presence of functional groups (crosslinkers: free carboxyl groups on citric acid and tertiary amino groups respectively) on the adsorbents that contributed to methylene blue and methyl orange adsorption, while the inclusion of bisphenol-A into the β-CD cavity was responsible for the Langmuir type adsorption. While studies have usually investigated the impact of OMP size, shape, and charge on adsorption mechanisms, the difference in adsorption isotherm types for different compounds on the same adsorbent suggests that the surface characteristics of the adsorbent structure affect the adsorption model.

2.2.5. Maximum adsorption capacity

The maximum adsorption capacity (Q_{max}) of an adsorbent is a key characteristic that will impact adsorbent consumption for a given application. Bisphenol-A was selected to facilitate a comparison of adsorbents on this characteristic (Figure 2-2). As a standard method for comparison of theoretical adsorption capacity does not exist and the differences between the adsorption isotherm models (Appendix A Table 2) were modest, Q_{max} values obtained from Langmuir isotherm models were employed for this purpose. The range of reported bisphenol-A Q_{max} values in Figure 2-2 shows that there is a significant difference in adsorption capacity between the reported adsorbents. Hence, the properties of the adsorbents were examined in detail to understand those that impact Q_{max}.

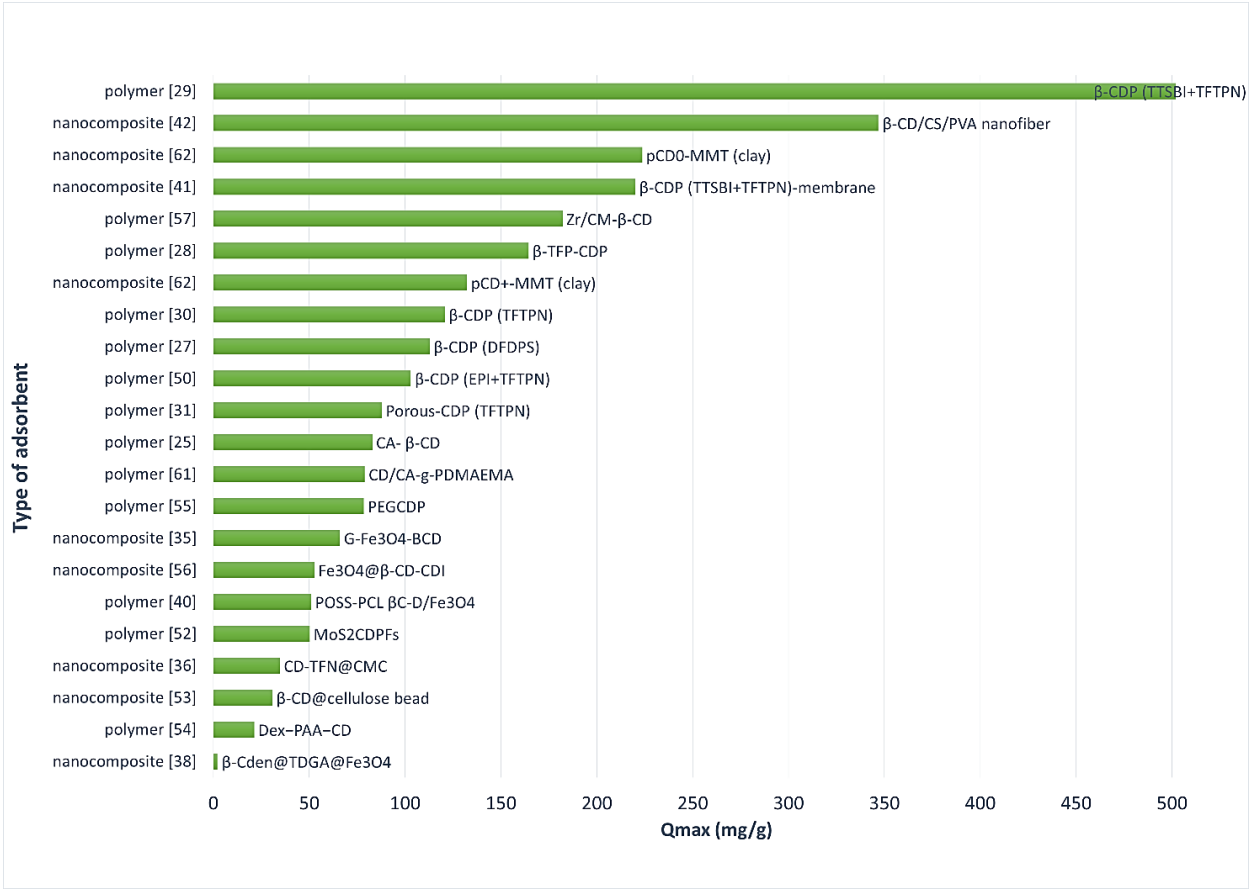

Figure 2-2: Reported Q_{max} values for adsorbents (obtained from Langmuir adsorption isotherms)

The use of crosslinked polymers for the adsorbent was found to generally result in higher Q_{max} values (Figure 2-2) as most of the Fe_3O_4 magnetic and bead composites lie in the lower range of the graph. The higher concentration of β-CD moieties, when expressed as mols/mass in the polymer structures as compared to the nanocomposite structures likely contributed to the greater Q_{max} values. This was illustrated in a study where bisphenol-A Q_{max} values for the functional adsorption site alone (β-CD@TFTPN) and the composite adsorbent structure (β-CD@TFTPN@CMC) after β-CD@TFTPN were compared [23]. It was found that both structures provided similar adsorption capacities when based on the mass of β-CD, whereas they differed (193.6 mg/g and 34.7 mg/g) when based on total adsorbent mass. Hence, the difference in the range of adsorption capacities can be related to the β-CD concentration in the adsorbent configurations.

2.2.6. Partitioning of OMPs in a mixture

As OMPs typically exist as mixtures in water the potential for competition between OMPs for available adsorption sites on β-CD functionalized adsorbents was examined. While a number of studies have

examined multiple OMPs, Q_{max} values have only been estimated individually [18], [36]-[38], These studies revealed the significance of OMP properties such as pKa, hydrophobicity, aromaticity, 3D conformation (chirality), size, and shape, that collectively impact the interactions between OMPs and β-CD adsorbents. However, the potential for competition has received limited attention [24], [32], [39], [67]. The few studies that have assessed competition have reported reductions in the adsorption of individual compounds when present in mixtures. However, these studies have been conducted at OMP concentrations in the mg/L range [24], [32], [39], while in natural waters they are usually present in the µg/L to ng/L range [1], [4]. Hence, there is a need to assess the partitioning in a mixture at environmentally relevant concentrations.

Concerns related to the occurrence and fate of chiral contaminants (i.e., pharmaceuticals) in water have increased recently as enrichment of specific enantiomers through conventional water treatment processes has been observed [68]. The chiral recognition ability of β-CD has been widely employed in separation techniques however, the impacts of chirality on adsorption in terms of competition have not been investigated thoroughly. Table 2-3 shows studies that have investigated the adsorption of chiral amino acids with two different β-CD nanoparticles. Both studies showed that the L-enantiomers had higher adsorption capacities when compared to D-enantiomers [69], [70]. Based upon these limited studies it was concluded that there is a need for more research into the impact of the chirality of OMPs on adsorption by β-CD functionalized adsorbents.

Table 2-3: Impact of chirality on adsorption capacity

Adsorbent	Adsorbate	Adsorption capacity (mg/g)
β-CD grafted magnetic nanoparticle [70]	L-Tryptophan	3.7
	D-Tryptophan	2.2
β-CD grafted magnetic nanoparticle [69]	L-Tryptophan	83.7
	D-tryptophan	61.3
	L-Phenylalanine	64.4
	D-Phenylalanine	33 .0
	L-Tyrosine	5.4
	D-Tyrosine	2.2

2.2.7. Effect of pH on adsorption of organic micropollutants

The literature reveals that a majority of reported Q_{max} values were determined at neutral pH. However, pH can vary between water sources and can be manipulated in treatment processes. Hence, studies

that investigated the effect of pH on adsorption in terms of either removal efficiency or adsorption partitioning were reviewed. It was anticipated that an analysis of pH effects would also provide additional insights into the nature of the interactions between adsorbates and adsorbents.

Many OMPs have functional groups that can protonate/deprotonate depending on the solution pH relative to their pKa. As the extent of protonation of an OMP will influence the polarity of the molecule it can be expected that the solution pH will influence adsorption mechanisms and, by extension, adsorption capacity. Studies that have examined bisphenol-A reported decreased removal efficiencies and adsorption capacities of the deprotonated (charged) molecule at pH values higher than the pKa [24], [39], [47], [53], [54]. This decrease was attributed to the alteration of hydrogen bonding between bisphenol-A and β-CD moieties [29], [44]. A change in the hydrophobicity of bisphenol-A with pH has also been hypothesized to influence the interaction with the β-CD cavity [24]. However, it was noted that other interactions might impact the adsorption mechanism, and the relationship between adsorption and pH to be complex. Further study of the impact of pH on Q_{max} values for a variety of OMPs would facilitate an analysis of the impact of pH on adsorption mechanisms and be valuable when designing processes that could be employed for the capture and recovery of the adsorbents.

β-CD functionalized adsorbents have functional groups that can protonate to alter the surface charge and thereby the Q_{max} of OMPs [37]. For instance, a decrease in the adsorption of BPA due to the protonation of β-CD under acidic conditions has been reported [36]. Low pH conditions also caused reduced adsorption of positively charged OMP (Bisphenol-S and procaine) due to the positive surface charge of a chitosan/EDTA crosslinked β-CD adsorbent [33]. In contrast, the adsorption of bisphenol-A and chloroxylenol to a TFTPN crosslinked β-CD polymer decreased when the pH was higher than 10, due to the establishment of repulsive forces between the negatively charged adsorbent and adsorbates [32]. Viewed collectively, it is clear that a detailed understanding of the functional groups on the adsorbent and their associated pKa values is required to predict the dependence of Q_{max} values on pH.

2.2.8. Effect of natural organic materials on adsorption

Natural organic matter (NOM) is a well-known competitor for trace organic contaminants when natural waters are being addressed and a challenge for conventional adsorption processes due to reduced adsorption capacities and reduced lifespans of the adsorbent [71]. As NOM components have a number of functional groups (i.e., aromatic, carboxylic acid, hydroxyl) that could interact with β-CD it might be anticipated that the adsorption will be altered in its presence [64]. The impact of humic acids on the

adsorption of OMPs by β-CD adsorbents under environmentally relevant conditions has been found to be modest [32], [37], [53], [66], [72]. The absence of competition by humic acids has been attributed to the inability of humic acids to fit into the cavity of β-CD thereby leaving access for smaller OMPs [37]. Although there have been few studies the results imply that large NOM constituents would not be a significant competitor regardless of the type of the OMPs.

Fulvic acids, which are a smaller NOM constituent might be expected to compete with OMPs for access to the cavity of β-CD and thereby reduce adsorption capacity. The presence of fulvic acids reduced the uptake of carbamazepine and chloroxylenol to a TFTPN crosslinked polymer while bisphenol-A adsorption was unaffected [32]. The decrease in adsorption was explained by interactions of OMPs with the fulvic acid that could potentially limit their complexation with the β-CD cavity [32]. In addition, the interaction of functional groups such as quaternary ammonium groups on the adsorbent with fulvic acids (i.e., ionic exchange) has been proposed as a means by which the β-CD cavity remained available for OMP adsorption in the presence of fulvic acids [53]. The results show that fulvic acid might compete with the OMPs depending on the adsorbent composition. Therefore, competitive adsorption with fulvic acid that might fit into the β-CD cavity should be investigated when natural waters are being employed.

2.2.9. Effect of inorganic ions on adsorption of organic micropollutants

The potential for inorganic ions to impact OMP adsorption by β-CD adsorbents was examined since both the adsorbates and adsorbents typically have functional groups that may interact with the ions. The presence of common cations such as sodium and calcium has been reported to have a limited impact on OMP (i.e., bisphenol-A, chloroxylenol, carbamazepine) adsorption with β-CD functionalized cross-linked polymers [32], [53], [72]. However, the presence of a very high concentration of sodium (2000 mg/L) was reported to compete with the adsorption of unidentified OMPs [72]. In contrast, the adsorption of PFAS with β-CD functionalized cross-linked polymers was reported to reduce in the presence of cations due to electrostatic attraction between cations and PFASs [73]. It might be anticipated that the extent of competition will depend on the charge of the OMP, the type of cations, and the surface charge of the adsorbent however, limited information is available in this regard. Future studies of natural water systems should consider the potential impacts of ionic strength and the types of inorganic ions on adsorption.

2.3. Reuse of β-CD functionalized adsorbents

The viability of an adsorbent will be enhanced if it can be easily recovered and reused after adsorption is complete. β-CD functionalized adsorbents are promising due to the reversible nature of the interactions with OMPs. Table 2-4 highlights key aspects of the studies that examined the reuse of β-CD adsorbents. The adsorbents were pre-loaded with target contaminants prior to the desorption study [24], [32], [42], [43], [47], [55], [57]. The OMPs were then desorbed by contacting with a desorption solution to regenerate the adsorbents. The reusability of β-CD adsorbents has typically been evaluated by conducting a series of adsorption/desorption cycles, where adsorption capacity (or removal efficiency) was assessed after each cycle. The factors impacting the reuse have been discussed subsequently.

Table 2-4: Reuse of β-CD functionalized adsorbents

	Adsorption (saturation)				Desorption				Reuse			
Adsorbent Configuration	**Reference**	**Reduction in adsorption**	**Contaminants**	**Concentration (mg/L)**	**Desorption Solvent**	**Contact Time (min)**	**Desorption Efficiency, %**	**Regeneration Process**	**Type**	**Max. cycle**	**Decrease in adsorption capacity**	**Decrease in removal efficiency**
Polymer	[28]	Minimal	PFOA	0.2	MeOH	24 h	>90	Suspense	C	4	NSC	NA
Polymer	[49]		Bisphenol-A	22.8	MeOH	5	NA	Filtration	B	5	NA	NSC
Polymer	[60]		Bisphenol-A	22.8	EtOH	NA	90	Eluted	C	5	NA	NSC
Polymer	[32]		Chloroxylenol Bisphenol-A	50	MeOH	120	NA	Filtration	B	5	NA	NSC NSC
Polymer	[48]		Bisphenol-A E2 EE2	22.8 10.9 11.9	EtOH	10	NA	Filtration	B	5	NA	NSC
Polymer	[39]		3-phenylphenol	17.0	MeOH	10	NA	Filtration	B	5	NA	NSC
Composite (Cellulose microcrystalline)	[23]		Bisphenol-A	22.8	MeOH	NA	>90	Eluted	C	3	NSC	NA
Composite (clay)	[66]		Bisphenol-A	NA	0.1 N NaOH	NA	80	Eluted	C	2	NSC	NA
Polymer	[56]		Bisphenol-A	NA	EtOH and Water	NA	NA	Drying	B	10	NA	NSC
Polymer	[40]		Bisphenol-A	300	EtOH	NA	NA	Centrifugation	B	5	NSC	NA
Composite (Membrane)	[42]		Bisphenol-A	Saturation reached	EtOH	NA	NA	Filtration	C	6	NSC	NA
Composite (Carbon nanotubes)	[55]		Disperse Red 1	NA	MeOH, EtOH, DMF, Acetone, HCl, NaOH (0.1M)	NA	NA	Centrifugation Drying	B	7	NA	NSC

Polymer	[37]	Slight	Bisphenol-A Methylene Blue	100	0.5 M HCl in EtOH 0.5 M HCl EtOH	240	NA	Centrifugation	B	5	20%	NA
Composite (membrane)	[50]		Bisphenol-A	22.8	70% EtOH	NA	NA	Eluted	C	5	7%	NA
Composite (magnetic)	[43]		Congo Red	NA	1mol/L NaOH	3	NA	Ultrasound	B	5	NA	10%
Composite (magnetic)	[36]		Bisphenol-A	NA	MeOH	30	NA	Magnetic decantation	B	6	NA	10-20%
Composite (magnetic)	[24]		Carbamazepine Naproxen Bisphenol-A	20	EtOH	360	80.2 75.0 89.3	Magnetic decantation	B	3	Slight decrease	NA
Composite (magnetic)	[44]		E2	2	NaOH and Acetone	1440	NA	Acetone wash Drying	B	6	11%	NA
Composite (magnetic[)]	[41]		Bisphenol A	20	5% Acetic acid in MeOH	NA	NA	Magnetic separation Filtration Washing	B	5	NA	17%
Composite (bead)	[47]		Bisphenol-A	NA	MeOH	120	NA	Filtration Washing	B	4	30%	NA
Composite	[57]		Methylene blue Methyl orange Acid blue Disperse red	NA	MeOH, EtOH, DMF, Acetone, HCl, NaOH (0.1M)	NA	NA	Centrifugation	B	6	NA	Slight decrease
Composite (carbon nano tubes)	[55]	Moderate	Methylene Blue Acid Blue Methyl Orange	NA	MeOH, EtOH, DMF, Acetone, HCl, NaOH (0.1M)	NA	NA	Centrifugation Drying	B	7	NA	53% 51% 59%
Polymer	[32]		Carbamazepine	50	MeOH	120	NA	Filtration	B	5	NA	40%

NA: not available
NSC: no significant change
B: Batch C: Continuous

2.3.1. Desorption of organic micropollutants

For the effective reuse of adsorbents, a high level of desorption of OMPs is needed to maintain the number of active adsorption sites in sequential adsorption/desorption cycles. The desorption efficiency is defined as the fraction of the adsorbed OMP that is released to the desorption solution [23], [24], [28], [60], [66]. Overall, relatively high desorption efficiencies (75%-90%) have been reported (Table 2-4), which supports the potential reusability of β-CD adsorbents. Studies that did not report desorption efficiency evaluated the success of desorption by examining performance in subsequent adsorption cycles. Desorption was deemed to be satisfactory when consecutive adsorption/desorption cycles maintained consistent adsorption capacity (or removal efficiency) [48], [49]. Although these studies suggest desorption of OMPs from the adsorbents is feasible, several factors might impact the desorption efficiency which is discussed subsequently.

The desorption solvents employed have been investigated as it is a key design feature and should provide high desorption efficiency for a range of contaminants. Table 2-4 shows that ethanol and methanol have been the most commonly used solvents The use of other organic solvents (i.e.; acetone and DMF), inorganic solvents (i.e., acids, bases), or mixtures of these have also been reported [37], [41], [43], [44], [55], [57], [66]. Alcohols have been found to outperform other solutions in some cases [55], [57]. Where the use of acid/base solutions or their combination with organic solvents has provided better results [37], [43], [44], [66], desorption has been attributed to the establishment of repulsive forces between the adsorbate and adsorbents [43], [66]. Although alcohols have been shown to be successful for a range of OMPs, using these solvents may not be feasible in water treatment applications. Hence, alternatives that will not negatively affect the quality of the water generated in subsequent adsorption cycles should be developed. pH adjustment might be employed for this purpose to enhance desorption however more research is needed in this regard as the enhancement will depend on the charge of the OMP or surface charge of the adsorbent.

The kinetics of OMP desorption will impact the size and cost of desorption processes. Based upon the previously described rapid adsorption kinetics it was anticipated that desorption contact times would be short. The contact times that have been reported (Table 2-4) were typically in the range of 5 minutes to 6 hours making them practical for water treatment. While the contact time for desorption has commonly been reported, the effect of contact time on the extent of the desorption has not commonly been reported and opportunities for optimization remain to be assessed.

2.3.2. Reuse of β-CD functionalized adsorbents

The classification of reuse responses represented studies with different adsorbents, adsorbates, desorption solutions, and numbers of reuse cycles. The absence of standardization in this regard is a challenge when comparing reuse studies. Of particular interest was the absence of any long-term studies of adsorbent reuse as the maximum number of cycles evaluated across all studies was 10. Based upon the reported responses (Table 2-4) the adsorbents were classified on the basis of minimal decrease, a slight decrease (<20%), and a moderate decrease (between 40% and 60%) in adsorption capacity (or removal efficiency) and these results were discussed subsequently based on the common features employed.

The studies that reported a minimal reduction in performance over multiple cycles were examined to identify common features (Table 4) [23], [28], [39], [40], [42], [48], [49], [56], [66]. From Table 2-4 it can be seen that the majority of these studies employed crosslinked polymers as the adsorbent and only a few of these adsorbents had composite structures. Alcohols were employed as the regeneration solvent in all but one study where NaOH was used. Based on the reported results, the combination of cross-linked polymers with alcohol regeneration has significant potential in reuse applications.

The studies that reported modest decreases (less than 20%) in adsorption capacity (or removal efficiency) were also examined to identify common features (Table 2-4) [24], [32], [36], [37], [41], [43], [44], [47], [50], [57]. From Table 2-4 it can be seen that a majority of these studies involved applications of nanocomposite structures and alcohols were commonly employed for regeneration. Alternative desorption solutions including NaOH, HCl, acetic acid, DMF, and acetone were also investigated. The factors responsible for the slightly reduced adsorption capacities have not been fully elucidated in the studies however, it appears that composite structures may be more subject to loss of capacity than the crosslinked polymers that demonstrated consistent reuse. It was noted that the chemicals employed in regeneration might result in loss or degradation of active adsorption sites or physical separation operations (i.e.; centrifugation) can cause agglomeration of the adsorbent which can reduce the available adsorption sites [40], [44]. These factors can potentially lead to reduced adsorption capacity in reuse. Given the limited information available, more research on the stability of β-CD functionalized adsorbents is needed to identify design and operating parameters that maintain adsorbent integrity if they are to be used in multiple cycles.

Relatively low recoveries of adsorption capacity (40-60%) of adsorbates (carbamazepine and methylene blue/methyl orange/acid blue) were reported in some cases despite the use of alcohols as desorption eluents [32], [55]. Inefficient desorption and/or degradation of surface functional groups on the adsorbent resulting in a reduction in the active adsorption sites were identified as possible causes of poor recovery [32], [55]. However, the β-CD functionalized crosslinked polymer and the β-CD functionalized carbon nanotube composite employed in these studies demonstrated good reusability with minimal decrease in adsorption capacity for other OMPs (bisphenol-A/chloroxylenol and disperse red). The results show that the recovery and reuse of adsorbent differed substantially between OMPs. Although limited types of OMPs have been investigated in the reuse schemes, the regeneration of the adsorbent might depend on the stability of β-CD-OMP complexes that are involved in adsorption which needs further investigation.

2.4. Summary and recommendations

This review provides an overview of the application of β-CD adsorbents for the removal of OMPs from water. According to the literature;

- There is limited information on the adsorption of OMPs at environmentally relevant concentrations.
- Adsorption depends on the physicochemical properties of the OMPs; however, the adsorption mechanism is complex and the competition between OMPs should be investigated.
- It is necessary to describe the impact of water chemistry on the host-guest interactions in detail to understand the adsorption mechanism.
- The impact of the chirality of OMPs and small NOM components on adsorption in terms of competitive adsorption should be investigated.
- Capture and recovery of β-CD functionalized adsorbents make them promising for future water treatment applications in terms of reusability however, methods that can be employed in sequential capture and recovery of the β-CD functionalized adsorbents are needed.

To enhance the application of β-CD functionalized adsorbents future studies should focus on the following subjects;

- The type of crosslinkers or grafting agents on β-CD functionalized adsorbents can be altered to provide enhanced adsorption and selectivity for OMPs, hence further developments in this regard could expand future applications of β-CD adsorbents.

- The selection of OMPs for the investigation of adsorption should include highly prioritized organic micropollutants in the environment for future applications of β-CD functionalized adsorbents.
- The application of computational chemistry tools to characterize noncovalent interactions in the adsorption of OMPs, screen OMPs, and investigate surface properties of adsorbent structures has the potential to be an efficient means of improving these adsorbents for applications in water treatment.
- QSAR tools that can predict adsorption properties based upon physicochemical properties can reduce the amount of testing of adsorbents however, more development of the tools is required to address additional adsorbents and OMPs.

Chapter 3

Adsorption of pharmaceuticals by a novel β-CD functionalized adsorbent

3.1. Abstract

The presence of pharmaceuticals in water has raised concerns due to the potential risks they pose to living organisms, which has led to the development of novel treatment technologies. In this study, a novel β-cyclodextrin functionalized magnetic nanoparticle was assessed for adsorption of target pharmaceuticals. The β-CD functional group on the adsorbent was expected to provide an adsorption site for pharmaceuticals due to its hydrophobic cavity. A maximum adsorption capacity of 3.4 mg/g for ibuprofen was obtained by fitting a Langmuir adsorption isotherm to experimental data. pH and the presence of calcium ions significantly impacted the adsorption partitioning due to changes in the charge state of ibuprofen and the surface charge of the model adsorbent, respectively. The adsorption of a mixture of pharmaceuticals at an environmentally relevant concentration (1 µg/L) resulted in a range of solid phase concentrations between 0.1 mg/g and 0.4 mg/g. The differences in liquid-solid partitioning did not correlate with the hydrophobicity of the target pharmaceuticals and were suggestive of a complex sorption mechanism. An investigation of the molecular geometry of the pharmaceuticals revealed that planar geometries (naproxen) yielded higher partitioning than bent molecular geometry (sulfamethoxazole) where more than one aromatic ring was present in the pharmaceutical hence the molecular geometry impacted the affinity of the pharmaceuticals for the hydrophobic cavity of β-CD.

3.2. Introduction

β-cyclodextrin (β-CD) functionalized nano adsorbents are receiving increasing attention for the removal of organic micropollutants (OMPs) from water as β-CD's hydrophobic cavity provides noncovalent interactions with small organic molecules [26]. These noncovalent interactions have been described as a host-guest complexation where β-CD is the host and the organic molecule is the guest [18]. The backbone of the β-CD functionalized adsorbents can be modified to optimize the size, adsorption capacity, mechanical stability, and selectivity of target OMPs based on specific applications [17]. While these features make β-CD functionalized adsorbents promising for the removal OMPs, a number of gaps in the knowledge base have been identified and are discussed subsequently.

Adsorption of OMPs via β-CD functionalized adsorbents has usually been investigated at elevated concentrations (mg/L) (Appendix A Table 2) although OMPs are present in water at very low concentrations [5]-[7]. These studies have typically been conducted to gain insight into maximum adsorption capacity by saturating the adsorption sites [24], [39], [47], [53], [54]. Hence, there is limited information on the adsorption of OMPs at environmentally relevant concentrations [28], [40]-[42]. Adsorption capacities should be quantified at environmentally relevant concentrations to establish the potential of β-CD functionalized adsorbents for water treatment applications and further investigation is needed on this subject.

The adsorption of OMPs has usually been assessed individually and a comparison of adsorption capacities has shown that their physicochemical properties such as size, and hydrophobicity have impacted their adsorption [18], [36]-[38]. Only a limited number of studies have investigated OMP adsorption as a mixture where competition between target OMPs was reported [24], [32], [39]. Most OMPs are present as a mixture in water systems and the partitioning to β-CD functionalized adsorbents will likely differ between OMPs that have different affinities for the β-CD cavity. Hence, partitioning should be assessed for a mixture of target OMPs that span a range of physicochemical properties to gain insight into the affinities of the target OMPs for the adsorbents under environmentally relevant conditions.

Various types of OMPs have been investigated in the literature for adsorption with β-CD functionalized nano adsorbents. Among these, the adsorption of pharmaceutical compounds has received little attention despite their suitable size for host-guest complexation with β-CD cavity [23], [24], [32]-[34], [35]. The $LogK_{ow}$ and $LogD_{ow}$ values of pharmaceuticals have been assessed to relate to the adsorption mechanism and hydrophobicity of the pharmaceuticals, however conflicting results between the studies have been observed [24], [32]. Further investigation is needed to gain insight into the adsorption of pharmaceutical compounds via β-CD functionalized adsorbents.

The water chemistry can impact the partitioning of OMPs due to the functional groups on the OMPs and the adsorbent. In this regard, the effect of pH and common ions (i.e., divalent cations) present in the water have been investigated in the literature [24], [32], [53], [72]. However, water chemistry can also be used to manipulate host-guest interactions. β-CD functionalized adsorbents might be employed for concentrating OMPs as part of an analytical method where desorption of the OMPs can be achieved by conditions such as extreme pH or ion concentrations [37], [43], [44], [66]. Hence, there is a need

for evaluating the performance of the adsorbent at those extreme conditions to gain insight into the potential analytical applications of β-CD functionalized adsorbents.

In this study, a model β-CD functionalized magnetic nanoparticle (β-CD FMNP) was investigated for adsorption of pharmaceuticals. The β-CD FMNP is a spherical magnetic nanoparticle developed using a nonmagnetic nanogel scaffold made magnetic with embedded Fe_3O_4 [45]. The adsorbent was silica-coated prior to the grafting of β-CDs to minimize oxidation. β-CDs were modified to create carboxymethyl-β-CDs that were then grafted onto the silica-coated adsorbent. The model adsorbent has been demonstrated to provide enhanced adsorption of procaine via host-guest adsorption when compared to other β-CD functionalized core-shell nanoparticles [45]. However, the adsorption of other pharmaceuticals has not yet been examined for this adsorbent.

The objective of the study was to investigate the adsorption of seven target pharmaceuticals that span a range of physicochemical properties. The target pharmaceuticals have been identified to be high-priority OMPs based on their impact on health and their contribution to global water pollution [4], [8], [10]. The adsorption of ibuprofen was initially investigated to gain insight into the adsorption mechanism. The impact of pH and Ca^{+2} concentration on adsorption was examined. An adsorption isotherm was developed to benchmark the maximum adsorption capacity of the model adsorbent to those in the literature. Finally, the adsorption of seven target pharmaceuticals was assessed as a mixture at an environmentally relevant concentration. The impact of physicochemical properties of pharmaceuticals (i.e., hydrophobicity, molecular geometry) on the partitioning of the target contaminants when present in the mixture was examined.

3.3. Methods

3.3.1. Selection of target pharmaceuticals

Target pharmaceuticals were selected based on their frequency of occurrence in the environment and the physicochemical properties that are relevant to adsorption [74]-[77]. Table 3-1 shows the target contaminants and corresponding physicochemical properties [62]. These properties were investigated as they were found to be significant factors in host-guest complexation of OMPs with β-CD functionalized adsorbents and explained subsequently.

Table 3-1: Physicochemical properties of target pharmaceuticals

Pharmaceutical	Chemical Formula	Molecular weight (g/mol)	pKa	LogKow	LogDow pH: 7.4
Sulfamethoxazole	$C_{10}H_{11}N_3O_3S$	253.3	pKa1:1.6 pKa: 2:5.7	0.9	1.6
Gemfibrozil	$C_{15}H_{22}O_3$	250.3	4.5	4.4	1.6
Diclofenac	$C_{14}H_{11}Cl_2NO_2$	296.1	4.2	4.5	1.4
Carbamazepine	$C_{15}H_{12}N_2O$	236.3	13.9	2.5	2.3
Ibuprofen	$C_{13}H_{18}O_2$	206.3	5.3/4.9	4.0	0.5
Naproxen	$C_{14}H_{14}O_3$	230.3	4.2	3.2	0.5
Ketoprofen	$C_{16}H_{14}O_3$	254.3	4.5	2.8	0.1

The target pharmaceuticals were chosen considering their molecular weight as the size of the OMP was an indicator for fitting into the β-CD cavity (diameter: 4-8 Å) and for host-guest complexation [78]. Pharmaceutical compounds were considered to be small organic molecules in the literature as their molecular weight was less than 1000 g/mol [64]. The target pharmaceuticals were low molecular weight compounds similar to the OMPs employed in the literature (i.e., bisphenol-A 228 g/mol, phloxine: 829.6 g/mol) [24], [30]. Hence, it was anticipated that the size of the selected contaminants was suitable for host-guest complexation with the β-CDs grafted onto the model adsorbent, and the adsorption of pharmaceuticals with the range of molecular weight shown in Table 3-1 was investigated.

Octanol-water partitioning coefficient (K_{ow}) values of the target contaminants were collated as it is a commonly available physicochemical property that describes the hydrophobicity of organic molecules [63], [69]. $LogK_{ow}$ of the selected pharmaceuticals ranged between 0.9 and 4.5 (Table 3-1) [62]. The adsorption capacity of the pharmaceuticals in a mixture was assessed with respect to reported $logK_{ow}$ values to understand the impact of hydrophobicity on adsorption.

While $LogK_{ow}$ can be employed to assess of hydrophobicity of neutral compounds, $LogD_{ow}$ is an improved indicator of the hydrophobicity of compounds that can be ionized [24]. The selected pharmaceuticals had functional groups that can deprotonate and protonate (i.e.; -COOH, $-NH_2$), hence the pH could impact their hydrophobicities. The $LogD_{ow}$ values of selected pharmaceuticals ranged from 0.1 – 2.3 (at neutral pH) indicating a wide range of hydrophobicity (Table 3-1). The selection was anticipated to allow an evaluation of a range of adsorptions including hydrophobic partitioning and affinities for the β-CD cavity.

3.3.2. Materials

Methacrylic acid (MAA), ethyl acrylate (EA), di-allyl phthalate (DAP), sodium persulfate, sodium hydroxide, iron (II) sulfate heptahydrate ($FeSO_4 \cdot 7H2O$), sodium nitrite ($NaNO_2$), ammonia solution (28–30%), tetraethyl orthosilicate (TEOS, 98%), sodium phosphate dibasic heptahydrate, sodium phosphate monobasic monohydrate, hydrochloric acid, β-Cyclodextrin, calcium chloride, chloroacetic acid, ethanol, and acetone were purchased from Sigma-Aldrich. Cyanamide (CH_2N_2, 95%), aerosol OT (AOT, 75%) and cyanamide (CH_2N_2, 95%) were supplied by Thermo Fisher Scientific. Ibuprofen, naproxen, ketoprofen carbamazepine, sulfamethoxazole, diclofenac, and procaine hydrochloride were purchased from Sigma Aldrich. The isotopically labeled standards were purchased from CND isotopes. The internal standards (chloramphenicol and lorazepam) were purchased from Sigma Aldrich. HPLC-grade methanol and ammonium acetate were obtained from Sigma Aldrich. Ultrapure water was obtained from a Milli-Q system.

3.3.3. Synthesis of β-CD functionalized magnetic nanoadsorbent

β-CD functionalized magnetic nanoparticles were synthesized according to the method described by Ju et. al. [45]. The synthesis consisted of 4 major steps. In the first step, a nanogel was synthesized via the emulsion polymerization technique to form the backbone of the adsorbent. To prepare the nanogel polymerized methacrylic acid (MAA) and ethyl acrylate (EA) crosslinked with diallyl phthalate (DAP) were mixed with surfactant (AOT) solution where the initiator solution was prepared with sodium persulfate. The product was purified via dialysis until no surfactant was observed in the water. The nanogel was made magnetic by reacting Fe_2SO_4 with $NaNO_2$ and NH_4OH to obtain Fe_3O_4 particles inside the nanogel. Excess iron was subsequently removed via several cycles of ultrafiltration. The magnetic nanoparticles were then washed with water and subsequently captured using an HGMS to remove nonmagnetic constituents. In the third step, the surface of the Fe_3O_4 embedded nanogel was coated with a silica layer via tetraethyl orthosilicate to make the β-CD-FMNP resistant to oxidation or other structural changes that might occur with time. The silica-coated particles were then washed in the HGMS to remove unreacted chemicals and any residual nonmagnetic particles. Prior to the grafting procedure, β-CD was modified to obtain carboxymethyl-β-CD. In the final step, the surface of the silica-coated magnetic nanoparticles was functionalized with the carboxymethyl-β-CD in the presence of cyanamide to provide adsorption sites. The product was purified and concentrated by washing with the HGMS to remove the reaction by-products and then releasing the captured particles into MQ water. The concentration of the wet particles was determined by the dry weight of the particles and the density

of the solution as determined by measuring the mass of 50 ml of the particle solution and dividing the mass of the solution by the volume of the solution [45].

The characterization of the β-CD functionalized magnetic nano adsorbent was previously reported in the literature [45]. The morphology and size of the nanogel, the magnetic nanoparticle and the silica-coated magnetic nanoparticle were examined by TEM (transmission electron microscopy). The magnetic properties of the particles were characterized by VSM (vibrating sample magnetometer). The presence of the silica shell was confirmed by XRD (X-ray diffraction) and the grafting of β-CD onto the silica surface was confirmed by FTIR (Fourier transform infrared spectroscopy) and TGA (thermogravimetric analysis). The average size and Z-potential of the β-CD functionalized adsorbent were measured by DLS (dynamic light scattering) [45].

The properties of the particles synthesized for the current study were evaluated to ensure that they were consistent with those previously reported. This was achieved by conducting procaine adsorption tests at pH 7 in an identical manner to that used to test the previously characterized [45]. The solid phase concentrations (15 mg/g) and removal efficiency (40%) that were obtained with an initial procaine concentration of 30mg/L was the same as that of the earlier study [45]. Further, the particle size distribution (average size of 400nm) and Z-potential (-38 mV) were consistent with that reported in the literature. Hence, it was concluded that the particles synthesized in the current study were similar to those of the particles that had been previously characterized in detail [45].

3.3.4. Adsorption of ibuprofen

Ibuprofen was selected as a model adsorbate for the initial assessment of adsorption as it has been previously demonstrated to form a host-guest complex with native β-CD [75]. The carboxylic acid functional group can deprotonate at pH 7 and protonate at pH lower than its pKa:4.5 (Table 3-1). Therefore, the adsorption was assessed at pH 7 to reflect natural waters and at pH 3 to understand the impact of protonation (pKa 4.5).

Batch adsorption tests were conducted in triplicate with a 10 mg/L ibuprofen solution. A 1000 mg/L stock ibuprofen solution was initially prepared from the standard ibuprofen solution (1.0 mg/mL). From the stock ibuprofen solution, 0.2 mL was transferred into a 20 ml vial via an automated volumetric pipette and 17.8 mL Milli Q water was added to the vial. Then, 2 ml of stock β-CD nanoparticle solution (10,000 mg/L) was transferred into the vial for a total solution volume of 20 mL. The initial concentration of Ibuprofen and β-CD FMNP in the final solution were 10 mg/L and 1000

mg/L respectively. pH was adjusted by titration to pH 7 ± 0.1 via 0.1 M NaOH solution and to pH 3 ± 0.1 via 0.1 M HCl respectively as verified by a pH meter.

The solutions were mixed for 1 hour in a temperature-controlled benchtop shaker (Innova 4230 Incubator Shaker, New Brunswick Scientific, Edison, NJ USA) at 20°C and 200 rpm. After the mixing the particles were separated via a high-gradient magnetic separator prior to analysis by UV-VIS. A blank solution including β-CD FMNP was prepared for UV-VIS analysis.

3.3.5. Adsorption isotherm

Isotherm experiments were developed to facilitate a comparison of the maximum adsorption capacity of the model β-CD FMNP to other FMNPs that have been reported. Prior to the adsorption tests, solutions of ibuprofen ranging between 5 to 20 mg/L that did not involve β-CD FMNP were analyzed in triplicate via UV-VIS to quantify the concentrations in the solution (Appendix B). The experiments were conducted in triplicate and were prepared by adding 5 ml of stock β-CD FMNP solution into ibuprofen solutions with concentrations ranging between 5 to 20 mg/L in 20 mL vials to have a constant adsorbent concentration of 1000 mg/L and a total volume of 20 mL. The same batch of nano-adsorbent was employed throughout the experiments. The solutions were mixed for 1 hour and the particles were separated via a high gradient magnetic separator prior to analysis by UV-VIS [45].

3.3.6. Effect of calcium concentration on adsorption of ibuprofen

The effect of the presence of calcium on the adsorption of ibuprofen was examined to assess the impact of common divalent cations on the adsorption mechanisms. Stock calcium chloride ($CaCl_2$) solutions of 0.1 M, 0.2 M and, 0.5 M were prepared by dissolving $CaCl_2.2H_2O$ MQ water. A volume of 4.5 mL of the solutions were transferred into 20 mL vials and spiked with 50 µl from the 1000 mg/L ibuprofen stock solution. The solutions were made up to 5 mL via the addition of 0.5 mL of stock β-CD nanoparticle solution (10 g/L). Hence, the initial concentrations of ibuprofen and the β-CD FMNP in the final solution were 10 mg/L and 1000 mg/L respectively. The solutions were prepared as duplicates and mixed for 1 hour. The particles were then separated via HGMS prior to analysis in UV-VIS. At the end of the test the Z-potential of the particles was measured to gain insight into the impact of calcium ions on the surface charge of the adsorbent. For this purpose, 3 ml samples which were drawn from the test solutions were analyzed by a Nanosizer ZS instrument (Malvern Co., UK)

3.3.7. Adsorption of the mixture of pharmaceuticals at environmentally relevant concentrations

Adsorption kinetics tests were carried out to assess the time required to reach equilibrium in subsequent tests. A stock solution that contained a mixture of the target compounds was employed for the tests. The stock solution contained 10 mg/L of each pharmaceutical and was prepared by adding 40 µL of each OMP standard solution (1000 mg/L) to a vial and making up the volume to 4 mL. A volume of 0.3 mL of the stock solution was then transferred via an automated volumetric pipette into 500 mL glass amber test bottles and 298 mL MilliQ water was added to the bottle. The total volume of the solution was completed to 300 mL with MilliQ water with the addition of 1.7 mL from the stock β-CD FMNP slurry (100 mg/L) in the final step. The initial concentrations of the pharmaceuticals and the β-CD FMNP in the final solution were 1 µg/L and 0.5 mg/L respectively. The pH was adjusted to a value of 7 ± 0.1 via 0.1 M NaOH before the experiment and measured after the mixing was complete. Samples with a volume of 100 mL were collected at 1, 2 and 3 h and then filtered via a 0.2 µm PES filter for SPE and LC/MS/MS analysis. To quantify the concentration of each OMP in the original solution, triplicate solutions without the β-CD FMNP were prepared and analyzed.

The equilibrium partitioning of the pharmaceuticals when present in a mixture at environmentally relevant concentrations was evaluated to explore the impact of adsorbate properties on adsorption under realistic conditions. It was recognized that the $LogK_{ow}$ and $LogD_{ow}$ have a molar basis, however, as the molecular weights of the target pharmaceuticals were similar the use of similar mass-based concentrations was deemed to not influence the interpretation of the results. A solution that contained a mixture of the target compounds was employed for the tests. Triplicate bottles were prepared from the previously described stock OMP solution (10 mg/L). A volume of 0.01 mL of stock pharmaceutical solution was transferred via an automated volumetric pipette into 300 mL glass amber test bottles and 99.3 mL MilliQ water was added to the bottle. The total volume of the solution was completed to 100 mL with MilliQ water with the addition of 0.67 mL from the stock β-CD FMNP slurry (100 mg/L) in the final step. The initial concentrations of the pharmaceuticals and the β-CD functionalized magnetic nanoparticles in the final solution were 1 µg/L and 0.5 mg/L respectively. pH was adjusted to pH 7 ± 0.1 via 0.1 M NaOH before the experiment and measured after the mixing is complete. The solutions were mixed for 1 hour. The solutions were filtered via a 0.2 µm PES filter after mixing was complete for SPE and LC-MS/MS analysis. To quantify the exact concentration of each pharmaceutical in the original solution, triplicate solutions without β-CD FMNP were prepared and analyzed via LC-MS/MS.

3.3.8. Analytical methods

The analysis of solutions containing elevated concentrations of ibuprofen was performed with HP Agilent 8453 UV-VIS (Waldbronn, Germany). The calibration curve was prepared as described previously [75]. The absorbance of the solutions was measured in a quartz cell (1 cm) that was washed with methanol prior to each measurement.

The solutions containing a mixture of pharmaceuticals were extracted to concentrate the pharmaceuticals into methanol prior to sample injection [79]. Extractions were done in a ThermoFisher AutoTrace™ automated solid phase extraction system (Dionex, Sunnyvale, CA). The extraction was performed using Bond Elut Plexa cartridges (6 cc, 500 mg, Agilent) that were preconditioned with methanol and MilliQ water. A 100 mL sample was brought to pH 2 ± 0.05 by 1 N HCl and spiked with 100 µL deuterated internal standard before loading onto the SPE cartridge. The cartridges were rinsed with 5 mL MilliQ water and 5mL 5% methanol in water prior to elution with 6 ml methanol (3 mL + 3mL). Next, the samples were evaporated until dryness under nitrogen prior to reconstitution with 500 µL of methanol with 75 µg/L lorazepam and chloramphenicol. The pharmaceuticals were analyzed using an Agilent 1200 HPLC with 6460 Triple Quadrupole mass spectrometer (Agilent, San Pedro, CA) with electrospray ionization (ESI) and the compounds were identified and quantitated according to the method described in the literature [79].

3.3.9. Data analysis

The solid phase concentrations were calculated for experiments that were conducted to determine the equilibrium time and equilibrium adsorption capacity. The solid phase concentration of pharmaceuticals at corresponding times was calculated via Equation 3-1;

$$Q_t = \frac{(C_0 - C_t)}{m} V \qquad (3\text{-}1)$$

where Q_t is the adsorbed mass concentration on the adsorbent (mg/g), C_0 and C_t are the concentrations at time zero and time t respectively, V is the volume of the solution (ml) and m is the mass of adsorbent (g).

The experimental data was fit with a Langmuir isotherm as given by Equation 3-2;

$$Q_t = \frac{Q_{max} \times K_L \times C_e}{1 + K_L \times C_e} \qquad (3\text{-}2)$$

where Q_t is the equilibrium mass of adsorbed contaminant on the adsorbent (mg/g), Ce is the equilibrium concentration of contaminant (mg/L) in the solution, Q_{max} is the maximum adsorption capacity, (mg/g) and K_L is the affinity parameter or Langmuir constant (L/mg) [30].

3.4. Results and discussion

3.4.1. The impact of pH on the adsorption of ibuprofen

The adsorption of ibuprofen was investigated at pH 7 and pH 3 to gain insight into the impact of pH on the adsorption mechanism. Minimal adsorption was obtained at pH 7 while a solid phase concentration of 2.5 ± 0.1 mg/g was obtained at pH 3. The results show that the adsorption of ibuprofen was enhanced at a pH that is lower than its pKa (pKa: 4.5). The observed results were investigated with respect to changes in hydrophobicity of ibuprofen and the surface charge of the model β-CD functionalized adsorbent that was each affected by pH.

The change in hydrophobicity of ibuprofen with respect to pH was reviewed by its $LogD_{ow}$ value to understand its effect on partitioning. When the pH was adjusted from pH 7 to pH 3, ibuprofen was protonated and the $LogD_{ow}$ value at pH 3 increased ($LogD_{ow}$ = 4.0) when compared to that at pH 7 (LogDow = 0.5). Hence ibuprofen was more hydrophobic at pH 3 when compared to pH 7 and this enhanced adsorption. This is consistent with the effect of pH on host-guest complexation between ibuprofen and native β-CD that has been reported in the literature [75]. The definitive conclusion that host-guest complexation with β-CD functionalized adsorbents was responsible for adsorption is difficult due make because of the complex chemical structure of the nanocomposite materials that may provide alternative types of adsorption. However, a previous study on the model adsorbent reported that the adsorption of procaine occurred after the β-CD grafting onto the silica-coated particles while procaine did not adsorb onto the particles that only had silica coating [45]. Hence, the adsorption mechanism has been defined as a host-guest complexation for the subsequent discussion.

The zeta potential of the β-CD functionalized nanoadsorbent was examined at the target pH values to evaluate its impact on the adsorption of ibuprofen. It was found that the zeta-potential of the model adsorbent was reduced from -37.6 ± 1.1 (pH 7) to -25.0 ± 1.8 mV (pH 3). The results suggest that reduced negative surface charge at pH 3, weakened the electrostatic repulsion between negatively charged ibuprofen species and the negatively charged surface of the adsorbent. However, as the adsorbent was still negatively charged, the increased adsorption was primarily attributed to the

increased hydrophobicity of ibuprofen at lower pH. Hence, it was concluded that the adsorption was hydrophobic and the mechanism was described as host-guest complexation.

3.4.2. Maximum adsorption capacity

Adsorption isotherm experiments were performed to establish the maximum adsorption capacity of the model adsorbent so that it could be benchmarked against other core-shell β-CD nano adsorbents reported in the literature. Figure 3-1 shows the experimental data and the fitted Langmuir adsorption isotherm for ibuprofen at a pH of 3. The experimental data shows that the solid phase concentration increased with increasing liquid phase concentration of Ibuprofen and was tending towards a plateau value at the highest liquid phase concentration. The maximum adsorption capacity (Q_{max}) of ibuprofen, as determined from the best-fit Langmuir isotherm, was 3.42 ± 0.2 mg/g. It should be noted that the R^2 value of the regression (0.82) was somewhat low and hence there was some uncertainty in the value of Q_{max}. While other isotherm models could have been evaluated it was unlikely that improved fits would have been achieved because of the scatter in the data and the limited number of available data points. The Q_{max} value obtained in the current study is subsequently compared with previously reported values for β-CD functionalized adsorbents to obtain insights into the impact of adsorbent properties on adsorption.

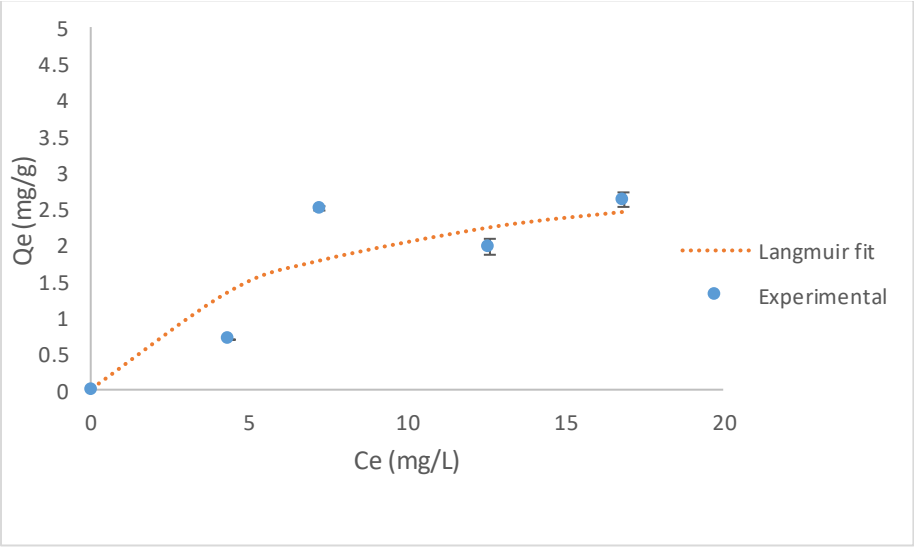

Figure 3-1: Ibuprofen adsorption isotherm at 25°C at pH 3

The Q_{max} value from this study was compared against those reported for β-CD functionalized core-shell nanoparticles. A core-shell β-CD functionalized nano adsorbent having a relatively similar nanocomposite structure (spherical, magnetic, silica-coated, and β-CD grafted nanoparticle) to the

model adsorbent in this study was reported to have Q_{max} values of 1.7 mg/g for naproxen and 2.2 mg/g for carbamazepine at pH 7 [24]. Hence, the limited data show that the Q_{max} values were similar for the current and prior studies However, the pH values differed substantially between the studies and hence the properties of the adsorbents were examined in greater detail to identify the cause of the discrepant adsorption behaviours.

The characteristics of the current and literature adsorbents were further reviewed to gain insight into the adsorption mechanism [24] [45]. It was found that the grafting agents that link β-CD to the surface of the adsorbents differed. The carboxymethyl group employed to graft β-CD to the silica surface on the model adsorbent in this study likely does not provide electrostatic attraction for the negatively charged ibuprofen. In contrast, the grafting agent employed in the literature adsorbent contained amine groups that could attract negatively charged naproxen [24]. Potential interactions that supported the adsorption of naproxen and carbamazepine simultaneously were reported in the prior study [24]. When the chemistry of the two grafting agents was considered along with the pH values at which adsorption was active it was concluded that the grafting agent composition is a significant factor in the design of adsorbents that are intended for removing negatively charged pharmaceuticals.

The Q_{max} value from the current study was considerably smaller than those reported for β-CD functionalized crosslinked polymers (50-300 mg/g) [32], [39], [56]. This is attributed to the high concentration of β-CD in polymer type adsorbents when compared to the core-shell nanoparticles. While crosslinked polymer adsorbents have higher Q_{max} values than those of the core-shell nanoparticles other factors such as diffusion limitations should be considered when designing applications.

3.4.3. Effect of calcium concentration on adsorption of ibuprofen

The results in the prior section demonstrated that electrostatic interactions likely affect the adsorption of ibuprofen. Hence the effect of calcium, that is commonly present in natural waters, on adsorption was investigated as it was expected to impact on electrostatic interaction. Figure 3-2 presents the solid phase concentration of ibuprofen versus calcium ion concentration for the various tests. It can be seen that the adsorption capacity was enhanced from 0.5 mg/g to 1.2 mg/g when the concentration of $CaCl_2$ was increased from 0.05 M to 0.2 M. It should be noted that the solution pH in these tests was 6.4 hence, the charge state of the ibuprofen was assumed to be negative. The results were inconsistent with prior reports where calcium had a negligible impact on the adsorption of bisphenol-A, chloroxylenol,

and carbamazepine by a TFTPN crosslinked β-CD polymer [32]. It was anticipated that this was due to differences in electrostatic interactions and hence the impact of calcium on the surface charge was investigated.

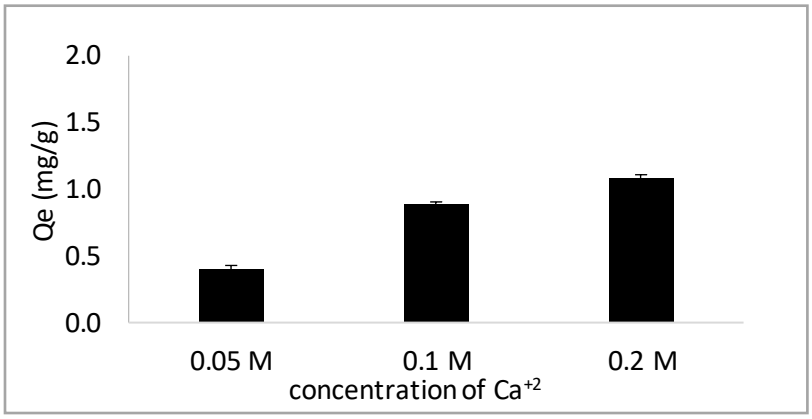

Figure 3-2: Equilibrium solid phase concentration of ibuprofen (10mg/L) versus $CaCl_2$ concentration (pH:6.4)

The zeta potential of the adsorbent was investigated to understand the impact of calcium ion on the surface charge of the adsorbent. (Figure 3-3). The zeta potential of the model adsorbent reduced from -37.6 ± 1.1 mV to -2.7 ± 0.2 mV when $CaCl_2$ concentration increased from 0 to 0.2M. The sharp change in the magnitude of potential between 0 to 0.05 M (-38 ± 1.1 mV to -12.4 ± 1.9 mV) was attributed to the neutralization of the surface charge of the adsorbent. [80][81The presence of calcium ions would increase the surface charge density. Due to increased surface charge density, more counterions (Ca^{+2}) entered the Stern layer and the thickness of the Stern layer decreased. This resulted in a quicker drop in zeta-potential initially [80]-[83]. The zeta potential continued to reduce gradually with increasing calcium ion concentration however it remained negative over the entire range of values. It was recognized that the increased ionic strength might cause the particles to become unstable in solution when the Z-potential as higher than -10 mV. However, visual observation of the solution did not indicate any coagulation or precipitation. The increased adsorption capacity at the elevated calcium concentrations was also consistent with stable adsorbent particles in the solution. Viewed collectively it appears that increased $CaCl_2$ concentrations reduced repulsive forces due to altered surface charge density of the adsorbent, and this led to enhanced adsorption of ibuprofen.

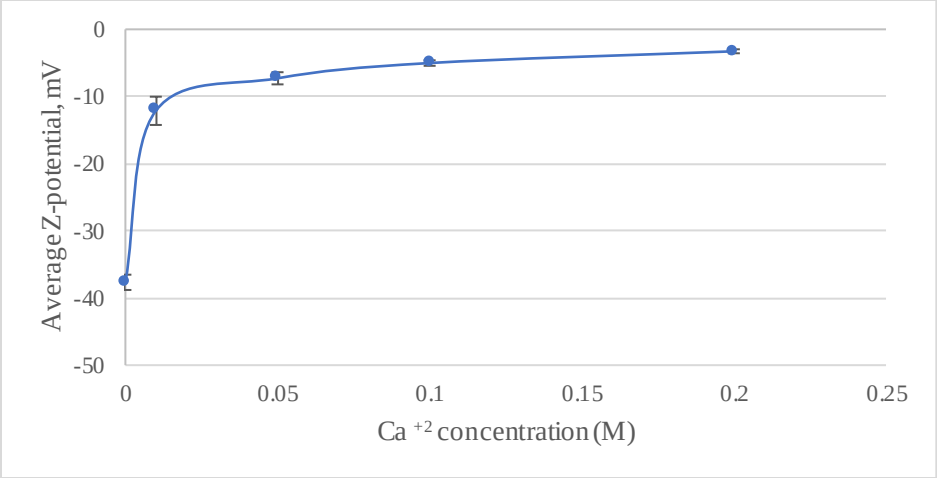

Figure 3-3: Average zeta-potential of β-CD magnetic nanoparticles versus $CaCl_2$ concentration

The results suggest ibuprofen adsorption occurred via host-guest complexation with the hydrophobic cavity of β-CD. Adsorption was impacted by the surface characteristics of the adsorbent that were influenced by the β-CD grafting agent. The model adsorbent was subsequently evaluated for adsorption of a list of pharmaceuticals with a range of physicochemical properties to gain insight into partitioning in a mixture at environmentally relevant concentrations.

3.4.4. Equilibrium adsorption of OMPs at environmentally relevant conditions

The effect of contact time on adsorbate uptake was examined to determine the equilibrium time that would be employed in subsequent equilibrium tests. Figure 3-4 illustrates the time that was needed to reach equilibrium for pharmaceuticals that were tested as a mixture. The aqueous concentration of the pharmaceuticals was reduced in the first hour and no significant decrease was observed during the next two hours. It was concluded that equilibrium was achieved in less than an hour and on the basis of these results, the subsequent equilibrium tests were conducted for 1 h.

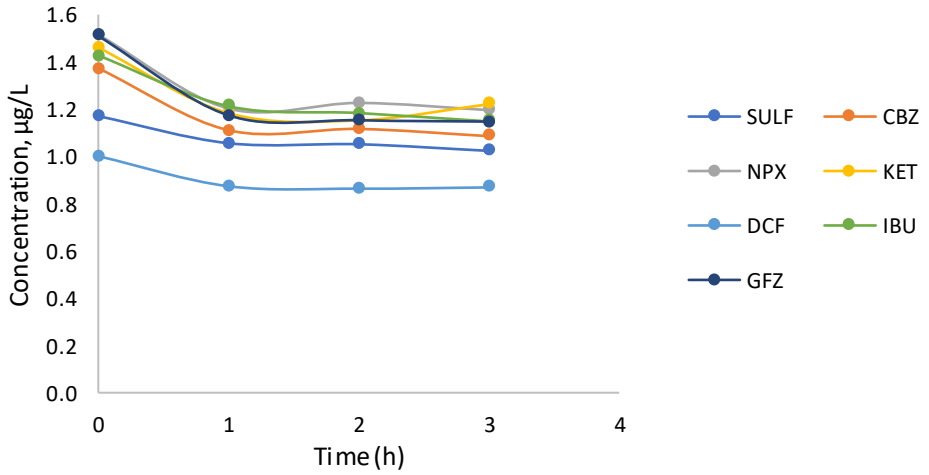

Figure 3-4: Effect of contact time on aqueous concentration of selected OMPs

The observed results were compared against those of studies conducted at environmentally relevant concentrations to assess the model adsorbent for water treatment applications. A mesoporous TFTPN crosslinked β-CD functionalized polymer reached equilibrium in less than 30 minutes [35] and an EPI crosslinked β-CD functionalized (nonporous) polymer reached equilibrium in 2 h for pharmaceuticals including naproxen, ibuprofen, ketoprofen, diclofenac [21], while a DFB crosslinked (porous) β-CD functionalized polymer required considerably longer times (13 h) to reach equilibrium for PFOA [28]. The apparent increased rate of mass transfer, when compared to non-porous β-CD functionalized polymers, was attributed to the elimination of diffusive limitations with nanoparticles.

The equilibrium adsorption of the mixture of target pharmaceuticals was studied at an environmentally relevant pharmaceutical concentration and around neutral pH to reflect real water systems. Figure 3-5 shows mean equilibrium solid phase concentrations and the standard deviations when an initial concentration of 1 µg/L was employed. The equilibrium solid phase concentrations of the target pharmaceuticals varied between 0.1 mg/g to 0.4 mg/g. The difference in adsorption capacities of the OMPs was attributed to differences in their affinity for the β-CD cavity due to their physicochemical properties such as hydrophobicity, pKa, size, and shape [35] and these characteristics were further investigated to understand the observed responses.

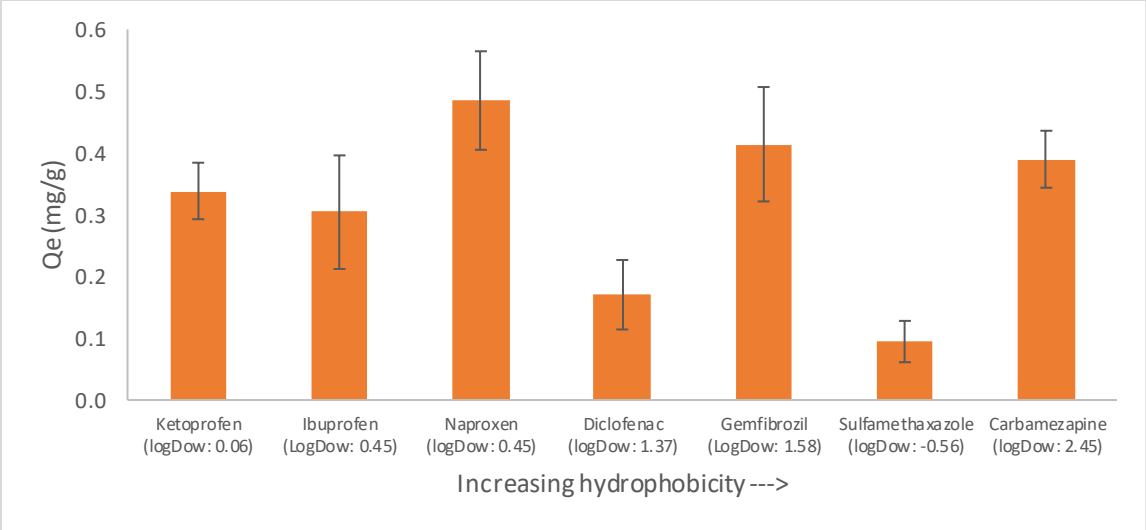

Figure 3-5: Average (± std dev) equilibrium solid phase concentration of pharmaceuticals. The X-axis shows the LogDow value of each pharmaceutical at pH 7 in increasing order from left to right.

The $LogD_{ow}$ and $LogK_{ow}$ values of the target pharmaceuticals at pH 7 were investigated to assess the impact of hydrophobicity on adsorption at their charged states and neutral states respectively. Figure 3-5 shows the solid phase concentrations of the target pharmaceuticals versus their $LogD_{ow}$ values. The observed responses did not provide a relationship with $LogD_{ow}$ values. Similarly, a trend with LogKow values was not observed. It might be expected that the hydrophobic interior of β-CD would provide an attractive adsorption site for the pharmaceuticals and therefore there would be a relationship between partitioning and LogKow values. The lack of trend with hydrophobicity indicators shows that the adsorption mechanism is more complex and is suspected to be impacted by other physicochemical properties of the target pharmaceuticals.

The target pharmaceuticals can be protonated or deprotonated depending upon the pH relative to their pKa values and hence the charge state of the target compounds was investigated at pH 7. Except for carbamazepine (pKa = 13.9), all of the target pharmaceuticals were in their negatively charged state due to deprotonation at pH 7 (Table 3-1). Based on previously described results for ibuprofen adsorption, it was expected that the positively charged species of carbamazepine might provide electrostatic attractions due to the negative surface charge of the adsorbent and yield better partitioning compared to other pharmaceuticals in the mixture, however, this was not observed from the mixture adsorption results. Hence, the charge state of the pharmaceuticals did not describe the adsorption properties of the pharmaceuticals.

The molecular geometry of the pharmaceuticals was reviewed as the shape of the OMPs has been reported to impact on host-guest interactions with β-CD functionalized adsorbents [24], [67], [72]. In particular, the molecular geometry of pharmaceuticals with more than one aromatic ring in the structure was found to influence partitioning. In the current study naproxen, which has a planar geometry due to the naphthalene moiety demonstrated the highest solid phase concentration. On the other hand, sulfamethoxazole and diclofenac yielded the lowest solid-phase concentrations. These compounds have two aromatic rings that are twisted with respect to each other due to the presence of $-SO_2$ and -NH functional groups between the aromatic rings respectively [84]. In addition, the adsorption capacities of carbamazepine and ketoprofen were in between the adsorption capacities of the planar and the twisted structures and this was attributed to the slightly angled aromatic rings of these compounds. The results are consistent with a literature report where the bent geometry of bisphenol-F and bisphenol-S resulted in reduced adsorption when compared to bisphenol-A which has a slightly nonplanar structure to a β-CD capped graphene-magnetite nanocomposite [36]. Based on these results, the molecular geometry impacts the partitioning of target contaminants onto β-CD functionalized nano adsorbent when present at environmentally relevant concentrations.

Based on the current study, the partitioning of pharmaceuticals onto the model adsorbent was influenced by the geometry of the adsorbates and the electrostatic interactions between the adsorbate and the adsorbent which was altered by the water chemistry. The modifications of β-CD (i.e., type of grafting agent, substitution degree of β-CD) employed to graft onto the nanocomposite structure can be a factor that impacts the non-covalent interactions and as a result partitioning. However, it is difficult to evaluate the impact of these factors by experimental techniques. Hence, characterization of the non-covalent interactions by molecular could provide further insight on this subject.

3.5. Conclusion

A novel β-CD functionalized magnetic nano adsorbent was evaluated for the adsorption of a range of target pharmaceuticals. The investigation of the adsorption of ibuprofen provided insights into the adsorption mechanism and the effect of water chemistry on adsorption. Based on the results;

- Solid phase concentration of ibuprofen was elevated when the solution pH was lower than the pKa of ibuprofen as the hydrophobicity was increased.
- The presence of calcium ions enhanced the adsorption of ibuprofen as the surface charge of the model adsorbent was reduced.

This study also provided insights into the adsorption of target pharmaceuticals as a mixture at an environmentally relevant concentration which has been rarely investigated in the literature. The results showed that;

- the hydrophobicity of the pharmaceuticals could not describe the adsorption mechanism alone.
- the molecular geometry of the OMPs that have more than one aromatic ring was determined as a factor impacting adsorption in the mixture, where planar geometry favored the partitioning when compared to nonplanar geometries.

Chapter 4

Molecular level investigation of adsorption of pharmaceuticals with β-CD functionalized adsorption sites

4.1. Abstract

The objective of this study was to investigate the partitioning of target pharmaceuticals onto β-CD functionalized nanocomposites at the molecular level. The use of molecular electrostatic surface potential mapping of β-CD derivatives was investigated to understand the impact of substitution degree and type of grafting agent on host-guest complexation. It was found that the substitution degree of β-CD was the most important factor that impacts the adsorption of ibuprofen which was consistent with experimental data. Molecular dynamics simulations revealed that fulvic acid is a competitor for ibuprofen for the cavity of the β-CD. The stability of the complexes of selected pharmaceuticals and β-CD derivatives was assessed. The results showed that the hydrophobicity of the guest molecules impacted the stability of the complexes when pH was altered and procaine provided the most stable complex (-75.9 kcal/mol) when compared to ibuprofen, naproxen and, sulfamethoxazole. It was also found that the presence of aromatic rings can provide additional electrostatic attractions by π-π interactions for the OMPs that have aromatic rings. Ultimately, this study showed that the molecular level simulations can be an effective tool for the investigation of the adsorption of OMPs by β-CD functionalized adsorbents, and could be employed to enhance their environmental applications.

4.2. Introduction

There has been a growing interest in β-CD functionalized adsorbents for the adsorption of organic micropollutants (OMPs) due to the hydrophobic cavity of β-CD [24], [29]-[31], [41], [43], [57]. The assessment of these adsorbents has typically included a screening of target OMPs for potential adsorption and assessing the impact of modifications to the adsorbent structures on the adsorption of target OMPs [32], [48], [49]. These studies have demonstrated that the development and application of β-CD functionalized adsorbents involves a large number of experiments and is resource intensive. Hence, there is considerable motivation to employ molecular-level investigations that can provide insight into the adsorption mechanism of OMPs and the factors that influence their adsorption with β-CD functionalized adsorbents.

Computational chemistry tools have potential in this regard as they allow the investigation of chemical systems at the molecular level to address issues that can be difficult to evaluate in physical studies [85]. These tools are based on the molecular mechanic, semi-empirical, ab-initio, and density functional theory quantum methods that use atomic and/or molecular level information [86], [87]. They can be employed to characterize and predict the structure and stability of chemical systems, estimate energy differences between different states, and suggest reaction pathways and mechanisms at the atomic level [87]. These features make computational chemistry tools promising for the investigation of the adsorption of OMPs on β-CD functionalized adsorbents.

Molecular simulations have significantly contributed to applications in other disciplines including drug design, development and delivery, protein binding, materials design, and synthesis [86]. Furthermore, they have also been employed to investigate equilibrium thermodynamics and reaction stoichiometry and to identify plausible reaction mechanisms involved in β-CD host-guest complexation with pharmaceuticals [74], [88]-[90]. The results have provided insight into the affinity of pharmaceuticals to β-CD, complex stability, and complex geometry. However, molecular simulations have been rarely used to investigate the adsorption of OMPs with β-CD functionalized adsorbents via host-guest complexation [48]. Molecular level investigation of OMP partitioning to β-CD functionalized adsorbents could help address the knowledge gaps associated with this subject which are discussed subsequently.

The secondary -OH groups of β-CD are typically modified prior to grafting onto the surface of nanocomposites [24], [30]. The substitution degree of the modified β-CD establishes the number of available functional groups for grafting. When the substitution degree is higher than 1, the functional groups available for grafting might not be utilized completely during the grafting procedure. The presence of functional groups that are not attached to the surface and that can be ionized can alter the surface characteristics of the adsorbent depending on the solution's pH [45], [91]. Hence, the substitution degree of β-CD that is grafted onto the surface of the nanocomposites can significantly impact the adsorption of OMPs. However, there is insufficient information on this subject, and more research at the molecular level is needed to evaluate the impact of the substitution degree of β-CD on the adsorption of OMPs.

Different functional groups (e.g., amine and diimidazole functional groups) have been employed to graft the β-CDs onto the coated surface of the nanocomposites [24], [34]. The linkages employed in the integration of β-CDs to polymers have been reported to significantly impact the adsorption of

certain OMPs [27], [28]. However, those employed in nanocomposites have not been investigated in detail for the impact on intermolecular interactions with the OMPs [24]. Hence, the type of grafting agent employed to link β-CDs onto the surface of the nanocomposites can significantly impact the adsorption of OMPs. Molecular level investigation of the effect of the type of grafting agents on the surface characteristics could provide insights into the adsorption of target OMPs with β-CD functionalized nanocomposites.

The partitioning of OMPs has usually been attributed to host-guest complexation with the hydrophobic β-CD cavity. However, the driving mechanism for the partitioning onto the adsorbent has been found to depend on the type of OMPs and their physicochemical properties [24], [32], [39]. A comparison of the stability of host-guest complexes of target OMPs with β-CD derivatives employed on the adsorbent structure can give insight into the affinities of OMPs and hence, the potential for competitive adsorption [88], [92]-[95]. Assessment of complex stability through the use of molecular dynamics simulations has the potential to efficiently address this issue but needs to be critically developed and evaluated.

In this study, the host-guest interactions of target pharmaceuticals with selected β-CD derivatives representing the adsorption site were investigated via molecular simulations. The reactivity of β-CD derivatives for potential noncovalent interactions was systematically investigated to understand the impact of the substitution degree and the type of grafting agents. This was achieved via the use of surface electrostatic potential maps of β-CD derivatives based upon molecular mechanics and semi-empirical quantum mechanics methods. The impact of the physicochemical properties of the target pharmaceuticals and fulvic acid on host-guest complexation with selected β-CD derivatives in an aqueous matrix was examined via molecular dynamics simulations. The results were employed to understand the competition between the adsorbates.

4.1. Computational methods

4.2.1. Selection of β-CD derivatives (host molecules)

The literature reveals that the adsorption of OMPs is impacted by the grafting agents employed for integration of β-CD into the adsorbent structures and hence representative β-CD derivatives were chosen to conduct simulations that cover a range of substitution degrees of β-CD and a range of functional groups used in β-CD modification prior to grafting step. The selection criteria of the β-CD derivatives are provided subsequently.

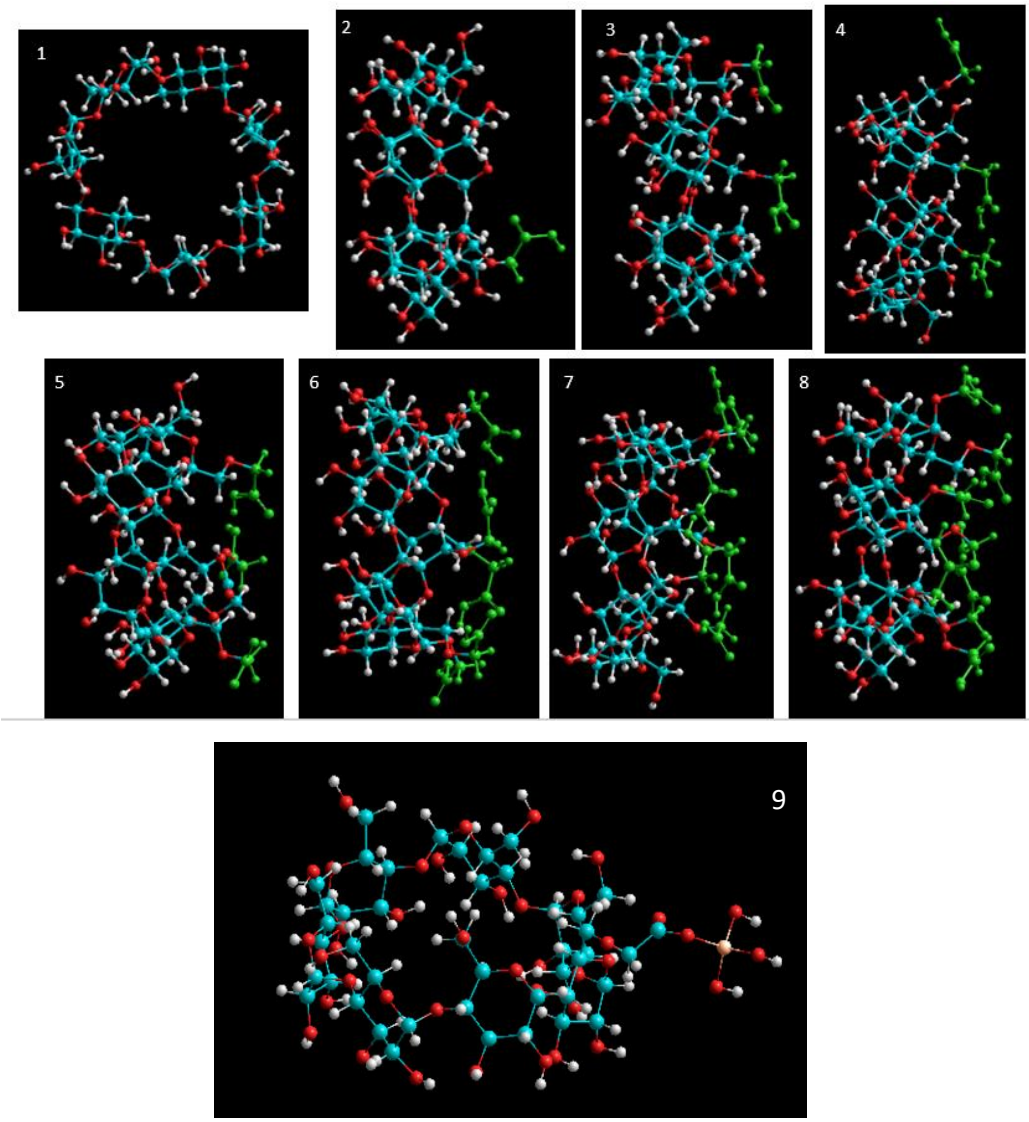

Figure 4-1: CM-β-CD derivatives 1) β-CD (sd: 0) 2) CM-β-CD (sd:1) 3) CM-β-CD (sd:2) 4) CM-β-CD (sd:3) 5) CM-β-CD (sd:4) 6) CM-β-CD (sd:5) 7) CM-β-CD (sd:6) 8) CM-β-CD (sd:7) 9) Si-CM-β-CD. The atoms are color-coded where blue is carbon, red is oxygen, white is hydrogen and orange is silicon. The green labelled parts on the modified β-CDs indicate the substituted carboxymethyl functional groups (1-8) and $Si(OH)_3$ (9).

The substitution degree (sd) of CM-β-CD employed in grafting β-CD onto the model adsorbent in this study was of interest hence the reactivity of CM-β-CD derivatives was investigated [45], [96]. Figure 4-1 shows the molecular structures of CM-β-CD derivatives that represented different substitution degrees (1-8). The CM-β-CD derivatives with a substitution degree higher than 1 were built by adding carboxymethyl groups to the adjacent carbon atom of CM-β-CD with a substitution degree of 1. A CM-β-CD derivative that represented the silica linkage was also included in Figure 4-1 (9) as the CM-β-CD is attached to the silica surface in the adsorbent structure. The reactivity of CM-β-CD derivatives and the stability of the host-guest complexes by the selected CM-β-CD were investigated via molecular simulations.

The impact of water chemistry on the surface properties of selected CM-β-CD derivatives was also investigated since the adsorption of pharmaceuticals was found to be impacted by the pH and the presence of calcium ions in experiments. For this purpose, the selected CM-β-CD derivatives from Figure 4-1 were employed by adjusting their molecular structure based on their pKa and in the presence of one calcium ion to further investigate the experimental results. The change in the reactivity and the host-guest interactions were examined via molecular simulations.

The impact of the type of grafting agents on host-guest interactions was assessed as the functional groups employed for grafting of β-CD have been reported to impact the adsorption of OMPs. Figure 4-2 shows the β-CD derivatives that were chosen for molecular simulations. CM-β-CD was selected as a relatively short-chain functional group. MDE-β-CD was selected to represent a grafting agent that has a longer carbon chain and an amine functional group that could provide electrostatic interactions when compared to carboxymethyl-β-CD. It has been previously employed in a β-CD functionalized core-shell magnetic nanoparticle that was tested for adsorption of naproxen (pKa: 4.2) [24]. DFB-β-CD was selected to represent a grafting agent that is more rigid when compared to CM-β-CD due to the presence of aromatic rings and fluorine atoms that can impact noncovalent interactions [28]. This functional group was reported to enhance the adsorption of negatively charged PFASs in a β-CD crosslinked polymer. The impact of these grafting agents on the reactivity and stability of the selected host-guest complexes was examined.

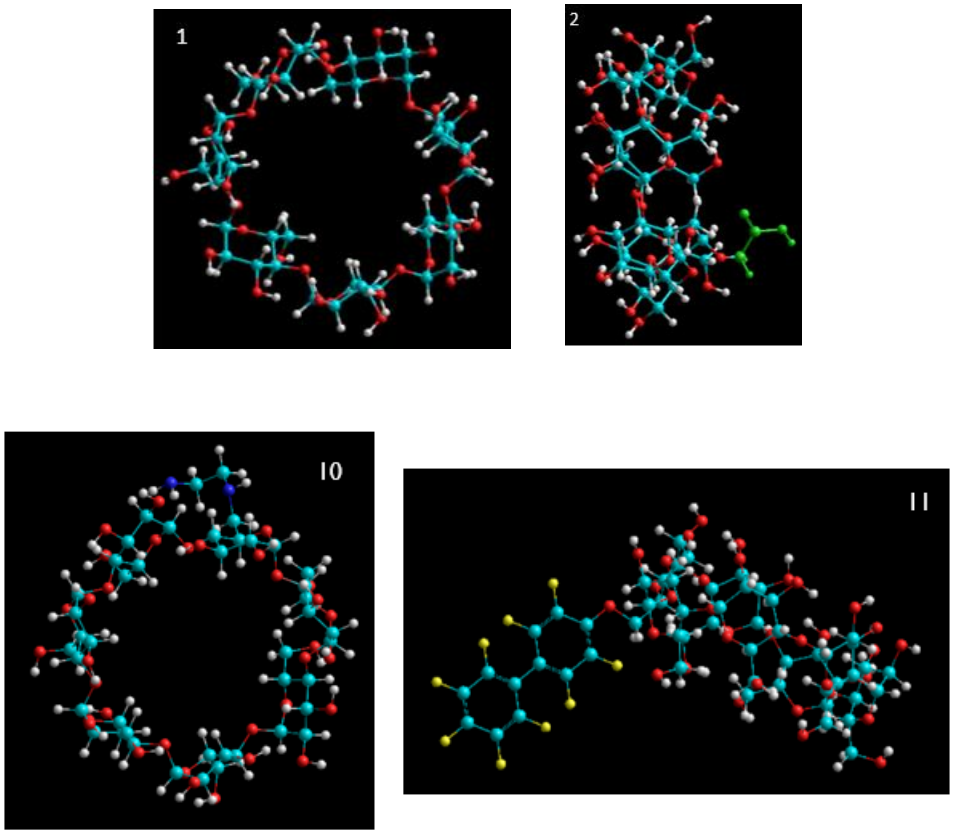

Figure 4-2: 1) β-CD 2) CM- β-CD 10) MDE-β-CD 11) DFB-β-CD white: hydrogen, green: carbon red: oxygen blue: sulphur, yellow: fluorine

4.2.2. Guest molecules

In this study, it was recognized that the adsorption is impacted by the properties of the adsorbate and hence selected representative compounds were chosen to conduct simulations that spanned a range of key properties. For this purpose, ibuprofen, procaine, naproxen, sulfamethoxazole and fulvic acid (Figure 4-3) were selected as the target contaminants based on their physicochemical properties and the results of the previously described adsorption study. The identified physicochemical properties of the target pharmaceuticals for investigation at the molecular level are explained subsequently.

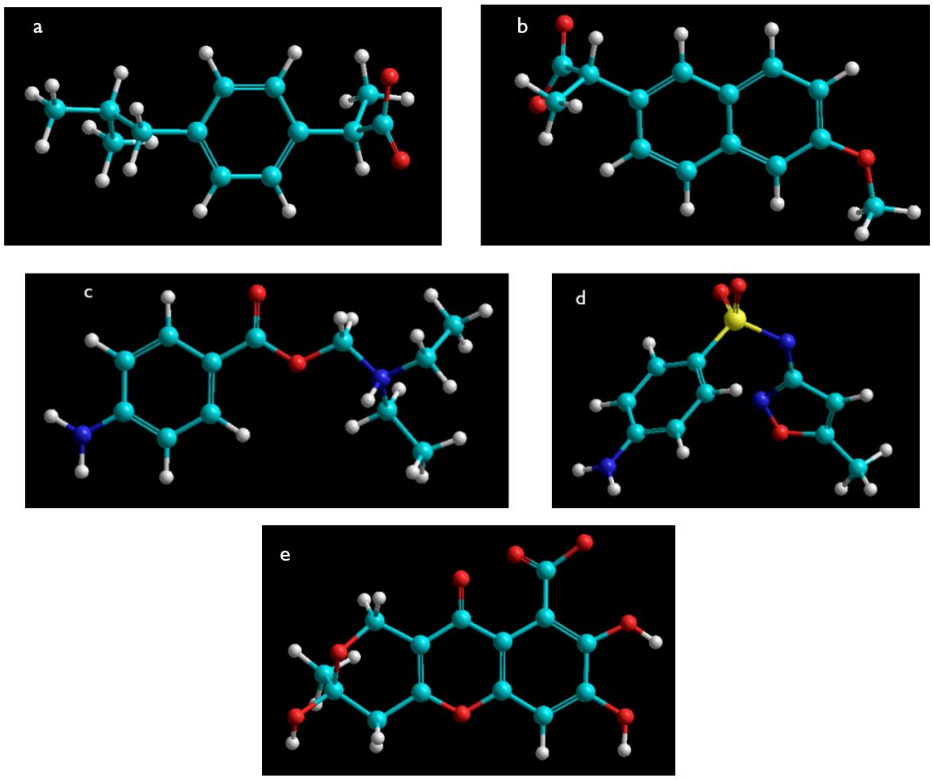

Figure 4-3: Target contaminants built via HyperChem (red: oxygen, green: carbon, blue: nitrogen, white: hydrogen, yellow: sulphur) a) ibuprofen b) naproxen c) procaine d) sulfamethoxazole e) fulvic acid

The hydrophobicity of the target molecules was investigated to gain insight into its impact on the host-guest complexation. For this purpose, ibuprofen and procaine were selected as the guest molecules. Ibuprofen is a pharmaceutical that is known to form a host-guest complexation with native β-CD [45]. Procaine has been previously demonstrated to be adsorbed with a high adsorption capacity by the model adsorbent employed in this study [75]. Both compounds have an aromatic ring that provides hydrophobicity and is suitable for entering the cavity of β-CD with respect to size. However, ibuprofen (pKa:4.5) has a carboxylic acid functional group that deprotonates at pH 7 and it is predominantly present in the negatively charged form around neutral pH [75]. In contrast, procaine (pKa: 8.9) has an amine functional group that is protonated at pH 7 and is predominantly present as a positively charged state [45]. Hence, the hydrophobicity of these compounds is influenced by the pH of the solution in which that they reside. It was expected that the differences in the host-guest complexes formed between these compounds and selected β-CD derivatives would provide insight into the impact of hydrophobicity on their adsorption.

The molecular geometry of the compounds was of interest as the shape of the OMPs has been previously identified as a factor that impacts host-guest complexation with β-CD functionalized adsorbents. For this purpose, naproxen and sulfamethoxazole were selected as the target guest molecules. Naproxen has two adjacent aromatic rings (naphthalene moiety) that provide a planar molecular geometry [24]. Sulfamethoxazole differs from naproxen in this regard, as the -SH bond creates a bent shape with aromatic rings twisted relative to each other that provides a nonplanar molecular geometry [84]. The host-guest complexation of these compounds was investigated to gain insight into the impact of molecular geometry on the noncovalent interactions.

The presence of dissolved background organic matter in water sources (also known as natural organic material (NOM)) is known to provide competitors for trace organic contaminants and challenge conventional adsorption processes [34]. Fulvic acid was selected in this study as it is a NOM component that is relatively small compared to other NOM components (molecular weight of 308.2 g/mol) [32]. Hence, it was assumed to be a potential competitor with the pharmaceuticals for the β-CD cavity. It has a nonplanar molecular geometry and a carboxylic acid functional group that can be protonated/deprotonated based on the solution pH. Therefore, its interaction with selected β-CD derivatives was investigated to gain insight into competitive adsorption.

4.1.1. Building molecules and geometry optimization

The molecular geometries of the selected host and guest molecules were optimized to prepare them for subsequent molecular simulations by minimizing their surface potential. The initial molecular structure of β-CD was obtained from the crystal database (BUXKIR from Cambridge Crystallographic Database [97]. The modified β-CDs and the selected guest molecules were built in HyperChem 8.0 software package (AMBER03 parametrization). β-CD was modified starting from the same carbon on the narrow rim of β-CD to be consistent with comparisons of the simulated condition of β-CD derivatives. The chemical structure of the guest molecules was verified by checking for odd bond lengths and bond angles after AMBER03 parametrization [93]. The Polak Ribiere conjugant gradient algorithm was chosen for the geometry optimization step (AMBER03) as a good general-purpose optimizer and is the default method in HyperChem [98]. The geometry optimization was stopped when the calculation converged with an RMS gradient of 0.1 kcal/mol/Å, which is the root mean square of the derivative of the energy with respect to the Cartesian coordinates. The optimized geometry of the molecules was then employed in the subsequent simulations.

4.1.2. Simulating aqueous medium

It was deemed important to represent the aqueous medium in molecular simulations for environmental applications of β-CD functionalized adsorbents as the water chemistry influences the non-covalent interactions between target OMPs and the β-CD adsorption site [99]. Explicit water molecules were used in the simulations by employing a periodic boundary conditions-imposed box that is illustrated in Figure 4-4 for a host-guest system. The explicit water molecules (described by the TIP3P function in HyperChem) typically have a molecular geometry closely matching actual water molecules and have a minimum distance of 2.3 Å (length of a hydrogen bond) from the solute atoms [99], [100]. Water molecules that were beyond a radius that was greater than half the largest box dimension were excluded by a switched cutoff function. This step was employed to reduce the nonbonded energy values (i.e., van der Waals, hydrogen bond and electrostatic) smoothly to zero. A second geometry optimization step was performed to minimize the energy of the systems prior to molecular simulations. This condition enabled the simulation to mimic the aqueous medium through the use of explicit water molecules during the calculations.

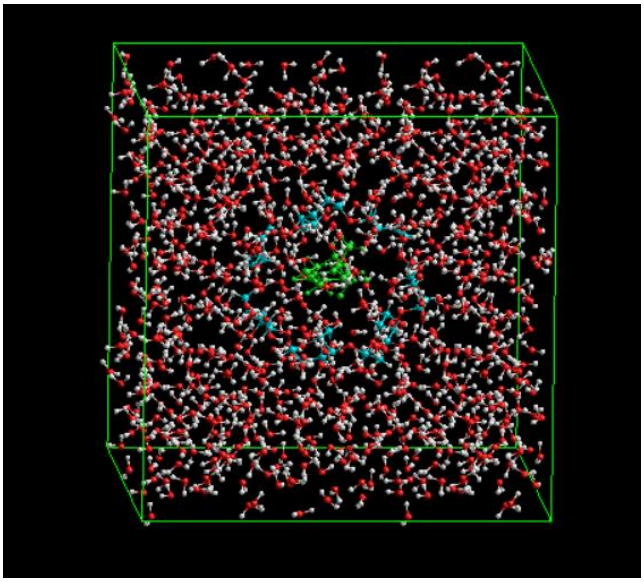

Figure 4-4: Illustration of an example molecular system in a water box: Ibuprofen-β-CD host-guest complex in water box (29.67 $Å^3$) with 934 water molecules. Green: Ibuprofen, blue ring-like structure: β-CD, red-white: water molecules

4.1.3. Investigation of the electrostatic surface potential of β-CD derivatives via semi-empirical quantum method

Molecular electrostatic surface potential (MESP) mapping was performed to evaluate the reactivity of β-CD derivatives (host molecules) for grafting and the potential intermolecular interactions with OMPs. MESP elucidates the reactivity of a molecule by describing its electronic charge distribution and the presence of the nucleophile and the electrophile sites on the molecular structure. Hence, it gives insight into potential covalent and noncovalent interactions [101], [102].

The electrostatic surface potential (V) (kcal/mol) for a molecule with a continuous electron charge distribution and nuclear point charge can be calculated by semi-empirical quantum methods in HyperChem [98] which is described by Eq 4-1;

$$V(r) = \sum_A \left[\frac{Z_A}{R_A - r} - \sum_{\mu\nu}^{on\ A} P_{\mu\nu} \int \frac{\rho(r')}{|r' - r|} dr' \right] \qquad (4\text{-}1)$$

where the point r is the position of a positive charge Z_A is the nuclear charge on atom A located at the position of R_A, $(\rho(r'))$ is the electron density function on atom A (Appendix C), dr' represents the distance between the volume element and point r. Hence, the electrostatic potential expression includes the contribution of the nuclei to the electrostatic potential by the first term and the electronic contribution by the second term. The mapped electrostatic potential surface shows the electron-rich (nucleophilic) and electron-deficient (electrophilic) regions using a colored scale and quantifies the maximum and the minimum potential on the surface (kcal/mol) [98], [101]. Therefore, MESP analysis was employed as a tool to evaluate the reactivity for the grafting onto surfaces and the potential noncovalent interactions with the guest molecules [98], [103], [104].

A series of three steps were employed to obtain the MESP maps of β-CD derivatives. The β-CD derivatives that were optimized in a water box were isolated from the water medium. The electronic structure (Eq 4-1) of the β-CD derivatives was calculated by single point calculation which provides information on the surface potential of the molecule conformation that was formed after geometry optimization. The PM3 semiempirical quantum mechanical method was chosen for this calculation as it has been found to provide a better approximation for macro-organic molecules by using parameters obtained from experiments to approximate wavefunctions [98][105]. The results were then employed in electrostatic surface potential mapping that was conducted with the molecular properties tool of

HyperChem 8. MESP calculations enabled a comparison of β-CD derivatives with respect to the impact of substitution degree and grafting agents on reactivity and potential host-guest interactions.

4.1.4. Investigation of complex stability via molecular dynamics simulations

The impact of the physicochemical properties of the selected guest molecules on host-complexation was investigated by the stability of host-guest complexes via molecular dynamics (MD) simulations The lower complex energy describes a more stable complex hence gives insight into competition between the guest molecules for a target host [92], [93], [94], [95].

The molecular mechanical method was employed for MD simulations and AMBER force field (Amber03 parametrization) was chosen as it is widely used for comparing large chemical systems and allows simulation under the explicit water condition in HyperChem [93] [98]. AMBER uses the equations of classical mechanics to describe the potential energy surfaces and physical properties of molecules. A molecule is described as a collection of atoms that interact with each other by simple analytical functions. This description is called a force field. The potential energy of a molecular system in a force field is the sum of individual components of the potential. For a molecule, the potential energy (V) (kcal/mol) is described by Equation 4-2;

$$V = V_{stretch} + V_{bend} + V_{dihedrals} + V_{VdW} + V_{Hbonds} + V_{EEL} \quad (4\text{-}2)$$

where $V_{stretch}$ describes the bond potential, V_{bend} describes the potential from bond angles, $V_{dihedrals}$ describe the torsional potential that arises from torsions, V_{VdW} describes the Van der Waals potential due to attractive London-dispersions and repulsive interactions due to Pauli exclusion, V_{Hbonds} describes the potential due to the distance between atoms that can have H-bonding and V_{EEL} describes the electrostatic potential due to electrostatic interactions that occur via a positive point charge that can be attracted and inversely related to the distance between two atoms. Each value in Eq (4-2) is the sum of all contributions of a molecule (Appendix C). To assess the stability of the complexes, the contribution of van der Waals and electrostatic potential terms were employed in the calculation of total energies of the host, the guest and the complexes as they provide insight into intermolecular interactions between the host and the guest.

A series of steps were employed to obtain the total energies of the host-guest complexes. Prior to the MD simulation the selected host and guest molecules were docked to obtain the complexes using the standard protocol for docking in the Glide program [106]. MD simulations were performed in an

explicit water box at a constant temperature (298 K) to mimic experimental conditions. The length of the simulations was 120 picoseconds with a time step of 0.001 picoseconds as these conditions have been indicated to yield an equilibrium condition [98]. Equilibrium was evaluated by the potential energy against time plots and it was assumed that equilibrium was reached when the change in average potential energy was minimized approaching a constant value during the simulation [98]. After the MD simulations were complete, the host, guest and host-guest complexes were isolated from the water box. Single point calculation with Amber force field was performed to obtain the total energies of the molecules in vacuo [107]. The MD simulations provided potential, kinetic and total energy at the end of the run which was employed for the assessment of the stability of the host-guest complexes.

The stability of the complexes was assessed on the basis of the complexation energy (ΔE) (kcal/mol) that was calculated as described in Eq 4-3;

$$\Delta E_{complexation} = E_{complex} - E_{host} - E_{guest} \qquad (4\text{-}3)$$

where $E_{complex}$ is the energy of the complex (kcal/mol), E_{host} is the energy of corresponding β-CD derivatives (kcal/mol) and E_{guest} is the energy of guest molecules (kcal /mol) [108]-[110]. The calculated complexation energy was employed to investigate the stability of the complexes with respect to the physicochemical properties of the host and guest molecules.

4.2. Results and Discussion

4.2.1. Investigation of molecular electrostatic surface potential (MESP) mapping of β-CD derivatives

The MESP analysis provides information on the electron-deficient and electron-rich regions on a molecule hence, the MESP of CM-β-CD derivatives was investigated to evaluate the impact of substitution degree on their reactivity through noncovalent interactions. Figure 4-5 presents the MESP of CM-β-CD with different substitution degrees (sd) where the electron-rich and deficient regions on the surfaces are delineated with different colors. It was found that increasing the substitution degree increased the presence of electron-rich regions due to the presence of additional carboxymethyl functional groups on β-CD. Hence, this initial assessment of the molecular electrostatic surface potential of CM-β-CD derivatives indicated that higher substitution degrees will provide attraction towards positively charged OMPs and repulsion of negatively charged OMPs [103], [104] [109], [111], The substitution degree was therefore identified as a factor that impacts the potential host-guest

interactions. The results were further investigated with respect to the impact of substitution degree on the reactivity of CM-β-CD for grafting of β-CD onto the silica surface.

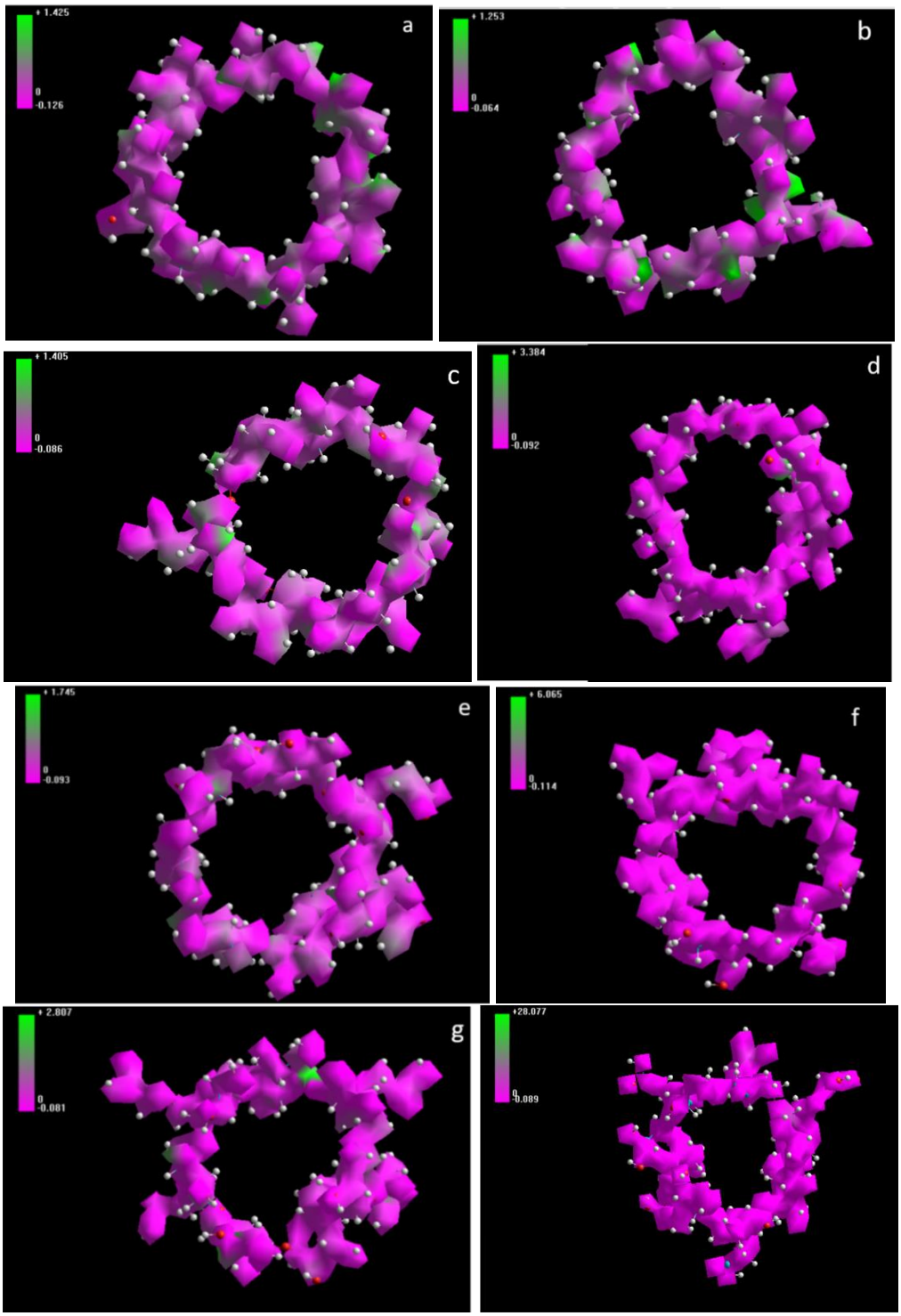

Figure 4-5: Electrostatic surface potential map of a) β-CD b) CM-β-CD (sd:1) c) CM-β-CD (sd:2) d) CM-β-CD (sd:3) e) CM-β-CD (sd:4) f) CM-β-CD (sd:5) g) CM-β-CD (sd:6) h) CM-β-CD (sd:7). The

pink color represents electron-rich and the green color represents electron-deficient regions on the surface. The scale on the left shows the maximum and minimum electrostatic surface potential on that position.

The grafting of CM-β-CD onto silica or iron oxide surface was investigated to gain insight into the reaction mechanism as a function of substitution degree. Grafting has been reported to occur via carbodiimide activation of the carboxylic acid (-COOH) group on CM-β-CD (Appendix C) [45], [112]. The average substitution degree of CM-β-CD has been reported to be 3 for both commercial and lab-scale synthesis [112]. Hence, more than one -COOH group on the CM-β-CD molecule was available for binding to the -OH groups on the adsorbent surface (i.e., silica or iron oxide) [45], [112]. The grafting was usually characterized via the presence of a C=O stretching peak of the carboxylate group on CM-β-CD when attached to the surface of the adsorbent in FTIR [45][112]. However, further characterization by XPS pointed out the potential presence of carboxyl groups on the CM-β-CD in the literature [112], [113]. Therefore, the MESP of CM-β-CD with a substitution degree of 3 (sd:3) was further investigated to assist in determining the presence of free carboxyl groups.

The MESP of the CM-β-CD (sd:3) derivative was reviewed considering the reactivity of CM-β-CD (sd:3) for grafting onto the silica surface. Figure 4-6 shows the MESP of CM-β-CD (sd:3) and carboxymethyl groups attached to β-CD. It was found that a large positive electrostatic surface potential occurred on one of the available -COOH groups of CM-β-CD (sd:3) around the carbon atom. Hence, it was hypothesized that the activation is more likely to occur from the oxygen on the -COOH group identified via MESP analysis [98]. This mechanism would explain the presence of free -COOH groups on CM-β-CD (sd:3) supporting the reports in the literature [112], [113]. Therefore, the MESP analysis provided an improved understanding of the reaction mechanism that is difficult to study via experimental techniques.

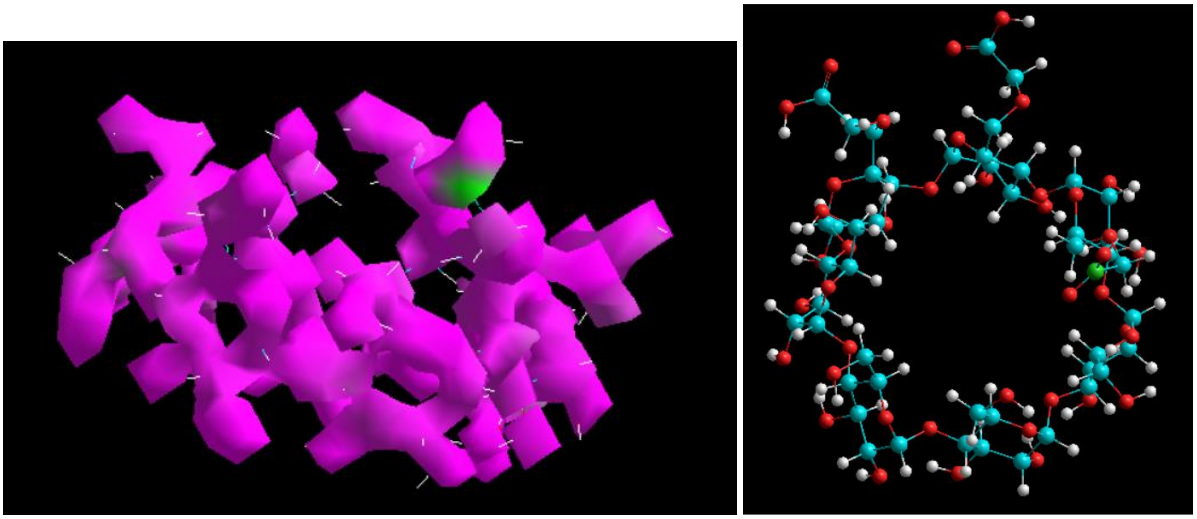

Figure 4-6: The carbon with the highest electrostatic surface potential labelled with green color on a) the MESP of 3-substituted CM-β-CD b) the chemical structure of 3-substituted CM-β-CD

The presence of free -COOH groups around neutral pH can impact the host-guest interactions hence, the literature was reviewed for relevant studies that focus on the adsorption mechanism of OMPs with CM-β-CD functionalized adsorbents or host-guest complexations of CM-β-CD. It was seen that the CM-β-CD could complex with cadmium (Cd^{+2}) around neutral pH with the negatively charged -COOH groups (pKa lower than 5), while simultaneously hosting anthracene in the β-CD cavity [114]. The same adsorption mechanism was reported where CM-β-CD functionalized nanoparticles were employed for the adsorption of copper (Cu^{+2}) [112]. Moreover, other CM-β-CD functionalized nanoparticles reported the adsorption of methylene blue and procaine both of which reside in a positive charge state around neutral pH [45], [96]. These examples clearly show that the free -COOH groups on CM-β-CD provided opportunities for electrostatic attraction of positively charged pollutants although the main adsorption mechanism was reported to be hydrophobic inclusion by the β-CD cavity. Hence, the average substitution degree of CM-β-CD should be considered as a factor that can alter the host-guest interactions and the adsorption of OMPs.

The effect of pH on the reactivity of CM-β-CD (sd:3) for noncovalent interactions was investigated using the MESP analysis. Figure 4-7 shows the electrostatic surface potential maps of CM-β-CD (sd:3) and Si-CM-β-CD (sd:3) in their neutral states and where one of the -COOH groups is deprotonated. Based on the MESP analysis, the presence of negatively charged $-COO^-$ groups increased the presence of electron-rich regions as anticipated for CM-β-CD (sd:3) and Si-CM-β-CD (sd:3). Hence, the

deprotonation of free -COOH groups changed the reactivity of the adsorption site indicating attraction toward positively charged compounds at around neutral pH.

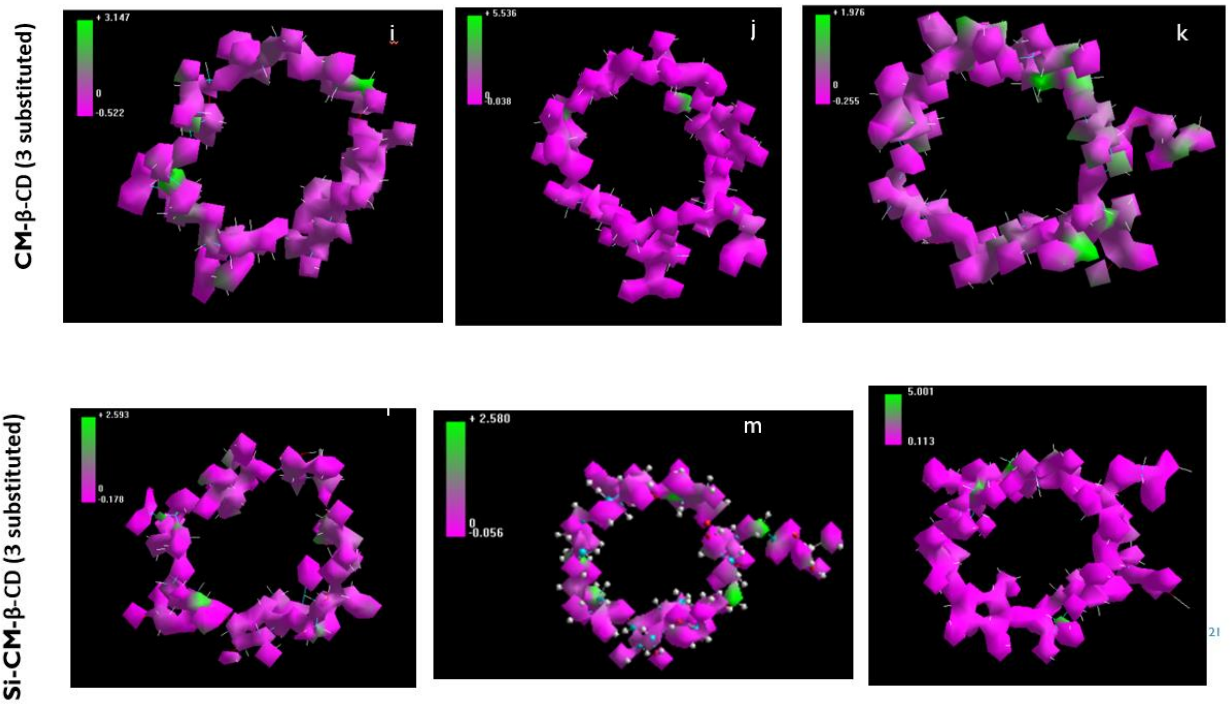

Figure 4-7: The molecular electrostatic surface potential of 3 substituted CM-β-CD derivatives. Upper row: CM-β-CD Lower row: Si-CM-β-CD. The molecular structures from left to right: deprotonated state (pH<5), neutral state (pH> 5), and in the presence of magnesium ion (pH<5).

The results of the MESP analysis were reviewed based on the experimental results of the current study and the literature. In the previously described adsorption tests ibuprofen did not adsorb significantly to the CM-β-CD functionalized magnetic nano adsorbent at neutral pH and this was initially attributed to the negative charge on the ibuprofen. Based on the MESP analysis, the altered reactivity due to the presence of free -COOH groups significantly reduced the complexation at pH higher than the pKa of ibuprofen. On the other hand, in a study where a citric crosslinked β-CD functionalized adsorbent was employed for the adsorption of methylene blue, the adsorption capacity was decreased at low pH due to protonation of the free -COOH groups that were identified via XPS analysis [37]. In this regard, MESP analysis can help understand the effect of pH on the adsorption of OMPs when there are functional groups on the grafting agent that can be ionized.

The effect of the presence of cations on the reactivity of CM-β-CD (sd:3) was also investigated as it was anticipated to impact the host-guest interactions. Figure 4-6 shows the electrostatic surface potential maps of CM-β-CD (sd:3) and Si-CM-β-CD (sd:3) where one of the -COOH groups is attached to a calcium ion at around neutral pH. The electrostatic potential maps show that the presence of calcium increased the presence of electron-deficient regions indicating the potential host-guest complexation with negatively charged OMPs would be enhanced. In this regard, the enhanced adsorption of ibuprofen in the presence of calcium ions in the current study was attributed to the increased surface charge density in the bulk phase. The MESP analysis reveals that the complexation of calcium ion with the negatively charged free -COO^- groups can decrease the repulsion between the adsorption site and ibuprofen around neutral pH which supported the experimental data. Hence, the investigation of β-CD via MESP analysis assisted in understanding the chemistry behind the effect of cations on the adsorption of OMPs which depend on the ionizable groups on the grafting agent.

The literature was reviewed to understand the relationship between the effect of the cations on the adsorption and the use of different grafting agents. It was found that the studies that observed negligible impacts of cations on the adsorption employed aromatic-rigid crosslinkers (TFTPN) [53][32][72]. The negligible effect can be due to the absence of functional groups that can complex or interact with Ca^{+2}. However, the impact of cations on adsorption where grafting agents or crosslinkers that had ionizable functional groups such as carboxymethyl or citric acid has not been reported [37]. While there is limited information in the literature, the MESP analysis helped to clarify that the impact of the cations on the adsorption of OMPs will depend on the presence of ionizable functional groups on the grafting agent.

The reactivity of β-CD derivatives with different types of grafting agents was investigated to understand their impact on potential host-guest interactions. Figure 4-8 shows the electrostatic surface potential of three different grafting agents attached to β-CD. The number of substitution degree was limited to 1 to prevent any effects from additional substitutions that might not be attached to the surface of the adsorbent. Figure 4-8 shows that MDE-β-CD and DFB-β-CD provided more positively charged (electron deficient) regions on the β-CD cavity when compared to the CM-β-CD. The use of DFB-β-CD as a crosslinker has been reported to enhance the adsorption capacity of negatively charged PFASs [115]. The combination of increased positively charged regions on the cavity due to aromatic rings in DFB-β-CD would be expected to reduce repulsion or even promote the attraction of the negatively charged PFAS. Similarly, MDE-β-CD with the amine moiety has been reported for adsorption of negatively charged naproxen around neutral pH [24]. Hence, the employment of these grafting agents

can enhance the adsorption of negatively charged species of ibuprofen. The results revealed that the MESP analysis can assist in understanding the potential alterations in the host-guest complexations that would occur when the type of the grafting agents changes and could be employed prior to experimental studies when developing β-CD functionalized adsorbents.

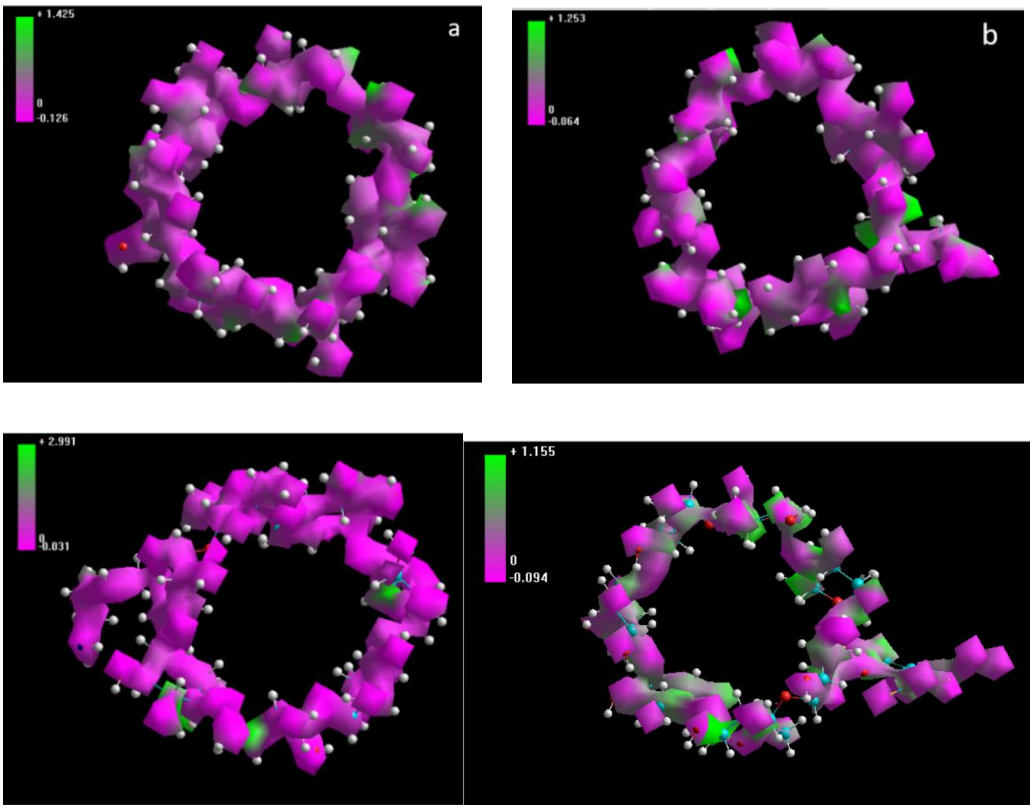

Figure 4-8: The molecular electrostatic surface potential maps of a) β-CD b) CM-β-CD c) MDE-β-CD d) DFB-β-CD

4.2.2. Molecular dynamics simulation

The impact of the grafting agents on the stability of the host-guest complexes was investigated using molecular dynamics simulations to gain insight into the competition between the OMPs. For this purpose, ibuprofen and procaine were selected as the two guest molecules that have different charge states at neutral pH. Table 4-1 shows the complexation energies of the corresponding host-guest complexes of ibuprofen and procaine. The contributions of Van der Waals and electrostatic potential energy components of each molecule (i.e., host, guest, and complexes) are summarized in Appendix C. The MD simulations showed that the ibuprofen complex with EDB-β-CD (29 kcal/mol) and DFB-β-CD (7kcal/mol) was more stable when compared to CM-β-CD (54.9 kcal/mol) and this differed from

procaine complexation that had lower complexation energy with CM-β-CD (-60 kcal/mol) than EDB-β-CD (12.8 kcal/mol) and DFB-β-CD (-5.2 kcal/mol). The change in complex stabilities as determined by MD was consistent with the differing electrostatic surface potentials as discussed by MESP analysis.

Table 4-1: $\Delta E_{complexation}$ (kcal/mol) of the corresponding host-guest complexes

	Ibuprofen	Procaine
β-CD	-24.7	-35.2
CM-β-CD	54.9	-60
EDB-β-CD	29	12.8
DFB-β-CD	7	-5.2

The results were further investigated to understand the differences between the ibuprofen complexes of EDB-β-CD and DFB-β-CD. MD simulations revealed that the ibuprofen complex with DFB-β-CD (7 kcal/mol) provided a lower complex energy than EDB-β-CD (29 kcal/mol) (Table 4-2). The results show that the presence of the aromatic rings (DFB-β-CD) can be more effective than the presence of an amine functionality (EDB-β-CD) on the grafting agent for enhanced adsorption of ibuprofen. Therefore, MD simulations can be employed to evaluate the impact of the type of grafting agents on the intermolecular interactions that can be complementary to the results of the MESP analysis.

The results were reviewed to identify factors that led to a more stable DFB-β-CD complex of procaine (-5 kcal/mol) when compared to ibuprofen (7 kcal/mol). For this purpose, the effect of the aromatic ring on the host-guest interactions via π-π interactions was investigated [116]. The conformation of the complexes after the MD simulation revealed that the distance between the closest carbon atom on the aromatic ring of the host molecule and the procaine was 3.27 Å while the distance between the closest carbon atom on the aromatic ring of the host molecule and ibuprofen was 4.75 Å (Appendix C). Based on the results, the lower complex energy of procaine in the presence of the aromatic ring bearing grafting agent was attributed to the electrostatic interactions arising from the geometry of the host-guest complexes. Hence, molecular dynamics simulations can be employed for the investigation of specific intermolecular interactions that can impact the host-guest complexation of the OMPs with β-CD functionalized adsorbents.

The stability of the host complexes was investigated to gain insight into the competition between the OMPs for the β-CD FMNP employed in the current study [92]-[95]. Table 4-2 shows the complexation energies of the target guests with β-CD derivatives that represented the different grafting stages of β-CD to the model adsorbent. The contributions of Van der Waals and electrostatic potential energy components of each molecule (i.e., host, guest and complexes) are summarized in Appendix C. The results show that procaine yielded the most stable complex which is consistent with those of the MESP analysis as positively charged OMPs was attracted more around the neutral pH when compared to the negatively charged ones. The competition between the OMPs is discussed subsequently with respect to their physicochemical properties (i.e., hydrophobicity and molecular geometry).

Table 4-2: $\Delta E_{complexation}$ (kcal/mol) of the host-guest complexes

	Ibuprofen	Procaine	Sulfamethoxazole	Naproxen	Fulvic acid
β-CD	-24.7	-35.2	-32.1	-24.5	-26.1
CM-β-CD	54.9	-60	79.9	65.6	75.3
Si-CM-β-CD	25.9	-75.9	6.5	22	32.5

The impact of the hydrophobicity of guest molecules on the stability of the host-guest complexes was investigated. For this purpose, the complex stability of ibuprofen and procaine was compared as their hydrophobicity changes with the solution pH. The LogDow value of ibuprofen is 0.5 while procaine has a LogDow value of 0.3 hence, it was anticipated that the more hydrophobic compound would result in a more stable complex. However, the results showed that (Table 4-2) procaine has a more stable complex (-60 kcal/mol) with CM-β-CD and Si-CM-β-CD (-75.9 kcal/mol) when compared to ibuprofen (54.9 kcal/mol and 25.9 kcal/mol respectively). In addition, the stability of the ibuprofen-β-CD complex was decreased while the procaine-β-CD complex was increased when β-CD was modified to CM-β-CD and Si-CM-β-CD. This was attributed to the charge state of the host and guest molecules although the inclusion mechanism was responsible for the complexation due to hydrophobic aromatic rings. MD simulations showed that the adsorption did not depend solely on the hydrophobicity of the guest molecules and the adsorption was impacted by the electrostatic interactions.

The impact of the molecular geometry of the guest molecules on the stability of the host-guest complexation was investigated. For this purpose, naproxen and sulfamethoxazole complexes were

compared as it was anticipated that naproxen would yield a more stable complex due to the planar geometry when compared (Table 4-2) to sulfamethoxazole that has a bent geometry based on the results of the previous experiments. However, it was found that naproxen had a more stable complex with only CM-β-CD when compared to sulfamethoxazole. A prior study showed reduced adsorption capacity of (bent geometry) bisphenol-S and bisphenol-F when compared to slightly nonplanar bisphenol-A which employed a graphene oxide nanocomposite [36]. In the prior study, the β-CDs were grafted onto a surface via a short-chain grafting agent similar to the EDB-β-CD and β-CD FMNP discussed in the current study [36],[45], [69]. The structures of these adsorbents suggest that there might be a steric hindrance when the host molecules are attached to the surface, which might result in reduced available space for the movement of the guest molecules while the aromatic rings reside inside the β-CD cavity. Hence, the results suggest that the impact of the molecular geometry of the target pharmaceuticals might differ when compared to the MD studies.

The complexation of fulvic acid with β-CD derivatives was investigated due to its potential for being a competitor to the adsorption of the target OMPs. This is the first reported use of MD simulations to characterize the competition between fulvic acid and OMP for the native β-CD. Table 4-3 shows that fulvic acid had a lower complexation energy (-26.1 kcal/mol) than ibuprofen (-24.7 kcal/mol) for β-CD, hence it was speculated that fulvic acid would compete with ibuprofen for the β-CD cavity. However, the stability of the fulvic acid complexes changed when the β-CD was modified to CM-β-CD and Si-CM-β-CD. In this regard, fulvic acid had a lower complex energy (75.3 kcal/mol) than sulfamethoxazole (79.9) with CM-β-CD while it might not compete with the OMPs when Si-CM-β-CD was employed. The negligible impact of fulvic acid on the adsorption of bisphenol-A was attributed to additional electrostatic interactions with quaternary ammonium groups [53]. Similarly, MD simulation shows that the competition by the fulvic acid will depend on the modifications on the β-CD. Hence, additional insights can be obtained with MD when compared to MESP analysis as it provides the differences between the complexes of OMPs for the same host and can be employed to evaluate the competitive adsorption between the OMPs.

4.2.3. Conclusions

Molecular simulations were employed to investigate the intermolecular interactions between target pharmaceuticals and β-CD derivatives. While the MESP analysis provided information on the reactivity of the β-CD via their electronic structure, MD provided information on the stability of the

host-guest complexes. Ultimately, this study compiled a series of simulation steps to investigate the adsorption of OMPs. Based on the results;

- MESP analysis showed that the substitution degree of β-CD should be considered as a factor for the development of β-CD functionalized adsorbents.
- MESP analysis also showed that the effects of pH and the presence of the cations will depend on the functional groups on the grafting agents that can ionize.
- MD simulations revealed that grafting agents with aromatic rings can provide additional electrostatic interactions due to the geometry of the host-guest complexes.
- The competition between the OMPs will depend on their charge state and molecular geometry.
- Fulvic acid was shown to compete for the β-CD cavity while the competition depends on the modification on the β-CD

Molecular simulations can be employed as a strategic tool for the development of β-CD functionalized adsorbents and could be useful for future studies;

- to enhance the adsorption for OMPs that have low affinity for the β-CD functionalized adsorbents by exploring different grafting agents.
- to assess the adsorption of metabolites, enantiomers or other type of compounds that are difficult to examine experimentally prior to experimental investigation of a model β-CD functionalized adsorbent.

Chapter 5

Evaluation of HGMS for capture and recovery of β-CD functionalized magnetic nanoadsorbent

5.1. Abstract

In this study, a bench-scale high gradient magnetic separator (HGMS) was assessed for the capture and recovery of a novel β-CD functionalized magnetic-nano adsorbent. The use of turbidity as a process monitoring parameter to quantify the mass of nanoparticles in the HGMS system was assessed. A multi-layer steel wool placement was able to increase the nanoparticle capture efficiency from 30 % to 98 %, compared to a typical matrix arrangement. On the other hand, the recovery efficiency decreased and this was attributed to the residual magnetization of the steel wool. The evaluation of common factors (i.e., external magnetic field, flow type, and flow velocity) revealed that flow velocity and external magnetic field were significant factors impacting capture and recovery efficiency. A 90% capture efficiency of the nano adsorbent was achieved at 2T and 0.22 mL/s. The HGMS process selectively captured and recovered larger particles, which led to smaller particles left in the effluent and the recovered solution. The results provide guidance for the design and operation of lab-scale HGMS systems that could be employed for the pre-concentration of OMPs as part of the workflow associated with OMP analysis.

5.2. Introduction

Magnetic nano adsorbents have been considered attractive for their ability to separate easily from the adsorption medium [117]-[123]. A number of β-CD functionalized magnetic nano adsorbents have been reported for the adsorption of a range of organic micropollutants (OMPs) [24], [36], [41], [43], [44]. The separation of these adsorbents has been achieved via magnetic decantation by permanent magnets, allowing reuse in further adsorption cycles after the desorption of OMPs [24], [36]. While adsorption properties make them promising for environmental applications, the potential for the development of lab-scale analytical applications for OMPs that take advantage of magnetic properties has not been investigated yet.

The current analytical methods (i.e., LC/MS-MS) for the OMPs that are present at low concentrations (i.e., pharmaceuticals) in the environment usually require pre-treatment techniques to

enhance the concentration of OMPs prior to analysis [72][79]. These techniques usually involve extraction and drying steps which are time-consuming [72][79]. Magnetic β-CD functionalized nanoparticles could be employed as adsorbents to pre-concentrate the OMPs and can potentially require simpler analytical methods (i.e., HPLC, UV-fluorescence). However, efficient separation techniques are needed for the capture and recovery of β-CD functionalized magnetic nano adsorbents from aqueous samples [24], [36].

High Gradient Magnetic Separator (HGMS) has been employed for the separation of magnetic nanoparticles (MNPs) from the aqueous medium [131] [133]. A typical HGMS system typically consists of permanent magnets that provide an adjustable external magnetic field and a chamber where a magnetically impacted matrix (i.e., steel wool) is placed [126], [128], [129]. Figure 5-1 describes the capture operation in a bench scale HGMS where the MNPs are captured onto the matrix from the solution by the applied external magnetic field. [130]-[132]. When the external magnetic field is removed, the captured MNPs are released and potentially can be recovered via washing with a solvent. The performance of HGMS systems has been estimated by quantifying the capture and recovery efficiencies of the MNPs [123]. Although it is a promising technique, HGMS has not been evaluated for the capture and recovery of β-CD functionalized magnetic nano adsorbents

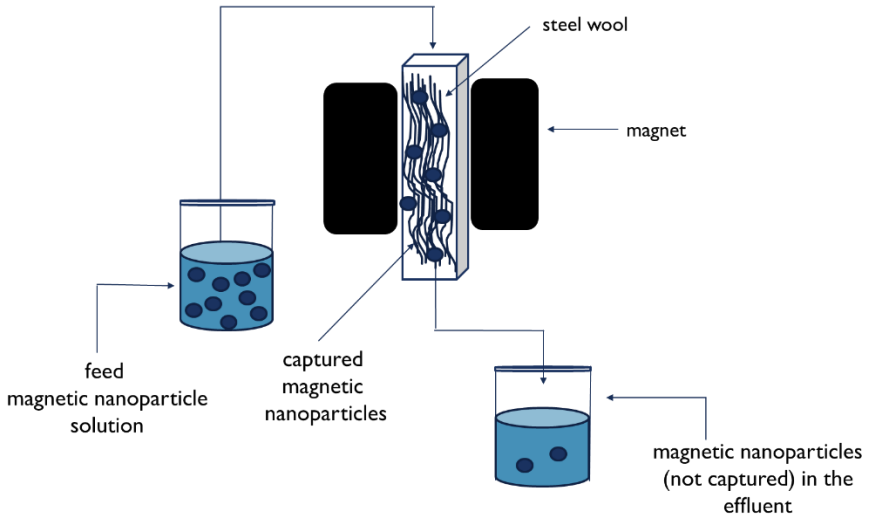

Figure 5-1: Capture operation in a bench-scale High Gradient Magnetic Separator

Quantification of the capture and recovery efficiencies in HGMS systems has been achieved by tracking the mass of MNPs in the streams entering and leaving. Gravimetric methods have been commonly employed to determine the mass of MNPs in the discharge of the HGMS or in the recovery solution where the MNPs are collected. The method includes drying the samples and gravimetrically weighing the MNPs [118]-[123], [126], [127], [131], [133], [134]. UV-VIS and ICP-OES methods have been reported as alternatives to the gravimetric method for the determination of the mass of MNP (i.e., Fe_3O_4) by its concentration [119], [126]. However, current analytical methods are impractical for regular monitoring of MNPs as gravimetric methods are time-consuming while the alternatives (i.e., UV-VIS, ICP-OES) are expensive [120], [126]. Therefore, fast, reliable, and cost-effective methods that can be employed for a range of adsorbent types are required to characterize the performance of HGMS in practice.

The use of turbidity measurements is a potential approach for quantifying MNPs in a fast, reliable and cost-effective way. Turbidity measures the light scattering of a solution containing suspended and colloidal particles and the extent of scattering has been found to depend on the particle size and shape [135], [136], [138]. In this regard, particles that have a spherical shape and size between 0.3 to 0.7 mm demonstrated more symmetrical scattering and hence more reproducible turbidity data, when compared to other types of particles [135]. Therefore, it is anticipated that for an MNP solution with these physical properties a relationship between mass-based concentrations and turbidity values can be obtained. If feasible, turbidity would be an attractive method for quantifying the mass of MNPs entering and leaving HGMS systems.

The magnetic separation of MNPs depends on the magnetic force (F_m) exerted by the magnetic field on the particle. The magnetic force acting on a particle is described by Equation 5-1;

$$F_m = \mu_0 V_p M_p \nabla \mathrm{H} \qquad (5\text{-}1)$$

where F_m is the magnetic force (N), μ_0 is the vacuum permeability constant (N/A^2), V_p is the particle volume (m^3), M_p is the magnetization of the particles (A/m^2), and H is the magnetic field at the location of the particle (A/m) [128] [130]. Based on Equation 5-1, the presence of a high external magnetic field, large particle sizes and high particle magnetization will lead to a larger magnetic force acting on the particle and, as a result, enhance capture efficiencies in HGMS systems [118], [119], [121], [133] [139].

Although a high external magnetic field has provided enhanced capture efficiency in experimental studies, it has been found that this has caused the recovery efficiency to decrease [119]-[122]. This was attributed to the residual magnetization that result in the continuation of interactions between the matrix and the MNPs and the presence of large aggregates that influenced the movement of particles during the recovery [118], [124], [126]. Therefore, the conditions that are established in the capture process can affect recovery efficiency.

Particle size impacts the capture of the MNPs based on Eq 5-1 due to increased magnetic force exerted on the particle. However, solutions of engineered MNPs typically contain a range of particle sizes [128], [129], [131]. The size distribution of particles present in HGMS discharge and recovery solutions may differ from the initial size distribution if there is preferential capture or recovery. This can potentially impact the adsorption capacity in consecutive cycles of adsorption which has not been assessed in HGMS systems. Hence, the potential for change in size distribution through the HGMS should be examined to better understand the impact of HGMS on the long-term adsorption performance of the magnetic nanoparticles.

The capture of the MNPs occurs when the magnetic force exerted by the magnetic field overcomes the other forces on the particle while an external magnetic field is being applied. Figure 5-2 illustrates the magnetic force (F_m), the fluid drag force (F_d) and, the gravitational force (F_g) [140]. Therefore, a large magnetic force is desired for the capture of the MNPs. As the magnetic force is relaxed during the recovery of MNPs, it can be anticipated that the recovery of the particles is more likely to be related to fluid movement. However, several subjects have been identified as gaps that require further investigation which has been explained subsequently.

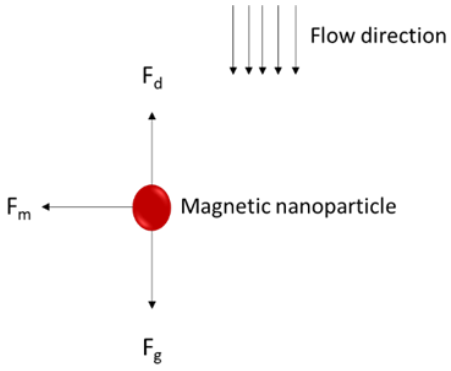

Figure 5-2: Major forces acting on a particle in HGMS chamber when the external magnetic field is applied

The flow direction can impact the capture and the recovery of the MNPs as the forces acting on a particle would presumably change based on Figure 5-2. Upward flow direction has been employed for the capture of MNPs and recovery has typically been the opposite of that employed for capture (down) [118], [120], [121], [122], [127]. However, the reason for these selections has not been discussed in the literature. Overall, the impact of flow direction on capture and recovery efficiencies has not been investigated in detail in the literature.

The flow velocity has been investigated in a limited number of studies to understand its impact on the capture and recovery efficiency of MNPs. It was found that decreasing flow velocity has enhanced the capture efficiency [119]-[122]. This was attributed to the longer interaction times of the MNPs with the magnetically impacted material. On the other hand, the impact of flow velocity on recovery has not been usually investigated although the recovery has been reported to be more related to flow characteristics [128], [129], [141]. Hence, further investigation is needed on this subject

Steel wool has been the most common matrix employed in HGMS systems as it can be placed in different designs of HGMS chambers due to being flexible and inexpensive [117], [123], [142]. Steel wool has usually been packed in the columns or wrapped around metal plates in HGMS systems, however, steel wool does not have a fixed geometry and its arrangement can be impacted by its placement which can result in short-circuiting that leads to reduced interaction between the steel wool and the particles [126], [130], [141]. The placement of multiple layers of matrices has been suggested to provide a more ordered arrangement and prevent problems related to agglomeration [130]. While layers of steel discs have been employed in HGMS designs for protein recovery applications, the placement of steel wool has not been explored for the characterization of HGMS performance.

The tangled geometry of the steel wool has been reported to induce an increased magnetic gradient when compared to other matrices such as steel rods or grooved plates which has provided enhanced capture [130], [142]. However, the recovery efficiency was reduced by 30% in the presence of the steel wool due to residual magnetization or agglomeration of MNPs [94][90]. This resulted in the need for frequent replacement of the matrix in HGMS systems and the MNPs in the system [90], [94], [117]. The recovery of MNPs for reuse may enhance the sustainability of adsorption processes hence the placement of steel wool requires further investigation [130].

In this study, the use of a bench scale HGMS was evaluated for the capture and recovery of a model β-CD functionalized magnetic nano adsorbent that could be employed to preconcentrate

pharmaceuticals [45]. The use of turbidity as a process monitoring parameter to quantify the mass of MNPs in process streams was assessed. The impact of external magnetic field strength, flow direction, and velocity on capture and recovery efficiencies was investigated. Furthermore, the effect of the steel wool arrangement on capture and recovery was assessed. The impact of HGMS processing on MNP size distribution was examined to obtain insights into the effect of HGMS on the reuse of the model adsorbent. The results of this study provide guidance for the design and operation of lab-scale HGMS systems that can be employed for the separation of β-CD functionalized magnetic nano adsorbents as part of the workflow associated with OMP analysis.

5.3. Methods

5.3.1. Development of turbidity-based calibration curves for FMNP concentrations

A HACH 2100Q model turbidimeter was employed for turbidity measurements. Calibration was performed with formazine standards (10/20/100/400/800 NTU) and was verified prior to each set of measurements with the 20 NTU standard. A 10 ± 0.1 NTU formazine standard was used as an additional quality control check solution prior to measurement.

To develop a turbidity calibration curve for MNPs, a solution containing model β-CD MNP was synthesized following the procedure provided in Appendix D [45]. A stock slurry of β-CD FMNP (1000 mg/L) was diluted by 50% to generate a solution with a turbidity of less than 800 NTU which was the upper limit of the measurement range of the turbidimeter. It was anticipated that turbidity of the effluent after the capture would potentially require lower turbidity measurements when compared to the original β-CD FMNP solution turbidity. Similarly, the turbidity of the recovered β-CD FMNP solution was expected to be relatively higher and similar to the feed β-CD FMNP solution. Hence, two sets of calibration standards were prepared for the measurement of turbidity after capture (low range: 2-10 mg/L) and recovery (high range: 10-500 mg/L).

The β-CD FMNP solutions were prepared by diluting the secondary stock β-CD FMNP solution (500 mg/L) in 50 ml HDPE bottles with MQ water to a final volume of 50 mL. Each FMNP calibration standard was prepared in triplicate. The method detection limits are provided in Appendix D which were calculated by measuring the turbidity of the lowest FMNP calibration standard in seven replicates in both ranges.

Gravimetric analysis was performed to validate the performance of the calibration curve for turbidity. For this purpose, 100 mg/L FMNP solutions were run through HGMS (0.5 g steel wool as 1 horizontal layer, 2T, 0.44 mL/s, downflow) in triplicate. A 10 g portion of each FMNP solution was weighed and then dried at 85 °C for 24 h to obtain the mass of MNPs. The mass concentration of the particles was then calculated by the ratio of the mass of the particles to the total mass of the FMNP solution (density: 1 g/cm^3). The concentration of the nanoparticles in the HGMS effluent obtained by the gravimetric analysis was compared to that of obtained by the turbidity method statistically by t-test (two-sample assuming unequal variances) which is provided in Appendix D.

5.3.2. HGMS system

A Frantz Model L-1 bench scale HGMS with a custom stainless steel rectangular column (volume: 25 mL) was employed (Appendix D). Steel wool was employed as the magnetically impacted material inside the column. A vertical HGMS configuration was employed as it has been reported to provide more contact availability of the magnetized matrix when compared to horizontal configuration [118]-[123], [126].

A longitudinal steel wool placement (Figure 5-3) was compared to several multiple-layer placement configuration to assess the impact of the matrix placement on capture and recovery efficiency. One rectangular piece with a mass of 1.5 g was placed in a longitudinal arrangement (parallel to the flow) inside the HGMS column in the first configuration and 1 (0.5 g), 3 (1.5 g) and 6 layers of (3 g) steel wool with open space between the layers (perpendicular to the flow) were employed for the multiple layer configurations. The thickness of the steel wool for both configurations was the same and large enough to prevent movement of the steel wool inside the column. The capture and recovery efficiencies were investigated at the highest magnetic field strength available in the HGMS system (2T)

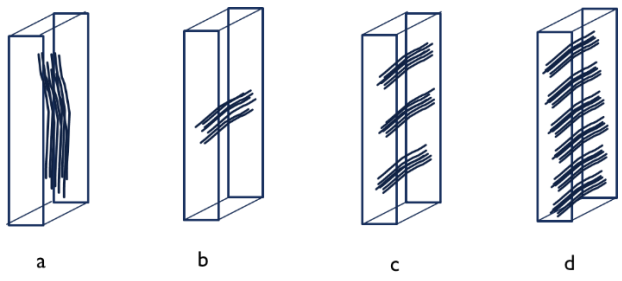

Figure 5-3: Steel wool placement configurations (a) Longitudinal 1.5 g and multiple layer placement of steel wool b) 1 layer 0.5 g, c) 3 layers 1.5 g (each layer: 0.5 g), c) 6 layers 3 g (each layer: 0.5 g)

The impacts of flow type, flow velocity and external magnetic field on the capture and recovery efficiency were assessed with a horizontal steel wool placement (0.5 g steel wool), using a reduced factorial experimental design (3 factors with two levels). The impact of the external magnetic field was investigated to assess the magnetic properties of β-CD FMNP with respect to capture and recovery. A field of 2 T was selected to provide maximum capture efficiency as the highest external magnetic field that can be employed in this system. A field of 0.5 T was also investigated as low external magnetic fields were desired for reduced energy consumption and for preventing heat caused by the magnets based on the literature [126]. An external magnetic field lower than 0.5 T was not investigated as the purification step in the synthesis of β-CD FMNP was conducted at 0.5 T [45].

Up-flow and down-flow configurations were assessed to understand the impact of flow direction on the capture and recovery of β-CD FMNP. In the downflow configuration, the feed β-CD FMNP solution was introduced from the top of the HGMS column while the external magnetic field was being applied and the entire volume of the solution was collected from the outlet of the HGMS column. In the up-flow configuration, the solution was introduced into the HGMS column from the bottom of the column that was modified with a plastic stopper to prevent drainage of water from the column. Sufficient MQ water was passed through the column until the same volume of feed solution (50 mL) was collected from the outlet. The same procedures described for the capture of the β-CD FMNP were followed for the recovery of β-CD FMNP with MQ water to collect the β-CD FMNP with respect to flow directions.

The impact of flow velocity was investigated to gain insight into its impact on the recovery of the β-CD FMNP. This was achieved via adjusting the flow to 0.44 mL/s and 0.22 mL/s in both up and down flow configurations. The same procedure described in the assessment of flow direction was employed to capture and recover the β-CD FMNP.

5.3.3. Capture and recovery of β-CD FMNPs

To evaluate the HGMS performance,100 mg/L β-CD FMNP feed solution was prepared as duplicates via volumetric dilution from the stock (1000 mg/L) β-CD FMNP to a volume of 50 mL MQ water. β-CD FMNP feed solutions were run through HGMS at the target conditions by a peristaltic pump. The effluent was collected into a beaker from the outlet of HGMS (50 mL). The turbidity of these solutions was measured directly after the HGMS run. Triplicate measurements from the same sample were performed to characterize analytical uncertainty.

The mass-based concentrations of the feed and effluent solutions were calculated on the basis of measured turbidity values and using the corresponding calibration curves. The mass of β-CD FMNPs captured via the HGMS process was calculated as described in Equation 5-2:

$$M_C = M_I - M_E \quad (5\text{-}2)$$

where M_I is the initial mass of MNPs introduced to the HGMS system, M_E is the mass of MNPs found in the effluent after passing through HGMS and M_C is the mass of β-CD FMNPs trapped inside the HGMS chamber. M_I and M_E were calculated by using the feed volume and the effluent volume which were 50 ml. The capture efficiency was then calculated as described in Equation 5-3:

$$Capture\ efficiency\ \% = \frac{M_C}{M_I} \times 100 \quad (5\text{-}3)$$

Recovery efficiency was calculated as described in Equation 5-4:

$$Recovery\ efficiency, \% = \frac{M_R}{M_I} \times 100 \quad (5\text{-}4)$$

where M_R is the mass of released β-CD FMNPs that were measured in the eluent (50 mL) that was generated by the washing step.

5.3.4. The effect of HGMS on the size distribution

Triplicate measurements of the Z-size distribution of FMNPs in samples from the inlet, effluent and eluent solutions were analyzed using a Nanosizer ZS (Malvern Co., UK). For this purpose, 3 mL samples were drawn from the solutions and placed in the analyzer's quartz cell prior to analysis. The mean particle size from the measurements was assessed to quantify the change in size distribution through the HGMS and thereby gain insight into the selective capture and recovery of FMNPs in the HGMS system. The instrument's analytics (i.e., polydispersity index and particle count) were examined to verify that the presence of substances other than the nanoparticles did not impact the particle size distribution.

5.4. Results and discussion

5.4.1. Relationship between the concentration and the turbidity of β-CD FMNP

Calibration curves of different batches of β-CD FMNPs were created to assess the feasibility of turbidity as a method for estimating the concentration of β-CD FMNPs. The observed turbidity values

are presented versus the β-CD FMNP concentrations in Figure 5-4 for the two concentration ranges. Linear relationships between turbidity and particle concentration were obtained with R^2 values of at least 0.99, and 0.99 for the low and high concentration ranges, respectively. The linear results indicate that turbidity can be employed to estimate mass-based concentrations of the model β-CD FMNP in adsorption/recovery systems.

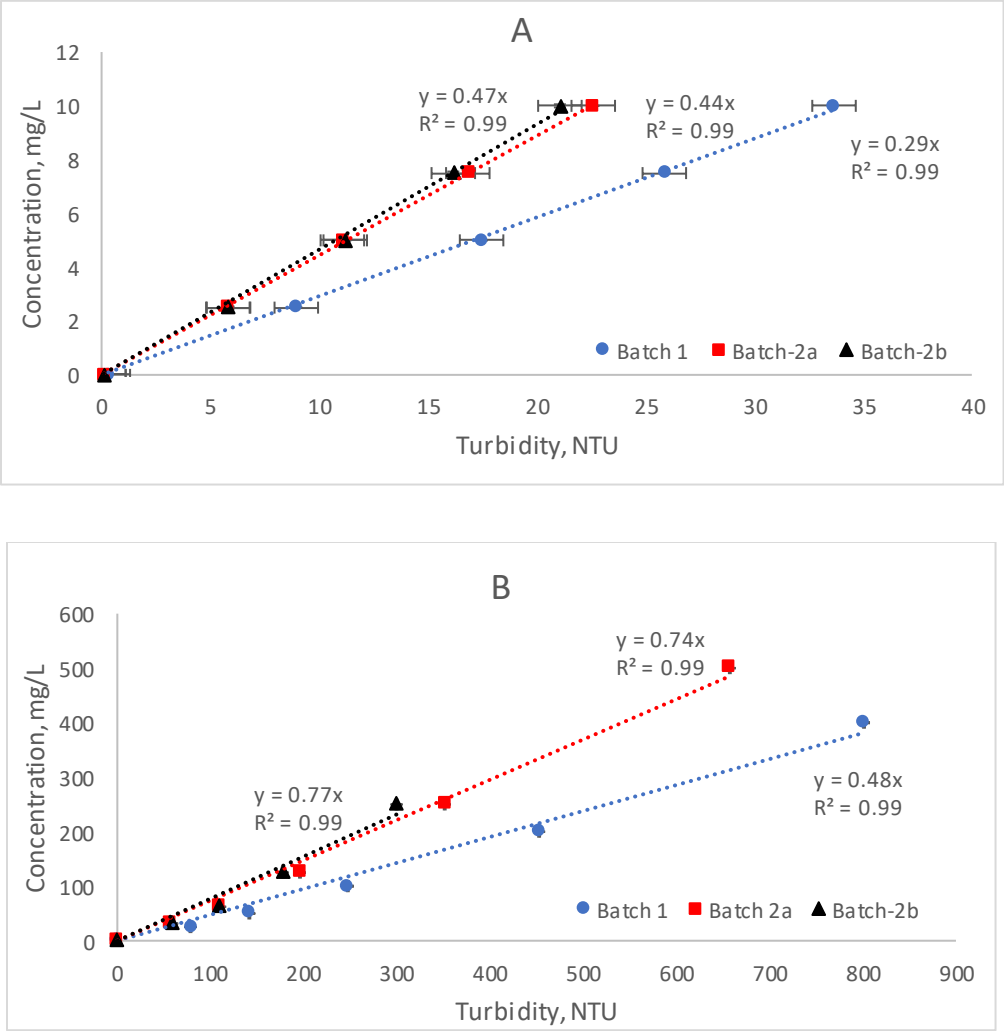

Figure 5-4: Correlation between turbidity and particle concentration A) low range B) high range (Batch 1 and Batch 2 represent nanogel batch, Batch 2 a and b represent same nanogel and separate synthesis of magnetic nanoparticle)

The calibration curves that were obtained from different batches of β-CD FMNPs were compared to assess the reproducibility of the results. From Figure 5-4 it can be seen that the calibration curves of β-CD FMNP that were synthesized from different nanogel batches (Batch 1 and Batch 2) had different

slopes implying that the light scattering properties differed based on the nanogel characteristics. In contrast, β-CD FMNP that were prepared from the same nanogel (Batch 2a and 2b) but separate synthesis steps (MNP synthesis, silica coating and β-CD grafting) had similar slopes (Figure 5-4). The nanogel synthesis step provided the backbone of the adsorbent, and establishes the size of the subsequent β-CD FMNPs [45]. It was hypothesized that the different calibration curves may have been due to differences in the particle sizes between the different nanogel batches.

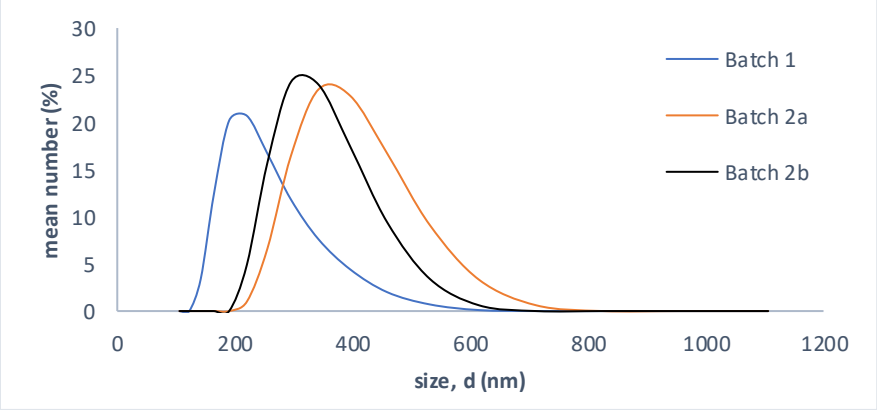

Figure 5-5: Particle size distribution of MNPs (Batch 1 and Batch 2: FMNP from different nanogel batch, Batch 2a and Batch 2b: separate synthesis steps after nanogel synthesis including MNP, silica coating, β-CD grafting steps

The size distribution of the particles was investigated to assess whether differences in this property were responsible for the different calibration curves. Figure 5-5 presents the particle size distribution for MNPs as number density (X-axis) from each size population (Y-axis) present in the mixture. Batch 1 has an average size of 170 nm while Batch 2a has 360 nm and Batch 2b has 310 nm. Therefore, the differences in turbidity between the two different batches of β-CD FMNP were attributed to the size distribution of the particles due to the nanogel synthesis. It was concluded that turbidity can be used for quantifying β-CD FMNP concentrations however there needs to be good quality control in the synthesis of the β-CD FMNPs such that consistent particle size distributions are produced. In the subsequent analysis of β-CD FMNP capture and recovery efficiencies, the calibration curves from the same batch of particles were employed as those used in the process testing to quantify the mass of particles.

The light scattering properties of a nanoparticle solution can be altered after the HGMS run if there is preferential capture which could change the size distribution of the particles. Hence, for an HGMS

effluent which was obtained by running 100 mg/L feed FMNP solution in the HGMS, the use of turbidity and concentration relationship was verified by gravimetric analysis. Based on the turbidity method and gravimetric analysis, the FMNP concentration in the HGMS effluent was 55.7 ± 0.9 mg/L and 57.1 ± 0.9 mg/L, respectively. Statistical analysis showed that the difference between the two methods was not statistically significant ($p>0.05$) (Appendix D). Therefore, the turbidity method was employed to determine the mass of nanoparticles throughout the HGMS system.

5.4.2. Evaluation of the capture and recovery efficiency of β-CD FMNP

The impact of steel wool placement configuration on the capture and recovery of the particles was assessed. Figure 5-6 shows these responses for the different arrangements (a-d). It was found that the capture efficiency was improved when the steel wool placement was changed to horizontal layers while the recovery decreased. The results are discussed subsequently.

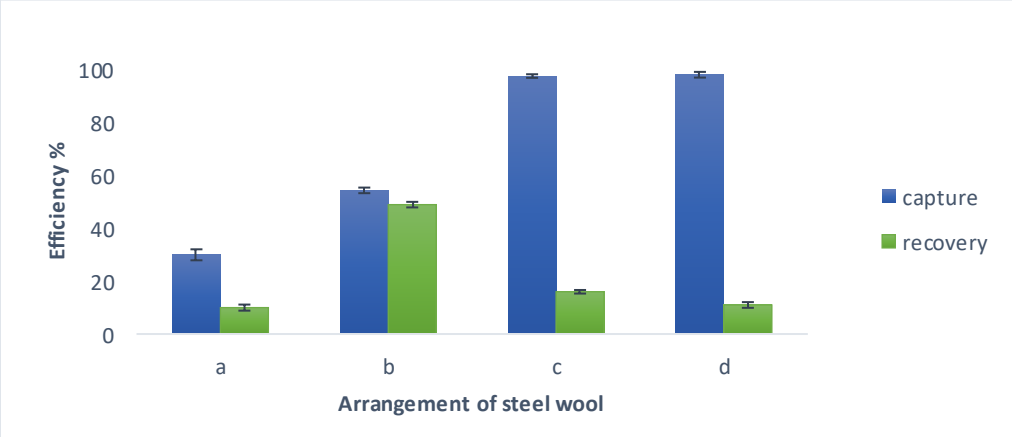

Figure 5-6: Capture and recovery efficiency of β-CD FMNP by the different configurations of steel wool arrangement. a) 1.5 g longitudinal b) 0.5g 1layer c) 1.5 g 3layer g d) 3.0g 6 layer

The impact of the matrix placement on the capture efficiency was investigated. The lowest capture efficiency (30%) was obtained with the longitudinal arrangement (1.5 g) and this was attributed to short-circuiting of the flow where the steel wool and the magnetic particles did not properly interact. The properties of steel wool make it difficult to completely eliminate short-circuiting due to the random geometry [130]. The results were consistent with prior studies that reported the nonuniform distribution due to the geometry of the matrix could be a potential cause for the low capture efficiency [130], [142]. The superiority of the horizontal configuration was indicated by the improved capture efficiency (54%) when considerably less steel wool (0.5 g) was employed in configuration (b). The enhanced capture

efficiency by the horizontal arrangement was attributed to a more uniformly distributed matrix inside the column.

The impact of employing multiple layers in a horizontal configuration on capture efficiency was assessed. The capture efficiency was increased to 98% (c) while maintaining the same mass of steel wool to that of the longitudinal configuration (a) in Figure 5-6. The better capture properties of layered steel wool configuration were attributed to the enhanced interactions between the steel wool and the particles due to uniformly distributed horizontal layers. However, increasing the mass of steel wool (3 g) and number of layers (6) beyond that of configuration (c) did not enhance capture efficiency. The results suggest that once sufficient layers and mass of steel wool were present the capture of FMNPs became limited by other factors that were not investigated in this study.

The impact of the matrix placement on recovery efficiency was also investigated as particle recovery was deemed to be an important feature of a system that would be used in an analytical workflow. The longitudinal arrangement of steel wool (a) resulted in poor particle recovery (10%) however, it was recognized that this configuration also yielded relatively low capture efficiency when compared to other arrangements (b, c and d). Hence, the recovery efficiency was limited by the poor capture conditions. When the steel wool placement was changed to horizontal layer arrangement (b), the highest recovery efficiency among all configurations (49%) was achieved. This was attributed to the decreased potential for residual magnetization due to the decreased mass of steel wool.

The impact of employing multiple layers of steel wool on the recovery of the particles was assessed. It was found that the recovery efficiency was reduced from 49% to 16% when the number of layers increased from 1 (b) to 3 (c) and further reduced to 11% when the number of steel wool layers was increased from 3 (c) to 6 (d) The results are consistent with prior reports that have indicated that the residual magnetization of steel wool which would increase with steel wool mass can cause difficulties in recovering particles [90], [94], [130]. This is further indicated where the matrix placement was altered from longitudinal (a) to horizontal placement (c) with the same mass of steel wool (1.5 g). The recovery efficiency did not change significantly and remained low despite the increase in capture efficiency (c) which can be attributed to the effect of residual magnetization by the same mass of steel wool. The results indicate that multiple layers of steel wool cause more particles to continue to interact with the matrix due to the residual magnetization hence reducing the recovery efficiency when compared to the lower mass of steel wool.

The impact of the external magnetic field, flow type and flow velocity on capture were investigated to identify preferred operating conditions for the system. Table 5-1 shows the capture efficiency in different operating conditions obtained by one horizontal layer (0.5 g) of steel wool. Maximum capture efficiency of 90 % was achieved by up flow configuration where 2 T and 0.22 mL/s were employed for the magnetic field strength and flow velocity respectively (Table 5-1). The effect of the operating conditions on the capture of the particles is discussed subsequently.

Table 5-1: Capture efficiency of β-CD FMNP with 1 layer (0.5 g) of steel wool

	0.5T		2T	
	0.44 mL/s	0.22 mL/s	0.44 ml/s	0.22 mL/s
Down flow	50%	83%	60%	88%
Up-flow	52%	85%	75%	90 %

The effect of the external magnetic field on particle capture was investigated. A high external magnetic field (2 T) yielded better capture efficiencies in each condition. The effect of the external magnetic field is consistent with the literature and Eq (5-1) where a larger magnetic force was exerted on the particles. However, employing a relatively low external magnetic field (0.5T) did not result in a significant decrease in the capture efficiency with low flow velocity (0.22 mL/s) condition. The results show that low external magnetic fields can be achieved by employing conditions that enhance the interactions of particles with steel wool (i.e., flow velocity) in the HGMS system. This can be advantageous in lab-scale applications of HGMS as low external magnetic fields are desired for reduced energy consumption and for preventing heat caused by the magnets [126].

The effect of flow velocity on particle capture was assessed. Low flow velocity (0.22 mL/s) provided better capture efficiencies when compared to high flow velocity (0.44 mL/s) in all conditions. This was attributed to the enhanced interaction of FMNPs with the steel wool. The results suggest that flow velocity is a significant factor as an operating condition in the HGMS system for capture when the steel wool is employed as the magnetically susceptible matrix. This might be due to the tangled geometry of steel wool and low flow velocities might be required for improved particle capture in scale lab-scale HGMS systems.

The effect of flow direction on particle capture was examined. It was found that the flow direction did not have a significant impact on the capture efficiencies except for one condition. At the high external magnetic field (2 T) and high flow velocity (0.44 mL/s), the capture efficiency increased from 60% to 75% when the flow direction was changed from downflow to flow up-flow configuration. This

might be due to more contact availability of the magnetized matrix in up flow configuration when compared to the downflow configuration which overcame the negative effect of high flow velocity on particle capture. Hence, up flow configuration enhanced the interactions between the steel wool and the particles in this condition.

The impact of the external magnetic field, flow velocity and flow type on the recovery of the particles was also investigated. Overall, moderate recovery efficiencies were obtained at the different operational conditions (Table 5-2). While capture efficiency has been commonly reported in the literature, this study showed that recovery efficiency was also impacted by the conditions established for FMNP capture. The effect of these capture operating conditions on the subsequent recovery efficiencies of the particles is discussed subsequently.

Table 5-2: Recovery efficiency of β-CD FMNP with 1 layer (0.5 g) of steel wool

	2 T		0.5 T	
	0.44 mL/s	0.22 mL/s	0.44 mL/s	0.22 mL/s
Down flow	45%	50%	42%	49%
Up-flow	30%	43%	32%	40%

The effect of residual magnetization on the recovery of the particles was investigated. It should be noted that the external magnetic field conditions reflect the capture conditions and the external magnetic field was turned off during recovery. However, it was anticipated that the effect of residual magnetization might change depending on the magnitude of the external magnetic field employed in the capture operation. It was found that the residual magnetization did not significantly impact the recovery efficiencies obtained at 2 T and 0.5 T at the same flow velocity and flow direction. This was attributed to the low mass of the steel wool layer (0.5 g) employed which was previously discussed.

The impact of flow velocity on the recovery of the particles was investigated. Low flow velocity (0.22 mL/s) provided better recovery efficiencies for all conditions when compared to high flow velocity (0.44 mL/s). The largest increase in the recovery efficiency (30% to 43%) was observed when the flow velocity was changed from 0.44 mL/s to 0.22 mL/s in up flow configuration. The effect was attributed to the enhanced movement of the particles inside the column due to low flow velocity which was consistent with the literature [112]. Based on the observed results, the flow velocity can be used to manipulate the recovery of the particles where efficient recovery of the particles is needed depending on the application of HGMS.

The up flow and downflow configurations were compared to understand the impact of the flow direction on the particle recovery. Up-flow configuration provided lower recovery efficiencies when compared to downflow configuration. When the external magnetic field is not present, the magnetic force on the particle is removed and the movement of the particle depends on the fluid drag force and the gravitational force acting on the particle (Figure 5-2). In the up-flow direction, the drag force and gravitational force will collectively reduce the movement of the particles. The issue of agglomeration of the particles has also been reported in the literature and might be enhanced in the up-flow configuration. Hence, the moderate decrease in the recovery efficiencies was attributed to the forces acting on the particles in the up-flow configuration.

5.4.3. The impact of HGMS on the size distribution of β-CD FMNP

The impact of HGMS on the size distribution of the β-CD FMNP was investigated to gain insight into the selectivity of capture. Figure 5-7 shows the size distribution of the β-CD FMNPs in the effluent of HGMS configurations that had 1 and 6 layers of steel wool over a range of operating conditions. From Figure 5-8 it can be seen that there was a consistent shift in the size distribution towards smaller particles when compared to the feed solution. The results showed that the size distribution in the HGMS effluent was impacted by operating conditions and the significance of this is discussed subsequently.

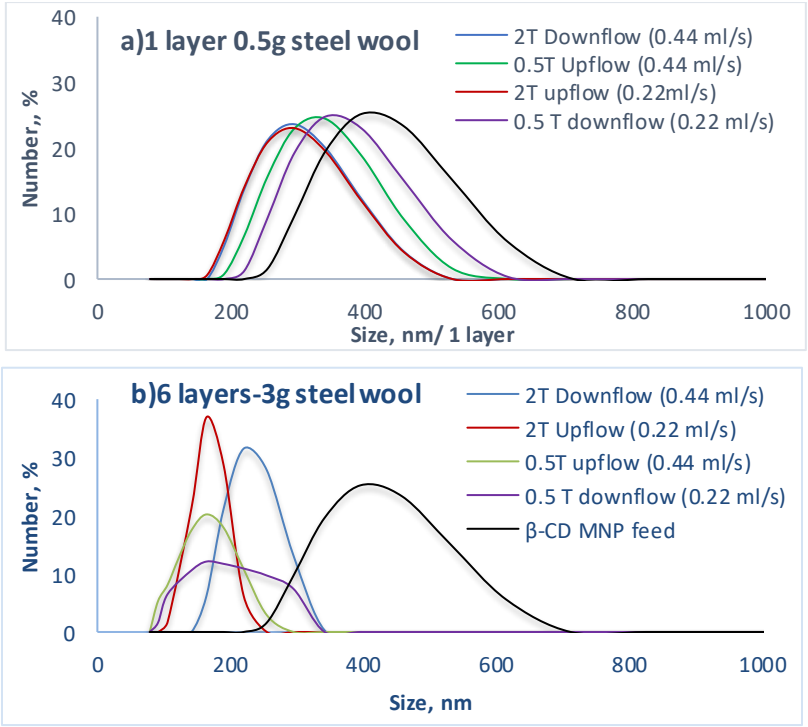

Figure 5-7: Size distribution of β-CD FMNP in HGMS effluent, steel wool: a) 1 layer b) 6 layers

The effect of HGMS conditions run on the particle size distribution in the effluent was examined as it provided insight into the distribution of particle sizes that were captured. It was found that the largest shift (400 nm to 161 nm) in the size distribution of the FMNPs was obtained with low flow velocity (0.22 mL/s). When the flow velocity is lower, it appears that the larger particles have enhanced interactions with the steel wool leaving the smaller particles in the discharge. Similarly, a high external magnetic field (2T) resulted in larger particles to be captured consistently. This was due to the higher magnetic force exerted on larger particles (Eq 5-1) hence, smaller particles remain in the discharge. The results show that the conditions that provided better capture efficiencies preferentially captured larger particles from the feed solution.

The impact of the mass of steel wool in the HGMS on the size distribution was also investigated. It was observed that increased mass (3 g) and layers of steel wool (6 layers) resulted in the capture of larger particles consistently. This was attributed to the preferential capture of larger size particles with increasing mass of steel wool in the HGMS according to Eq 5-1, and hence smaller particles contributed a larger fraction of those in the HGMS discharge. Based on the observed results, the placement of steel wool can also be used to manipulate the size distribution of the particles in the HGMS discharge based on the desired application.

The effect of HGMS conditions on the size distribution of the β-CD FMNP after recovery was also investigated. Figure 5-8 shows the number density-based size distribution of the β-CD FMNP for the various configurations and operating conditions. From Figure 5-9, it can be seen that the size distribution of the recovered β-CD FMNP was similar to that of the feed solution. It was previously found that there was selective capture of larger particles by the HGMS. Hence the similar distribution of recovered particles to the feed distribution in both 1 layer (0.5g) and 6 layer (3g) suggests that a greater number of larger size particles must have remained in the HGMS during the recovery operation.

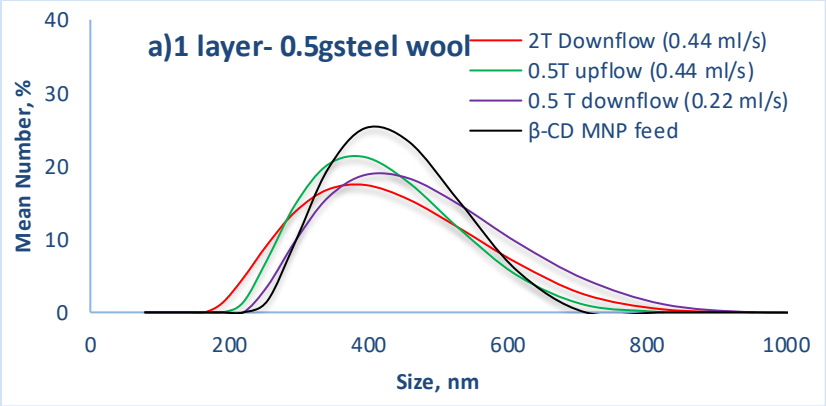

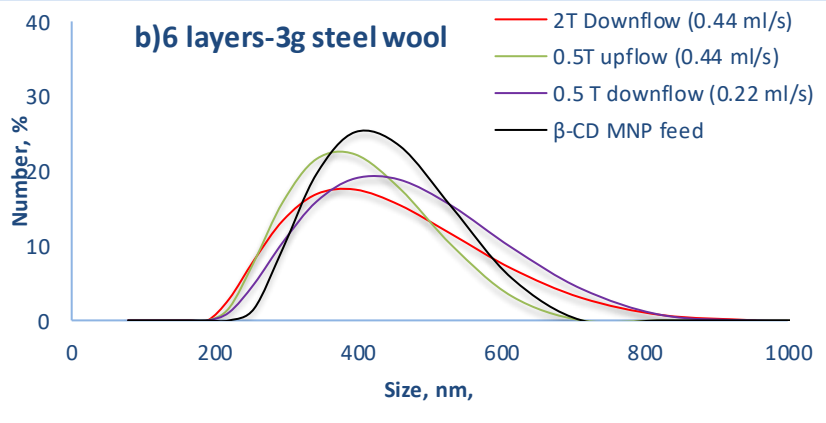

Figure 5-8: The size distribution of the β-CD FMNP after recovery a) 1 layer of 0.5 g steel wool b) 6 layers of 3 g steel wool (Legend entries describe capture conditions prior to recovery)

The impact of operational conditions on the size distribution of the particles was investigated. It should be noted that the legends describe the conditions that were set for the capture of the particles. It was found that the average particle size decreased when the flow velocity was changed from 0.22 mL/s to 0.44 mL/s consistently. The high flow velocity (0.44 mL/s) employed in the capture operation resulted in decreased capture efficiencies and less change in the size distribution of the particles in the discharge when compared to the low flow velocity (0.22 mL/s). Hence, the fraction of the particles trapped inside the HGMS column during the capture operation involved larger particles at high flow velocity. However, high flow velocity also yielded lower recovery efficiencies. In this regard, the results show that the reduced interaction of particles at high flow velocity during the recovery operation resulted in the recovery of smaller particles. As a result, the average size of the particles was reduced and the size distribution shifted to the left. Hence, the conditions employed in HGMS for recovery impacted the size distribution of the particles recovered.

To conclude, high capture efficiency was obtained with the HGMS showing that the system can be designed as a small-scale pretreatment method for concentrating OMPs as the OMPs can be desorbed while the 98% of the particles are trapped inside the HGMS column when the external magnetic field is on. The effect of HGMS treatment on the size distribution of particles might be a limitation for certain applications such as reuse in adsorption as it might influence the adsorption capacity in the long-term utilization of the particles. However, the selective capture of larger particles by the HGMS system can be advantageous for some applications such as the lab scale preconcentration method which could enhance the performance of the method. Further, the operational conditions investigated in the HGMS system provided moderate recovery efficiencies, hence improvements in this regard are needed to enhance the potential application of HGMS for lab-scale analytical methods.

5.5. Conclusions

This study evaluated a bench-scale HGMS for the capture and recovery of a novel β-CD functionalized magnetic nano adsorbent. Based on the results;

- Turbidity was successfully employed as a method to track the mass of the β-CD FMNPs in the HGMS system and to quantify the performance of the HGMS system.
- Matrix placement was shown to impact the capture and recovery efficiency. Multi-layer placement provided enhanced capture however the increased residual magnetization decreased the recovery efficiency.
- The external magnetic field and the flow velocity were the significant factors impacting the capture and recovery of the β-CD FMNPs.
- The impact of HGMS on the size distribution of a novel β-CD functionalized adsorbent was shown. It was found that the capture and recovery of β-CD FMNPs occur selectively where the capture of larger particles was promoted in HGMS with the conditions that provide higher capture efficiencies.
- The HGMS system attained high capture efficiencies of FMNPs (98%) and hence might be employed to pre-concentrate the OMPs as part of a sample preparation method prior to their analysis. However, an improvement in the recovery of the particles will be required to make this feasible.

Chapter 6

Conclusions and recommendations

6.1. Conclusions

This research established knowledge on the adsorption of selected pharmaceuticals from water by a novel β-CD functionalized magnetic nanoadsorbent. Helped to understand the underlying mechanism of adsorption. From this research, the following conclusions were made:

The partitioning was significantly impacted by the solution pH and the presence of calcium ions. Partitioning was enhanced in the presence of divalent cations indicating that the surface characteristics of nanocomposites with respect to the modifications on β-CD should be investigated in detail. The assessment of target pharmaceuticals as a mixture at environmentally relevant concentrations showed that the molecular geometries of the pharmaceuticals influence partitioning where nonplanar molecular geometry is favored. It was concluded that assessing host-guest complexation at the molecular level is important to gain insight into the fundamentals of the partitioning onto the β-CD functionalized adsorbents.

Although the literature suggested that β-CD functionalized adsorbents can be employed for a wide range of OMP types, the adsorption mechanism is complex as the noncovalent interactions are difficult to examine experimentally. Molecular simulations were used to investigate the factors impacting the host-guest interactions that are difficult to assess by experimental techniques. MESP analysis assisted understanding the reaction mechanism that takes place during the grafting of β-CD onto nanocomposite structures and the effect of grafting on the reactivity in terms of noncovalent interactions with OMPs in host-guest complexation. Furthermore, molecular dynamics simulations assisted in evaluating the competition between the target pharmaceuticals. The complexation of common organic competitors such as fulvic acid with β-CD functionalized adsorbents was demonstrated. Further, specific noncovalent interactions between the host and guest molecules were successfully demonstrated. Insights on this subject are valuable as this technique can enhance the investigation of different types of OMPs when evaluating novel β-CD functionalized adsorbents prior to experimental studies and can guide future environmental applications of β-CD functionalized adsorbents.

The reusability of the β-CD functionalized magnetic nanoadsorbent was reported in the literature however, techniques that allow sequential capture and recovery are needed. Hence, the use of a high

gradient magnetic separator was evaluated for the capture and recovery of the novel β-CD functionalized magnetic nanoadsorbent. An analytical method based on turbidity was demonstrated for quantification of HGMS performance which can enhance the application of magnetic β-CD functionalized adsorbents as a fast and reliable tool. A multi-layer arrangement of steel wool provided better capture of the particles and should be employed in future lab-scale applications of HGMS. Investigation of operational conditions showed that flow velocity is the most important condition that can be employed to manipulate the capture and recovery efficiency based on the desired application. The size distribution of the particles after the HGMs run showed that selective capture and recovery occurs which could be an advantage for employing HGMS as an analytical tool to preconcentrate pharmaceuticals.

6.2. Recommendations

The following recommendations are suggested for future studies of β-CD functionalized adsorbents;

- β-CD has chiral recognition abilities as it has been employed in separation technologies however, it is not known how this ability will impact the adsorption of chiral pharmaceuticals or other types of OMPs. Hence, there is a need for investigation of this subject with β-CD functionalized adsorbents. This issue can also be assessed via computational chemistry tools.

- QSAR studies can enhance the application of β-CD functionalized adsorbents. It is desirable to predict the behavior of a wide range of organic contaminants that may be present in water. Quantitative structure-activity relationships (QSARs) can be useful in this regard, as key physicochemical properties of OMPs can be estimated via molecular descriptors and can then be related to adsorption properties. The development of such QSARs for additional β-CD adsorbents and OMPs would support and enhance their use in water treatment applications.

- Exploring the relationship between the reaction equilibrium at the molecular level and the equilibrium in the bulk solution can potentially provide insights into the adsorption parameters obtained from the isotherm models based on the theory behind adsorption. The development of such techniques can improve the application of β-CD functionalized adsorbents.

References

[1] S. Kleywegt *et al.*, "Pharmaceuticals, hormones and bisphenol A in untreated source and finished drinking water in Ontario, Canada — Occurrence and treatment efficiency," *Sci. Total Environ.*, vol. 409, pp. 1481–1488, Mar. 2011.

[2] Y. Yang, Y. S. Ok, K. H. Kim, E. E. Kwon, and Y. F. Tsang, "Occurrences and removal of pharmaceuticals and personal care products (PPCPs) in drinking water and water/sewage treatment plants: A review," *Sci. Total Environ.*, vol. 596–597, pp. 303–320, Oct. 2017.

[3] Y. Luo *et al.*, "A review on the occurrence of micropollutants in the aquatic environment and their fate and removal during wastewater treatment," *Sci. Total Environ.*, vol. 473-474, pp. 619-641, Mar. 2014.

[4] L. Lishman *et al.*, "Occurrence and reductions of pharmaceuticals and personal care products and estrogens by municipal wastewater treatment plants in Ontario, Canada," *Sci. Total Environ.*, vol. 367, pp. 544–558, May 2006.

[5] B. Petrie, R. Barden, and B. Kasprzyk-Hordern, "A review on emerging contaminants in wastewaters and the environment: Current knowledge, understudied areas and recommendations for future monitoring," *Water Res.*, vol. 72, pp. 3-27, Apr. 2015.

[6] D. J. Lapworth, N. Baran, M. E. Stuart, and R. S. Ward, "Emerging organic contaminants in groundwater: A review of sources, fate and occurrence," *Environ. Pollut.*, vol. 163, pp. 287–303, Apr. 2012.

[7] C. Su, Y. Cui, D. Liu, H. Zhang, and Y. Baninla, "Endocrine disrupting compounds, pharmaceuticals and personal care products in the aquatic environment of China: Which chemicals are the prioritized ones?," *Sci. Total Environ.*, vol. 720, p. 137652, June 2020.

[8] A. Gogoi, P. Mazumder, V. K. Tyagi, G. G. Tushara Chaminda, A. K. An, and M. Kumar, "Occurrence and fate of emerging contaminants in water environment: A review," *Groundw. Sustain. Dev.*, vol. 6, pp. 169–180, Jan. 2018.

[9] J. F. Shaheen, B. Sizirici, and I. Yildiz, "Fate, transport, and risk assessment of widely prescribed pharmaceuticals in terrestrial and aquatic systems: A review," *Emerg. Contam.*, vol. 8, pp. 216–228, Jan. 2022.

[10] Y. Yang *et al.*, "Which Micropollutants in Water Environments Deserve More Attention Globally?," *Environ. Sci. Technol.*, vol. 56, pp. 13–29, Jan. 2022.

[11] O. M. Rodriguez-Narvaez, J. M. Peralta-Hernandez, A. Goonetilleke, and E. R. Bandala, "Treatment technologies for emerging contaminants in water: A review," *Chem. Eng. J.*, vol. 323, pp. 361–380, Sept. 2017.

[12] E. N. Evgenidou, I. K. Konstantinou, and D. A. Lambropoulou, "Occurrence and removal of transformation products of PPCPs and illicit drugs in wastewaters: A review," *Science of the Total Environment*, vol. 505, pp. 905–926, Feb. 2015.

[13] P. Y. Nguyen, G. Carvalho, M. A. M. Reis, and A. Oehmen, "A review of the biotransformations of priority pharmaceuticals in biological wastewater treatment processes," *Water Res.*, vol. 188,

p. 116446, Jan. 2021.

[14] M. S. Diniz *et al.*, "Ecotoxicity of ketoprofen, diclofenac, atenolol and their photolysis byproducts in zebrafish (Danio rerio)," *Sci. Total Environ.*, vol. 505, pp. 282–289, Feb. 2015.

[15] C. Sophia A. and E. C. Lima, "Removal of emerging contaminants from the environment by adsorption," *Ecotoxicol. Environ. Saf.*, vol. 150, pp. 1–17, Apr. 2018.

[16] C. Santhosh, V. Velmurugan, G. Jacob, S. K. Jeong, A. Nirmala Grace, and A. Bhatnagar, "Role of nanomaterials in water treatment applications: A review," *Chem. Eng. J.*, vol. 306, pp. 1116-1137, Dec. 2016.

[17] Z. Cai *et al.*, "Application of nanotechnologies for removing pharmaceutically active compounds from water: development and future trends Environmental significance," *Environ. Sci.: Nano*, vol. 5, pp. 27-47, 2018,

[18] H. Dodziuk, Polymers involving cyclodextrin moieties, *Cyclodextrins and their complexes*, Wiley-VCH Verlag GmbH & Co. KGaA, pp. 65-92, 2006.

[19] Z. M. Nagy, M. Molnár, I. Fekete-Kertész, I. Molnár-Perl, É. Fenyvesi, and K. Gruiz, "Removal of emerging micropollutants from water using cyclodextrin," *Sci. Total Environ.*, vol. 485–486, pp. 711–719, July 2014.

[20] E. M. M. Del Valle, "Cyclodextrins and their uses: A review," *Process Biochem.*, vol. 39, no. 9, pp. 1033–1046, May 2004.

[21] N. Morin-Crini, P. Winterton, S. Fourmentin, L. D. Wilson, É. Fenyvesi, and G. Crini, "Water-insoluble β-cyclodextrin–epichlorohydrin polymers for removal of pollutants from aqueous solutions by sorption processes using batch studies: A review of inclusion mechanisms," *Prog. Polym. Sci.*, vol. 78, pp. 1–23, Mar. 2018.

[22] A. A. Basheer, "New generation nano-adsorbents for the removal of emerging contaminants in water," *J. Mol. Liq.*, vol. 261, pp. 583–593, July 2018.

[23] D. M. Alzate-Sánchez *et al.*, "β-Cyclodextrin Polymers on Microcrystalline Cellulose as a Granular Media for Organic Micropollutant Removal from Water," *ACS Appl. Mater. Interfaces*, vol. 11, no. 8, pp. 8089–8096, Feb. 2019.

[24] S. Ghosh, A. Z. M. Badruddoza, K. Hidajat, and M. S. Uddin, "Adsorptive removal of emerging contaminants from water using superparamagnetic Fe3O4nanoparticles bearing aminated β-cyclodextrin," *J. Environ. Chem. Eng.*, vol. 1, no. 3, pp. 122–130, Sept. 2013.

[25] S. D. Richardson and S. Y. Kimura, "Emerging environmental contaminants: Challenges facing our next generation and potential engineering solutions," *Environ. Technol. Innov.*, vol. 8, pp. 40–56, Nov. 2017.

[26] G. Chen and M. Jiang, "Cyclodextrin-based inclusion complexation bridging supramolecular chemistry and macromolecular self-assembly," *Chem. Soc. Rev.*, vol. 40, no. 5, p. 2254, Feb. 2011.

[27] M. J. Klemes *et al.*, "Water Treatment Hot Paper Reduction of aT etrafluoroterephthalonitrile-b-Cyclodextrin Polymer to Remove Anionic Micropollutants and Perfluorinated Alkyl Substances from Water." *Angew.Chem.Int.Ed.* vol. 85, pp. 12049-12053, Aug. 2019

[28] L. Xiao, Y. Ling, A. Alsbaiee, C. Li, D. E. Helbling, and W. R. Dichtel, "β-Cyclodextrin Polymer Network Sequesters Perfluorooctanoic Acid at Environmentally Relevant Concentrations," *J. Am. Chem. Soc.*, vol. 139, no. 23, pp. 7689–7692, May 2017.

[29] X. Zhang, Y. Wang, and S. Yang, "Simultaneous removal of Co(II) and 1-naphthol by core-shell structured Fe_3O_4@cyclodextrin magnetic nanoparticles," *Carbohydr. Polym.*, vol. 114, pp. 521–529, Sept. 2014.

[30] P. Kumari and H. Parashara, *Nat. Conf. on Sol. Stat. Chem.* "β-cyclodextrin modified magnetite nanoparticles for efficient removal of eosin and phloxine dyes from aqueous solution," Materials Today: Proceedings 5, 2018, pp. 15473–15480.

[31] W. Yuan, J. Shen, L. Li, X. Liu, and H. Zou, "Preparation of POSS-poly(-caprolactone)-cyclodextrin/Fe 3 O 4 hybrid magnetic micelles for removal of bisphenol A from water," *Carbohydr. Polym.*, vol. 113, pp. 353–361, July 2014.

[32] Y. Zhou, G. Cheng, K. Chen, J. Lu, J. Lei, and S. Pu, "Adsorptive removal of bisphenol A, chloroxylenol, and carbamazepine from water using a novel β-cyclodextrin polymer," *Ecotoxicol. Environ. Saf.*, vol. 170, no. 130, pp. 278–285, Apr. 2019.

[33] F. Zhao *et al.*, "One-pot synthesis of trifunctional chitosan-EDTA-β-cyclodextrin polymer for simultaneous removal of metals and organic micropollutants*." Sci Rep, vol.* 7, p. 15811 Nov. 2017.

[34] K. Cai, J. Li, Z. Luo, Y. Hu, Y. Hou, and X. Ding, "b-Cyclodextrin conjugated magnetic nanoparticles for diazepam removal from blood" *Chem. Commun*, vol. 47, p. 32, June 2011.

[35] É. Fenyvesi *et al.*, "Removal of hazardous micropollutants from treated wastewater using cyclodextrin bead polymer – A pilot demonstration case," *J. Hazard. Mater.*, vol. 383, no., p. 121181, Feb. 2020.

[36] K. V Ragavan and N. K. Rastogi, "β-Cyclodextrin capped graphene-magnetite nanocomposite for selective adsorption of Bisphenol-A," *Carbohydr. Polym.*, vol. 168, pp. 129–137, Mar. 2017.

[37] W. Huang *et al.*, "Citric acid-crosslinked β-cyclodextrin for simultaneous removal of bisphenol A, methylene blue and copper: The roles of cavity and surface functional groups," *J. Taiwan Inst. Chem. Eng.*, vol. 82, pp. 189–197, Jan. 2018.

[38] X. Jin and S. Peldszus, "Selection of representative emerging micropollutants for drinking water treatment studies: A systematic approach," *Sci. Total Environ.*, vol. 414, pp. 653–663, Dec. 2012.

[39] Y. Tu *et al.*, "Amphiphilic hyper-crosslinked porous cyclodextrin polymer with high specific surface area for rapid removal of organic micropollutants," *Chem. Eng. J.*, vol. 382, no. September 2019, p. 123015, Feb. 2020.

[40] Z. Wang *et al.*, "Hierarchically micro-mesoporous β-cyclodextrin polymers used for ultrafast removal of micropollutants from water," *Carbohydr. Polym.*, vol. 213, pp. 352–360, Mar. 2019.

[41] D. Liu, Z. Huang, M. Li, X. Li, P. Sun, and L. Zhou, "Construction of magnetic bifunctional β-cyclodextrin nanocomposites for adsorption and degradation of persistent organic pollutants," *Carbohydr. Polym.*, vol. 230, p. 115564, Feb. 2020.

[42] Z. Wang, B. Zhang, C. Fang, Z. Liu, J. Fang, and L. Zhu, "Macroporous membranes doped with

micro-mesoporous β-cyclodextrin polymers for ultrafast removal of organic micropollutants from water," *Carbohydr. Polym.*, vol. 222, p. 114970, May 2019.

[43] D. Cai, T. Zhang, F. Zhang, and X. Luo, "Quaternary ammonium β-cyclodextrin-conjugated magnetic nanoparticles as nano-adsorbents for the treatment of dyeing wastewater: Synthesis and adsorption studies," Journal of Environmental Chemical Engineering, Volume 5, Issue 3, 2017, pp 2869-2878, June 2017.

[44] L. Jiang *et al.*, "Fabrication of β-cyclodextrin/poly (L-glutamic acid) supported magnetic graphene oxide and its adsorption behavior for 17β-estradiol," *Chem. Eng. J.*, vol. 308, pp. 597–605, Jan. 2017.

[45] J. Xu, Y. Tian, Z. Li, B. H. Tan, K. Y. Tang, and K. C. Tam, "β-Cyclodextrin functionalized magnetic nanoparticles for the removal of pharmaceutical residues in drinking water," *J. Ind. Eng. Chem.*, Volume 109, pp 461-474, May 2022.

[46] J. C. G. Sousa, A. R. Ribeiro, M. O. Barbosa, M. Fernando, R. Pereira, and A. M. T. Silva, "A review on environmental monitoring of water organic pollutants identified by EU guidelines," *J. Hazard. Mater.*, vol. 344, pp. 146–162, Feb. 2018.

[47] Q. Lin, Y. Wu, X. Jiang, F. Lin, X. Liu, and B. Lu, "Removal of bisphenol A from aqueous solution via host-guest interactions based on beta-cyclodextrin grafted cellulose bead," *Int. J. Biol. Macromol.*, vol. 140, pp. 1–9, Nov. 2019.

[48] P. Tang *et al.*, "Rapid and efficient removal of estrogenic pollutants from water by using beta- and gamma-cyclodextrin polymers," *Chem. Eng. J.*, vol. 344, pp. 514–523, July 2018.

[49] A. Alsbaiee, B. J. Smith, L. Xiao, Y. Ling, D. E. Helbling, and W. R. Dichtel, "Rapid removal of organic micropollutants from water by a porous β-cyclodextrin polymer," *Nature* 529, pp 190–194, Jan. 2016.

[50] J. P. Fan *et al.*, "A novel electrospun B-CD/CS/PVA nanofiber membrane for simultaneous and rapid removal of organic micropollutants and heavy metal ions from water," *Chem. Eng. J.*, vol. 378, p. 122232, July, 2019.

[51] D. Zhao, L. Zhao, C. Zhu, Z. Tian, and X. Shen, "Synthesis and properties of water-insoluble β-cyclodextrin polymer crosslinked by citric acid with PEG-400 as modifier," *Carbohydr. Polym.*, vol. 78, pp. 125–130, Aug. 2009.

[52] H. Kono, T. Nakamura, H. Hashimoto, and Y. Shimizu, "Characterization, molecular dynamics, and encapsulation ability of β-cyclodextrin polymers crosslinked by polyethylene glycol," *Carbohydr. Polym.*, vol. 128, pp. 11–23, Sept. 2015.

[53] X. Hu *et al.*, "Multifunctional β-Cyclodextrin polymer for simultaneous removal of natural organic matter and organic micropollutants and detrimental microorganisms from water," *ACS Appl. Mater. Interfaces*, vol. 12, no. 10, pp. 12165–12175, Mar. 2020.

[54] P. Tang *et al.*, "A simple and green method to construct cyclodextrin polymer for the effective and simultaneous estrogen pollutant and metal removal," *Chem. Eng. J.*, vol. 366, pp. 598–607, Jun. 2019.

[55] A. Mohammadi and P. Veisi, "High adsorption performance of β-cyclodextrin-functionalized multi-walled carbon nanotubes for the removal of organic dyes from water and industrial wastewater," *J. Environ. Chem. Eng.*, vol. 6, pp. 4634–4643, Aug. 2018.

[56] J. Liu, Y. Yang, J. Bai, H. Wen, F. Chen, and B. Wang, "Hyper-Cross-linked Porous MoS 2 −Cyclodextrin-Polymer Frameworks: Durable Removal of Aromatic Phenolic Micropollutant from Water," *Anal. Chem.*, vol. 90., pp. 3621-3627, Feb. 2018.

[57] S. Hossein Mousavi and A. Mohammadi, "A cyclodextrin/glycine-functionalized TiO2 nanoadsorbent: Synthesis, characterization and application for the removal of organic pollutants from water and real textile wastewater," *Process Saf. Environ. Prot.*, vol. 114, pp. 1–15, Feb. 2018.

[58] Z. Yuan *et al.*, "Cyclodextrin Hydrogels: Rapid Removal of Aromatic Micropollutants and Adsorption Mechanisms," *J. Chem. Eng. Data*, vol. 65, no. 2, pp. 678–689, Jan. 2020.

[59] A. I. Schäfer *et al.*, "Poly(ether sulfone) Nanofibers Impregnated with β-Cyclodextrin for Increased Micropollutant Removal from Water," *ACS Sustain. Chem. Eng.*, vol. 6, no. 3, pp. 2942–2953, Jan. 2018.

[60] Z. Wang, P. Zhang, F. Hu, Y. crosslinked β-cyclodextrin polymer used for rapid removal of a broad-spectrum of organic micropollutants from water Zhao, and L. Zhu, "A crosslinked β-cyclodextrin polymer used for rapid removal of a broad-spectrum of organic micropollutants from water," *Carbohydr. Polym.*, vol. 177, pp. 224–231, Jul. 2017.

[61] Y. Zhou, Y. Hu, W. Huang, G. Cheng, C. Cui, and J. Lu, "A novel amphoteric B-cyclodextrin-based adsorbent for simultaneous removal of cationic/anionic dyes and bisphenol A," *Chem. Eng. J.*, vol. 341, pp. 47–57, Jun. 2018.

[62] Y. Ling, M. J. Klemes, L. Xiao, A. Alsbaiee, W. R. Dichtel, and D. E. Helbling, "Benchmarking micropollutant removal by activated carbon and porous β-cyclodextrin polymers under environmentally relevant scenarios," Environ. Sci. Technol., vol. 51, pp. 7590–7598, May 2017.

[63] J. C. Crittenden, R. R. Trussell, D. W. Hand, K. J. Howe, and G. Tchobanoglous, *MWH's Water Treatment: Principles and Design*, Third Edit. Hoboken, New Jersey: John Wiley & Sons, Inc, 2012.

[64] R. P. Schwarzenbach, P. M. Gschwend, and I. D. M., *Environmental Organic Chemistry*, Second Edi. Hoboken, New Jersey: John Wiley & Sons, Inc, 2003.

[65] H. N. Tran, S.-J. You, A. Hosseini-Bandegharaei, and H.-P. Chao, "Mistakes and inconsistencies regarding adsorption of contaminants from aqueous solutions: A critical review," *Water Res.*, vol 120, pp. 88-116, Sept. 2017.

[66] I. A. Shabtai and Y. G. Mishael, "Polycyclodextrin−Clay Composites: Regenerable Dual-Site Sorbents for Bisphenol A Removal from Treated Wastewater," *Appl. Mater. Interfaces.*, vol. 10, pp. 27088-27097 Aug. 2018.

[67] É. Fenyvesi *et al.*, "Removal of hazardous micropollutants from treated wastewater using cyclodextrin bead polymer – A pilot demonstration case," *J. Hazard. Mater.*, vol. 383, p. 121181, Feb. 2020.

[68] A. Dogan, J. Płotka-Wasylka, D. Kempińska-Kupczyk, J. Namieśnik, and A. Kot-Wasik, "Detection, identification and determination of chiral pharmaceutical residues in wastewater: Problems and challenges," *Trends Anal. Chem.*, vol. 122, Jan. 2020.

[69] S. Ghosh, A. Badruddoza, M. Uddin, and K. Hidajat, "Adsorption of chiral aromatic amino acids onto carboxymethyl-b-cyclodextrin bonded Fe_3O_4 /SiO_2 core-shell nanoparticles,"

Volume 354, pp 483-492, Feb. 2011.

[70] L.-D. Guo, Y.-Y. Song, H.-R. Yu, L.-T. Pan, and C.-J. Cheng, "Novel smart chiral magnetic microspheres for enantioselective adsorption of tryptophan enantiomers," *Appl. Surf. Sci.*, vol. 407, pp. 82–92, Jun. 2017.

[71] L. C. Schideman, V. L. Snoeyink, B. J. Mariñas, L. Ding, and C. Campos, "Application of a three-component competitive adsorption model to evaluate and optimize granular activated carbon systems," *Water Res.*, vol. 41, pp. 3289–3298, Aug. 2007.

[72] Y. Ling, M. J. Klemes, L. Xiao, A. Alsbaiee, W. R. Dichtel, and D. E. Helbling, "Benchmarking Micropollutant Removal by Activated Carbon and Porous β-Cyclodextrin Polymers under Environmentally Relevant Scenarios," *Environ. Sci. Technol.*, vol. 51, no. 13, pp. 7590–7598, May 2017.

[73] C. Wu, M. J. Klemes, B. Trang, W. R. Dichtel, and D. E. Helbling, "Exploring the factors that influence the adsorption of anionic PFAS on conventional and emerging adsorbents in aquatic matrices," *Water Res.*, vol. 182, p. 115950, Sep. 2020.

[74] A. A. Abdoh, M. B. Zughul, J. E. D. Davies, and A. A. Badwan, "Inclusion complexation of diclofenac with natural and modified cyclodextrins explored through phase solubility, 1H-NMR and molecular modeling studies," *J. Incl. Phenom. Macrocycl. Chem.*, vol. 57, pp. 503–510, Jan. 2007.

[75] S. Pereva, T. Sarafska, S. Bogdanova, and T. Spassov, "Efficiency of " cyclodextrin-ibuprofen " inclusion complex formation," *J. of Drug Delivery Sci. and Tech.*, Volume 35, pp, 34-39, Oct. 2016.

[76] C. Metcalfe, M. E. Hoque, T. Sultana, C. Murray, P. Helm, and S. Kleywegt, "Monitoring for contaminants of emerging concern in drinking water using POCIS passive samplers." *Environ. Sci.: Processes Impacts*, vol. 16, pp. 473-481, Feb. 2014,

[77] R. N. Hull, S. Kleywegt, and J. Schroeder, "Risk-based screening of selected contaminants in the Great Lakes Basin," *J. Great Lakes Res.*, vol. 41, pp. 238–245, Mar. 2015.

[78] A. A. Sandilya, U. Natarajan, and M. H. Priya, "Molecular View into the Cyclodextrin Cavity: Structure and Hydration," *ACS Omega*, vol. 5, no. 40, pp. 25655–25667, Oct. 2020.

[79] N. Srikanthan, "Analysis of temporal changes in estrogenic compounds released from municipal wastewater treatment plants.," UWSpace *.p. 122, 2019.*

[80] M. A. Brown, G. Volpe Bossa, and S. May, "Emergence of a Stern Layer from the Incorporation of Hydration Interactions into the Gouy−Chapman Model of the Electrical Double Layer," *Langmuir*, vol. 31, pp. 11477–11483, Oct. 2015.

[81] M. S. Reid, S. A. Kedzior, M. Villalobos, and E. D. Cranston, "Effect of Ionic Strength and Surface Charge Density on the Kinetics of Cellulose Nanocrystal Thin Film Swelling," *Langmuir*, vol. 33, no. 30, pp. 7403–7411, Aug. 2017.

[82] S. Pasche, J. Vo, H. J. Griesser, N. D. Spencer, and M. Textor, "Effects of Ionic Strength and Surface Charge on Protein Adsorption at PEGylated Surfaces," *J. Phys. Chem. B*, vol. 109, pp. 17545–17552, Aug. 2005.

[83] M. A. Brown, A. Goel, and Z. Abbas, "Effect of Electrolyte Concentration on the Stern Layer

Thickness at a Charged Interface," *Angew. Chemie - Int. Ed.*, vol. 55, no. 11, pp. 3790–3794, Feb. 2016.

[84] M. Kozlowska, P. Rodziewicz, and A. Kaczmarek-Kedziera, "Structural stability of diclofenac vs. inhibition activity from ab initio molecular dynamics simulations. Comparative study with ibuprofen and ketoprofen," *Struct. Chem.*, vol. 28, no. 4, pp. 999–1008, Jan. 2017.

[85] H. S. Muddana and M. K. Gilson, "Calculation of host-guest binding affinities using a quantum-mechanical energy model," *J. Chem. Theory Comput.*, vol. 8, no. 6, pp. 2023–2033, May 2012.

[86] C. N. Cavasotto, M. G. Aucar, and N. S. Adler, "Computational chemistry in drug lead discovery and design," *Int. J. Quantum Chem.*, vol. 119, no. 2, pp. 1–19, Jan. 2019.

[87] S. Genheden, A. Reymer, P. Saenz-Méndez, and L. A. Eriksson, "Chapter 1: Computational Chemistry and Molecular Modelling Basics," *Computational Tools for Chemical Biology* pp. 1–38, Oct. 2017.

[88] L. A. Felton, C. Popescu, C. Wiley, E. X. Esposito, P. Lefevre, and A. J. Hopfinger, "Experimental and Computational Studies of Physicochemical Properties Influence NSAID-Cyclodextrin Complexation," *AAPS PharmSciTech*, vol. 15, no. 4, pp. 872–881, Aug. 2014.

[89] F. B. De Sousa *et al.*, "Supramolecular complex of fluoxetine with-cyclodextrin: An experimental and theoretical study," *Int. J. Pharm.*, vol. 353, pp. 160–169, Apr. 2008.

[90] M. Jana and S. Bandyopadhyay.,"Molecular Dynamics Study of β-Cyclodextrin−Phenylalanine", *J. Phys. Chem. B*, vol. 117, pp. 9280−92, Jul. 2013,

[91] W. Khuntawee, M. Karttunen, and J. Wong-Ekkabut, "A molecular dynamics study of conformations of beta-cyclodextrin and its eight derivatives in four different solvents," *Phys. Chem. Chem. Phys.*, vol. 19, no. 35, pp. 24219–24229, Aug. 2017.

[92] L. Seridi, A. Boufelfel, and S. Soltani, "Structural, electronic and QTAIM analysis of host-guest interaction of Warfarin with β-cyclodextrin and calix[4]arene," *J. Mol. Liq.*, vol. 221, pp. 885–895, Sept. 2016.

[93] T. Simsek, S. Simsek, C. Mayer, and B. Rasulev, "Combined computational and experimental study on the inclusion complexes of β-cyclodextrin with selected food phenolic compounds," *Struct. Chem.*, vol. 30, no. 4, pp. 1395–1406, May 2019.

[94] M.J. Huang, Z. Quan, Y.M Liu, "Computational Modeling of Inclusion Complexes of β-CD.pdf." . *Int. J. Quantum Chem.*, vol. 109 (1), pp: 81–90, Aug. 2008

[95] J. Varady, X. Wu, and S. Wang, "Competitive and reversible binding of a guest molecule to its host in aqueous solution through molecular dynamics simulation: Benzyl alcohol/β-cyclodextrin system," *J. Phys. Chem. B*, vol. 106, no. 18, pp. 4863–4872, Jan. 2002.

[96] A. Badruddoza, G. Si Si Hazel, K. Hidajat, and M. Uddin, "Synthesis of carboxymethyl-Î²-cyclodextrin conjugated magnetic nano-adsorbent for removal of methylene blue," *Physicochem. Eng. Asp.*, vol. 367, pp. 85–95, Oct. 2010.

[97] T. Aree, "Supramolecular complexes of β-cyclodextrin with clomipramine and doxepin: Effect of the ring substituent and component of drugs on their inclusion topologies and structural flexibilities," *Pharmaceuticals*, vol. 13, no. 10, pp. 1–20, Sept. 2020.

[98] "HyperChem Release 7 for Windows", HyperCube Inc., Jan. 2002

[99] F. Castiglione, F. Ganazzoli, L. Malpezzi, A. Mele, W. Panzeri, and G. Raffaini, "Inclusion complexes of β-cyclodextrin with tricyclic drugs: An X-ray diffraction, NMR and molecular dynamics study," *Beilstein Journal of Organic Chemistry*, vol. 13. pp. 714–719, Apr. 2017.

[100] F. Fateminasab, A. K. Bordbar, and S. Shityakov, "Detailed chemical characterization and molecular modeling of serotonin inclusion complex with unmodified β-cyclodextrin," *Heliyon*, vol. 5, no. 4, p.1405, Apr. 2019.

[101] L. Liu *et al.*, "Molecular Electrostatic Potential: A New Tool to Predict the Lithiation Process of Organic Battery Materials," *J. Phys. Chem. Lett.*, vol. 9, no. 13, pp. 3573–3579, Jun. 2018.

[102] J. S. Murray and P. Politzer, "Molecular electrostatic potentials and noncovalent interactions," *Wiley Interdiscip. Rev. Comput. Mol. Sci.*, vol. 7, no. 6, pp. 1–10, Jul. 2017.

[103] A. Krid, L. Belkhiri, H. Allal, A. Kuznetsov, and · Abdou Boucekkine, "Host-guest binding selectivity of ethylated pillar[5]arene (EtP5A) towards octane, 1,7-octadiene, and 1,7-octadiyne: a computational investigation," *Journal of Drug Delivery Science and Technology*, vol. 1, p. 3, Jul. 2022.

[104] Z. Jia, H. Pang, · Hui Li, and X. Wang, "A density functional theory study on complexation processes and intermolecular interactions of triptycene-derived oxacalixarenes," *Theoretical Chemistry Accounts*, vol. 138, p. 113, Sept. 2019.

[105] A. S. Christensen, T. T. Kubař, Q. Cui, and M. Elstner, "Semiempirical Quantum Mechanical Methods for Noncovalent Interactions for Chemical and Biochemical Applications," *Chemical Reviews* 2016 vol. *116* (9), pp 5301-5337, Apr. 2016.

[106] R. A. Friesner *et al.*, "Glide: A New Approach for Rapid, Accurate Docking and Scoring. 1. Method and Assessment of Docking Accuracy," *J. Med. Chem.*, vol. 47, no. 7, pp. 1739–1749, Feb. 2004.

[107] A. Ferino-Pérez *et al.*, "Evaluation of the molecular inclusion process of β-hexachlorocyclohexane in cyclodextrins," *RSC Adv.*, vol. 9, no. 47, pp. 27484–27499, Sept. 2019.

[108] S. Chang, Q. Zhang, Y. Lu, S. Wu, and W. Wang, "High-efficiency and selective adsorption of organic pollutants by magnetic CoFe2O4/graphene oxide adsorbents: Experimental and molecular dynamics simulation study," *Sep. Purif. Technol.*, vol. 238, p. 116400, Sept. 2020.

[109] L. Ismahan *et al.*, "Computational study of inclusion complex of l-Glutamine/beta-Cycldextrin: Electronic and intermolecular interactions investigations," *J. Mol. Struct.*, vol. 1206, p. 127740, Apr. 2020.

[110] A. Banik, P. Gogoi, • Monali, and D. Saikia, "Interaction of naproxen with b-cyclodextrin and its derivatives/ polymer: experimental and molecular modeling studies*." J. Incl. Phenom. Macrocycl. Chem.*, vol. 72, pp. 449–458, Apr. 2012

[111] M. Lu, Q. Bin Lu, and J. F. Honek, "Squarate-based carbocyclic nucleosides: Syntheses, computational analyses and anticancer/antiviral evaluation," *Bioorg. Med. Chem. Lett.*, vol. 27, no. 2, pp. 282–287, Jan. 2017.

[112] A. Z. M. Badruddoza, A. S. H. Tay, P. Y. Tan, K. Hidajat, and M. S. Uddin, "Carboxymethyl-

β-cyclodextrin conjugated magnetic nanoparticles as nano-adsorbents for removal of copper ions: Synthesis and adsorption studies," *J. Hazard. Mater.*, vol. 185, no. 2–3, pp. 1177–1186, Jan. 2011.

[113] A. Z. M. Badruddoza, Z. B. Z. Shawon, W. J. D. Tay, K. Hidajat, and M. S. Uddin, "Fe_3O_4/cyclodextrin polymer nanocomposites for selective heavy metals removal from industrial wastewater," *Carbohydr. Polym.*, vol. 91, no. 1, pp. 322–332, Jan. 2013.

[114] X. Wang and M. L. Brusseau, "Simultaneous Complexation of Organic Compounds and Heavy Metals by a Modified Cyclodextrin," *Environ. Sci. Technol.*, vol. 29, no. 10, pp. 2632–2635, Oct. 1995.

[115] M. J. Weiss-Errico and K. E. O'Shea, "Enhanced host–guest complexation of short chain perfluoroalkyl substances with positively charged β-cyclodextrin derivatives," *J. Incl. Phenom. Macrocycl. Chem.*, vol. 95, no. 1–2, pp. 111–117, Oct. 2019.

[116] Y. Zhao *et al.*, "Conformational Preferences of π–π Stacking Between Ligand and Protein, Analysis Derived from Crystal Structure Data Geometric Preference of π–π Interaction," *Interdiscip. Sci. – Comput. Life Sci.*, vol. 7, no. 3, pp. 211–220, Sept. 2015.

[117] A. Mudhoo and M. Sillanpää, "Magnetic nanoadsorbents for micropollutant removal in real water treatment: a review," *Environ. Chem. Lett.*, vol. 19, no. 6, pp. 4393–4413, Jul. 2021.

[118] Z. Kheshti, K. Azodi Ghajar, A. Altaee, and M. R. Kheshti, "High-Gradient Magnetic Separator (HGMS) combined with adsorption for nitrate removal from aqueous solution," *Sep. Purif. Technol.*, vol. 212, pp. 650–659, Apr. 2019.

[119] Z. Qi, T. P. Joshi, R. Liu, Y. Li, H. Liu, and J. Qu, "Adsorption combined with superconducting high gradient magnetic separation technique used for removal of arsenic and antimony," *J. Hazard. Mater.*, vol. 343, pp. 36–48, Feb. 2018.

[120] A. Nakamura, K. Sugawara, S. Nakajima, and K. Murakami, "Adsorption of Cs ions using a temperature-responsive polymer/magnetite/zeolite composite adsorbent and separation of the adsorbent from water using high-gradient magnetic separation," *Colloids Surfaces A Physicochem. Eng. Asp.*, vol. 527, pp. 63–69, Aug. 2017.

[121] Z. Kheshti, K. A. Ghajar, R. Moreno-Atanasio, F. Neville, and S. Ghasemi, "Investigating the high gradient magnetic separator function for highly efficient adsorption of lead salt onto magnetic mesoporous silica microspheres and adsorbent recycling," *Chem. Eng. Process. - Process Intensif.*, vol. 148, p. 107770, Feb. 2020.

[122] T. Sugawara, Y. Matsuura, T. Anzai, and O. Miura, "Removal of ammonia nitrogen from water by magnetic zeolite and high-gradient magnetic separation," *IEEE Trans. Appl. Supercond.*, vol. 26, no. 4, Jan. 2016.

[123] H. W. Kwon, H. P. Hong, D. W. Ha, and Y. H. Kim, "Selective Removal of Pb from Aqueous Phase by HGMS and Ion-Imprinted Magnetic Adsorbent," *IEEE Trans. Appl. Supercond.*, vol. 31, no. 5, pp. 13–16, Feb. 2021.

[124] G. Mariani, M. Fabbri, F. Negrini, and P. L. Ribani, "High-Gradient Magnetic Separation of pollutant from wastewaters using permanent magnets," *Sep. Purif. Technol.*, vol. 72, pp. 147–155, Apr. 2010.

[125] S. Mirshahghassemi, A. D. Ebner, B. Cai, and J. R. Lead, "Application of high gradient

magnetic separation for oil remediation using polymer-coated magnetic nanoparticles," *Sep. Purif. Technol.*, vol. 179, pp. 328–334, May 2017.

[126] C. D. Powell *et al.*, "Magnetic nanoparticle recovery device (MagNERD) enables application of iron oxide nanoparticles for water treatment," *J. Nanoparticle Res.*, vol. 22, no. 2, Feb. 2020.

[127] T. Anzai, Y. Matsuura, T. Sugawara, and O. Miura, "Removal of Humic Acid in Water by Rice Hull Magnetic Activated Carbon and Magnetic Separation," *IEEE Trans. Appl. Supercond.*, vol. 26, no. 4, Jan. 2016.

[128] G. D. Moeser, K. A. Roach, W. H. Green, T. A. Hatton, and P. E. Laibinis, "High-Gradient Magnetic Separation of Coated Magnetic Nanoparticles," *AIChE J.*, vol. 50, p. 2835, Oct. 2004.

[129] A. Ditsch, S. Lindenmann, P. E. Laibinis, D. I. C. Wang, and T. A. Hatton, "High-gradient magnetic separation of magnetic nanoclusters," *Ind. Eng. Chem. Res.*, vol. 44, no. 17, pp. 6824–6836, Jul. 2005.

[130] W. Ge, A. Encinas, E. Araujo, and S. Song, "Magnetic matrices used in high gradient magnetic separation (HGMS): A review," *Results Phys.*, vol. 7, pp. 4278–4286, 2017.

[131] P. Fraga García, M. Brammen, M. Wolf, S. Reinlein, M. Freiherr Von Roman, and S. Berensmeier, "High-gradient magnetic separation for technical scale protein recovery using low cost magnetic nanoparticles," *Sep. Purif. Technol.*, vol. 150, pp. 29–36, Aug. 2015.

[132] K. Menzel, J. Lindner, and H. Nirschl, "Removal of magnetite particles and lubricant contamination from viscous oil by High-Gradient magnetic separation technique," *Sep. and Purif. Tech.*, vol. 92, pp. 122-128, May 2012.

[133] M. Ebeler, F. Pilgram, T. Wellhöfer, K. Frankenfeld, and M. Franzreb, "First comprehensive view on a magnetic separation based protein purification processes: From process development to cleaning validation of a GMP-ready magnetic separator," *Eng. Life Sci.*, vol. 19, no. 8, pp. 591–601, Aug. 2019.

[134] M. Ebeler, F. Pilgram, K. Wolz, G. Grim, and M. Franzreb, "Magnetic Separation on a New Level: Characterization and Performance Prediction of a cGMP Compliant 'Rotor-Stator' High-Gradient Magnetic Separator," *Biotechnol. J.*, vol. 13, no. 2, Nov. 2018.

[135] M. Sadar, "Turbidity Standards - Technical Information Series - Booklet No. 12," *Hach Co.*, no. 12, pp. 1–18, 2003.

[136] Tchobanoglous, G., Burton, F. L., Tsuchihashi, R., & Stensel, H. D., Wastewater engineering: Treatment and resource recovery (5th ed.). Metcalf & Eddy Inc., McGraw-Hill Professional, New York, NY, 2013.

[137] C. E. Bright, S. M. Mager, and S. L. Horton, "Predicting suspended sediment concentration from nephelometric turbidity in organic-rich waters," *River Res. Appl.*, vol. 34, no. 7, pp. 640–648, Jul. 2018.

[138] C. Bright, S. Mager, and S. Horton, "Response of nephelometric turbidity to hydrodynamic particle size of fine suspended sediment," *Int. J. Sediment Res.*, vol. 35, no. 5, pp. 444–454, Oct. 2020.

[139] G. D. Moeser, K. A. Roach, W. H. Green, T. A. Hatton, and P. E. Laibinis, "High-gradient magnetic separation of coated magnetic nanoparticles," *AIChE J.*, vol. 50, no. 11, pp. 2835–

2848, Oct. 2004.

[140] J. Ku, J. Xia, J. Li, X. Peng, B. Guo, and H. Ran, “Accurate calculation of major forces acting on magnetic particles in a high-gradient magnetic field: A 3D finite element analysis,” *Powder Technol.*, vol. 394, pp. 767–774, Dec. 2021.

[141] J. Liu, F. Wang, J. Chen, L. Xu, and Q. Cao, “Insights into the effect of magnetic interactions on the magnetization process of matrices in high gradient magnetic separation,” *Miner. Eng.*, vol. 174, p. 107269, Dec. 2021.

[142] X. Zheng, Z. Xue, Y. Wang, G. Zhu, D. Lu, and X. Li, “Modeling of particle capture in high gradient magnetic separation: A review,” *Powder Technol.*, vol. 352, pp. 159–169, Jun. 2019.

Appendices

Appendix A

Table 1: Summary of studies that evaluated adsorption kinetics of β-CD adsorbents.

Type	Ref.	Configuration	Contaminant Type	Initial Concentration (mg/L)	Rate constant, k_2 ((g/mg.min).10^2)	Equilibrium Time, t (min)
Polymer	* [37]	Cross-linked	Bisphenol-A	100	265.0	240
			Methylene Blue		772.0	30
	* [32]	Cross-linked	Bisphenol-A	50	0.7	60
			Chloroxylenol		0.6	
			Carbamazepine		3.0	
	*[48]	Cross-linked	E2	17.64	5.3	10
			EE2	11.85	5.9	
			Bisphenol-A	22.8	12.4	
	*[49]	Cross-linked	Bisphenol-A	22.8	150.0	10
	[60]	Cross-linked	Bisphenol-A	22.8	5.7	10
	[33]	Cross-linked	Bisphenol-S	25	0.6	180
			Ciprofloxacin		0.5	
			Procaine		0.6	
			Imipramine		0.3	
	*[40]	Hierarchically micro-mesoporous crosslinked	Bisphenol-A	22	13.4	10
				80	40.2	
				15	388.0	
			Propranolol HCl	25.9	387.0	
			2-napthol	14.4	392.0	
			2,4 dichlorophenol	16.3	366.0	
	[39]	Hyper crosslinked porous	3-phenylphenol	17	496.0	5
			2-naphthol	14.4	1187.0	
			p-nitrophenol	13.9	170.0	
			4-chlorophenol	12.8	372.0	
	[28]	Cross-linked	Per-fluorooctanoic acid	1	4.8	810
				200	108.0	120
	[51]	Cross-linked	Aniline	54.9	NA	100
	[52]	Cross-linked	Bisphenol-A	114	2.1	120
	[56]	Hyper crosslinked porous	Bisphenol-A	22.8	8.0	20
	[54]	Cross-linked	Bisphenol-A	22.8	31.7	30
			E2	27.2	17.8	
	[53]	Cross-linked	Fulvic acid	30	48.9	10
			2-naphthol	14.41	255.6	
			2,4,6trichlorophenol	19.7	218.3	
			3-phenyl phenol	17.02	263.4	

			Bisphenol-A	22.8	161.9	
			Bisphenol-s	25	129.0	
			Humic acid	10	586.6	2.5
	* [58]	Hydrogel	Bisphenol-A	25	34.1	20
			Methylene Blue	50	46.2	10
Nanocomposite	[55]	Multiwalled carbon nanotubes	Methylene Blue	20	4.9	20
			Acid blue		9.7	20
			Methyl orange		3.0	35
			Disperse Red 1		113.1	15
	[57]	TiO_2 nanoparticle	Methylene blue	20	4.7	30
			Methyl orange		2.5	30
			Acid blue		2.9	15
			Disperse red 1		2.1	15
	[42]*	Macroporous Membrane doped with microporous β-CDP	BPA	10	2.9	120
				50	1.4	
				100	1.6	
				150	3.0	
				300	2.5	
	[24]	Magnetic	Carbamazepine	20	16.0	60
			Naproxen		26.0	120
			Bisphenol-A		105.0	40
	[36]*	Magnetic (graphene)	BPA	25	205.0	240
	[44]	Magnetic (Fe_3O_4-GO) nanosheet	Estradiol	0.8	1.3	480
				2	0.1	
	[30]	Magnetite nanoparticles	Eosin/Phloxine	Na	Na	120
	** [43]	Magnetic nanoparticles	Congo Red	200	0.03	160
	[23]	Microcrystalline cellulose	Bisphenol-A	22.8	NA	2
	** [50]	Nanofiber membrane	Bisphenol-A	22.8	201.0	1
	* [29]	Magnetic	1-naphthol	50	-	420
	* [47]	Cellulose bead	Bisphenol-A	30	0.1	360
	* [41]	Magnetic	Bisphenol-A	40	2.9	60
				60	1.6	
				80	1.4	

*Studies were conducted at ambient temperature.

** Study was conducted at 30°C

Unit of rate constants and concentrations were converted to provide consistent units for comparison

Table 2: Studies reporting adsorption isotherms for β-CD adsorbents

Type	Ref.	Adsorbent	Contaminant	Best fit isotherm	Qmax* (mg/g)	K_L* (L/mg)	n	K_f (L/g)
Polymer	[37]	Cross-linked	Bisphenol-A	Langmuir	82.9	0.06	3.7	0.4
			Methylene Blue	Sips	269.7	0.41	5.1	0.9
	[32]	Cross-linked	Bisphenol-A	Langmuir	164.4	0.03	0.5	11.8
			Chloroxylenol	Freundlich	144.1	0.03	0.5	12.52
			Carbamazepine	Freundlich	136.4	0.01	0.6	4.6
	[48]	Cross-linked	E2	Langmuir	128.4	0.20	3.3	181.9
			EE2		151.8	0.19	3.6	210.2
			Bisphenol-A		120.7	0.14	3.2	158.5
	[49]	Cross-linked	Bisphenol-A	Langmuir	88.0	0.25	-	-
	[60]	Cross-linked	Bisphenol-A	Langmuir	113.0	30.32	2.5	186.3
	[33]	Cross-linked	Bisphenol-S	Sips	49.1	0.43	Na	Na
			Ciprofloxacin		53.3	0.34	Na	Na
			Procaine		47.0	2.54	Na	Na
			Imipramine		44.3	0.77		
	[40]	Hierarchically micro-mesoporous crosslinked	Bisphenol-A	Langmuir	502.0	0.03	0.3	75.0
	[58]	Hydrogel	Bisphenol-A	Sips	32.8	84.3	4.65	0.13
			Methylene Blue		1786	62.4	7.14	6.05
	[39]	Hyper crosslinked porous	3-phenylphenol	Freundlich	503.5	61.20	0.2	525.4
			2-naphthol		340.6	43.70	0.2	346.3
			p-nitrophenol		272.1	5.40	0.3	222.3
			4-chlorophenol		253.0	9.90	0.2	226.1
	[28]	Cross-linked	PFOA	Freundlich	34.0	0.53	2.4	12.0
	[52]	Cross-linked	Bisphenol-A	Langmuir	78.5	25.0	0.4	0.6
	[56]	Hyper crosslinked porous	Bisphenol-A	Langmuir	50.25	0.56	2.5	18.4
	[53]	Cross-linked	Fulvic acid	Freundlich	166.5	0.14	3.0	35.8
			2-Naphthol		74.5	0.03	2.2	7.3
			2,4,6 trichlorophenol		108.0	0.03	2.5	12.8
			3-Phenylphenol		100.7	0.07	2.7	17.1
			Bisphenol-A		103.2	0.15	3.4	25.4
			Bisphenol-S		117.0	0.06	3.0	20.8
			Humic acid		40.0	9.37	7.5	26
	[54]	Cross-linked	Bisphenol-A	Langmuir	182.2	56.16	3.2	861.2
			E2		210.5	0.24	2.7	847.8
	[61]	Cross-linked	Bisphenol-A	Langmuir	79	32.8	2.6	12.2

Nanocomposite			Methylene Blue	Sips	394	34.7	2.9	25
			Methyl Orange	Sips	177.1	33.4	2.5	49.5
	[55]	Multiwalled carbon nanotubes	Methylene Blue	Langmuir	90.9	0.20	0.7	15.4
			Acid blue		172.4	1.05	0.7	16.3
			Methyl orange		96.2	0.15	0.9	13.2
			Disperse Red 1		500	0.10	0.9	44.0
	[57]	TiO_2 nanoparticle	Methylene blue	Freundlich	82.0	0.20	0.5	16.9
			Methyl orange		384.6	0.01	0.9	4.6
			Acid blue		76.9	0.21	0.5	17.2
			Disperse red 1		138.9	0.53	0.3	56.7
	[42]	Macroporous Membrane	Bisphenol-A	Langmuir	280.0	0.02	0.4	26.0
	[24]	Magnetic	Carbamazepine	Freundlich	2.2	0.08	0.6	0.3
			Naproxen		1.7	0.10	0.6	0.2
			Bisphenol-A		2.2	0.04	0.7	0.1
	[36]	Magnetic (graphene)	Bisphenol-A	Langmuir	66.0	0.02	2.4	6.3
	[44]	Magnetic (Fe_3O_4-GO) nanosheet	E2	Langmuir	85.8	1.75	0.7	66.8
	[43]	Magnetic nanoparticles	Congo red	Freundlich	425.5	0.00026	0.5	32.3
	[23]	Microcrystalline cellulose	Bisphenol-A	Langmuir	34.7	9.6	-	-
	[50]	Nanofiber membrane	Bisphenol-A	Freundlich	346.8	3.26	1.2	645.7
	[29]	Magnetic	1-Naphtol	Langmuir	235.0	0.02	0.5	6.5
	[47]	Cellulose bead	Bisphenol-A	Langmuir	36.6	0.03	3.0	9.3
	[41]	Magnetic	Bisphenol-A	Langmuir	52.7	0.15	0.4	12.4
	[66]	Clay	Bisphenol-A	Langmuir	223.7	0.20	Na	Na
					132.4	0.49	Na	Na

*Obtained from Langmuir isotherm

The studies have been conducted around neutral pH except (F. Zhao et al., 2017.) (Zhou et

Appendix B

Table 3: Initial concentration check of ibuprofen at 10mg/L in UV-VIS for isotherm experiments

C_0	5 mg/L	10 mg/L	15 mg/L	20 mg/L
Vial 1	5.04	9.85	14.29	19.11
Vial2	5.13	9.98	14.45	19.04
Vial 3	4.99	10.08	14.30	19.20
mean	**5.06**	**9.97**	**14.35**	**19.11**
Standard deviation	0.07	0.11	0.09	0.08

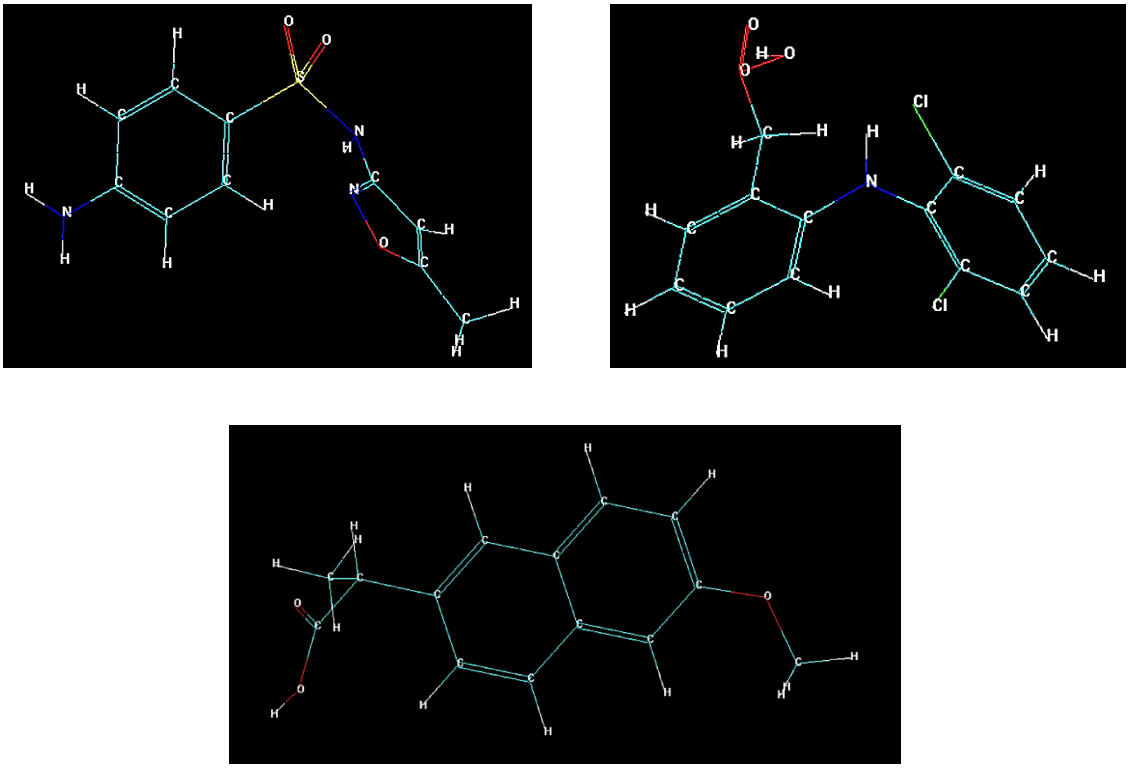

Figure 1: Chemical structures of a) Sulfamethoxazole b) Diclofenac c) Naproxen built in HyperChem 8.0 software

Appendix C

1. The individual components of the potential energy.

The dihedral potential is the torsional potential energy described by the Equation 1;

$$V_{dihedrals} = \sum_{dihedrals} \frac{V_n}{2} [1 + \cos (n\varphi - \varphi_0] \quad (1)$$

where Vn is the dihedral force constant, n is the periodicity of the Fourier term, φ_0 is the phase angle, and φ is the dihedral angle.

The bond stretch potential is described by the Equation 2;

$$V_{stretch} = \sum_{bond} K_r (r - r_0)^2 \quad (2)$$

where Kr is the stretch force constant and r is the distance from the equilibrium position r_0.

The bond angle potential is described by the Equation 3;

$$V_{stretch} = \sum_{angle} K_\theta (\theta - \theta_0)^2 \quad (3)$$

Where $K\theta$ is the bending force constant θ is the angle and θ_0 is the equilibrium angle.

The van der Waals potential is described by the Equation 4;

$$V_{VdW} = \sum_{i<j} \frac{A_{ij}}{R^{12}} - \frac{B_{ij}}{R^6} \quad (4)$$

Rij is the nonbonded distance between two atoms. Aij and Bij are van der Waals parameters for the interacting pair of atoms. The R^6 term describes the attractive London dispersion interaction between two atoms and the R^{12} term describes the repulsive interaction caused by Pauli exclusion.

The hydrogen bond potential is described by the equation 5;

$$V_{HB} = \sum_{i<j} \frac{C_{ij}}{R^{12}} - \frac{D_{ij}}{R^{10}} \quad (5)$$

where, Rij is the nonbonded distance between two atoms. Cij and Dij are H bonding parameters for the interacting pair of atoms.

The electrostatic potential is described by the Equation 6;

$$V_{EEL} = \sum_{i<j} \frac{q_i q_j}{\varepsilon R_{ij}} \quad (6)$$

Where two atoms (I and j) have point charges qi and qj. The magnitude of the electrostatic energy (V_{EEL}) varies inversely with the distance between the atoms, Rij. The effective dielectric constant is ε.

2. Electron density function

$$\rho(r) = \sum_{\mu\vartheta} P_{\mu\vartheta} \varphi_{\mu}(r) \varphi_{\vartheta}(r)$$

3. Carbodiimide activation

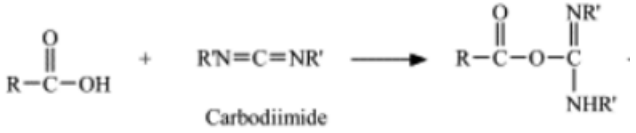

Table 4: van der Waals and electrostatic potential of host, guest and host-guest complexes

Host	Guest	V_{Vdw} host	EEL host	Vdw guest	EEL guest	Vdw complex	EEL complex	Vdw adsorption	EEL adsorption	total
β-CD	Ibuprofen	11.3	0.0	3.2	2.1	-8.1	0.0	-22.6	-2.1	**-24.7**
	Procaine	11.3	0.0	5.2	13.1	-5.6	0.0	-22.1	-13.1	**-35.2**
	Sulfamethoxazole	11.3	0.0	4.0	11.8	-5.1	0.0	-20.3	-11.8	**-32.1**
	Naproxen	11.3	0.0	7.9	-8.7	-14.1	0.0	-33.2	8.7	**-24.5**
	Fulvic	11.3	0.0	10.5	0.0	-4.4	0.0	-26.1	0.0	**-26.1**
CM-β-CD	Ibuprofen	-7.3	-35.1	3.2	2.1	11.4	6.4	15.5	39.4	**54.9**
	Procaine	-7.3	-35.1	5.2	13.1	8.9	-93.1	11.0	-71.1	**-60.0**
	Naproxen	-7.3	-35.1	7.9	-8.7	5.7	16.6	5.1	60.5	**65.6**
	Sulfamethoxazole	-7.3	-35.1	4.0	11.8	13.2	39.9	16.6	63.3	**79.9**
	Fulvic acid	-7.3	-35.1		0.0	6.2	26.6	13.6	61.8	**75.3**
Si-CM-β-CD	Ibuprofen	-5.9	4.3	3.2	2.1	9.3	20.3	12.0	13.9	**25.9**
	Procaine	-5.9	4.3	5.2	13.1	-5.6	-53.5	-5.0	-70.9	**-75.9**
	Naproxen	-5.9	4.3	7.9	-8.7	2.5	17.1	0.5	21.5	**22.0**
	Sulfamethoxazole	-5.9	4.3	4.0	11.8	-3.8	24.5	-1.9	8.4	**6.5**
	fulvic	-5.9	4.3		0.0	10.0	20.9	15.9	16.6	**32.5**
EDB-β-CD	Ibuprofen	6.8	-45.6	3.2	2.1	-4.5	0.0	-14.5	43.5	**29.0**
	Procaine	6.8	-45.6	5.2	13.1	-7.7	0.0	-19.7	32.5	**12.8**
DFB-β-CD	Ibuprofen	15.8	-42.6	3.2	2.1	-14.5	0.0	-33.5	40.5	**7.0**
	Procaine	15.8	-42.6	5.2	13.1	-13.7	0.0	-34.7	29.5	**-5.2**

4. Configuration of the aromatic rings of host and guest in complexation

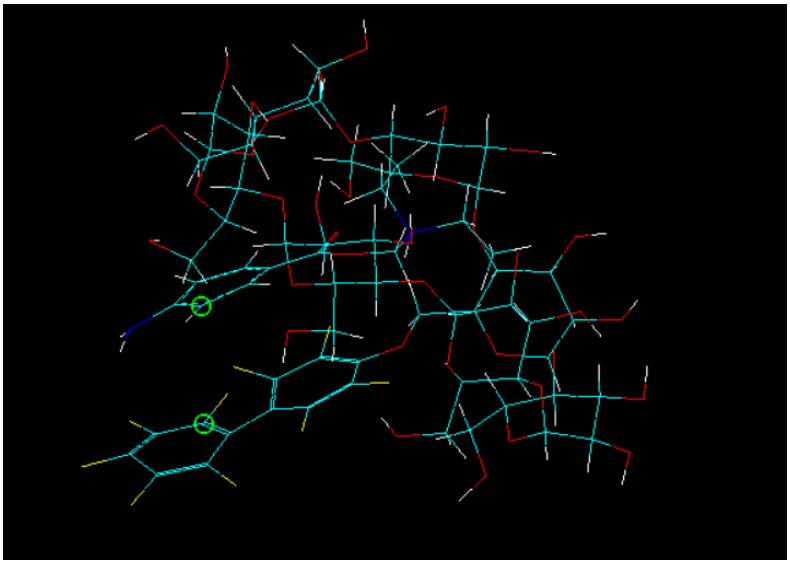

Figure 2: Procaine-DFB-β-CD complex. The distance between the labeled carbon atoms is 3.27 Å

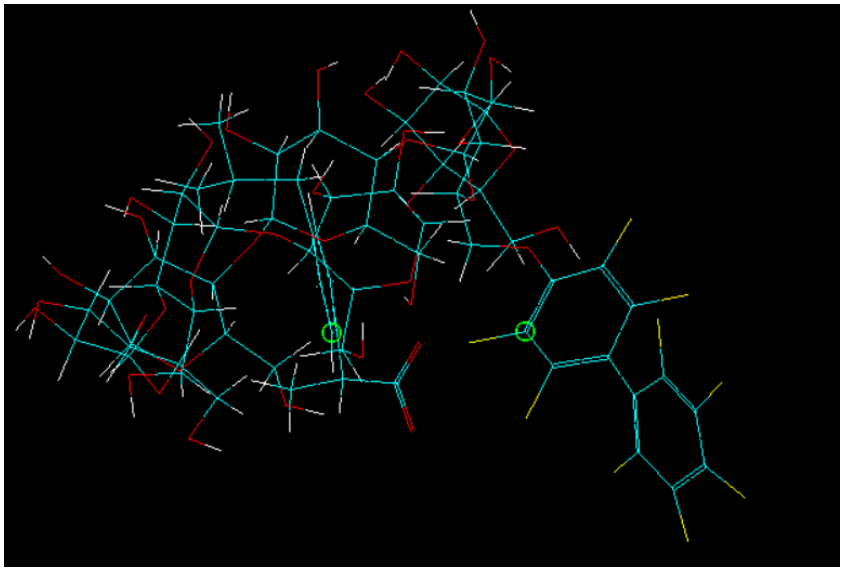

Figure 3: Ibuprofen-DFB-β-CD complex. The distance between the labeled carbon atoms is 4.75 Å

Appendix D

1. HGMS

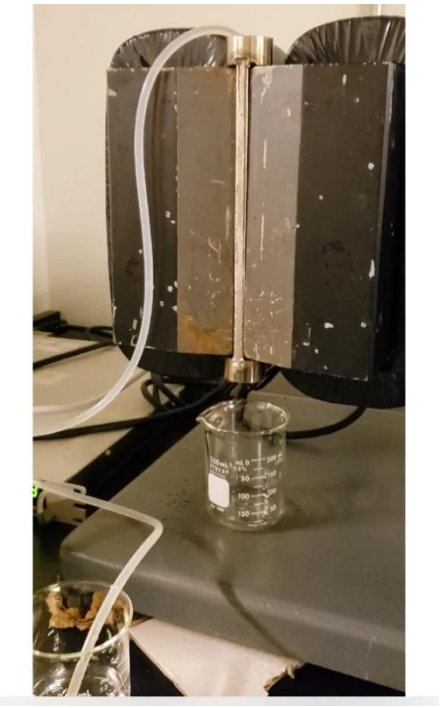

2. The synthesis of β-CD functionalized magnetic nanoparticles

β-CD functionalized magnetic nanoparticles were synthesized according to the method described by Ju et. al. [45]. The synthesis consisted of 4 major steps. In the first step, a nanogel was synthesized via the emulsion polymerization technique to form the backbone of the adsorbent. To prepare the nanogel polymerized methacrylic acid (MAA) and ethyl acrylate (EA) crosslinked with diallyl phthalate (DAP) were mixed with surfactant (AOT) solution where the initiator solution was prepared with sodium persulfate. The product was purified via dialysis until no surfactant was observed in the water. The nanogel was made magnetic by reacting Fe_2SO_4 with $NaNO_2$ and NH_4OH to obtain Fe_3O_4 particles inside the nanogel. Excess iron was subsequently removed via several cycles of ultrafiltration. The magnetic nanoparticles were then washed with water and subsequently captured using an HGMS to remove nonmagnetic constituents. In the third step, the surface of the Fe_3O_4 embedded nanogel was coated with a silica layer via tetraethyl orthosilicate to make the β-CD-FMNP resistant to oxidation or other structural changes that might occur with time. The silica-coated particles were then washed in the HGMS to remove unreacted chemicals and any residual nonmagnetic particles. Prior to the grafting

procedure, β-CD was modified to obtain carboxymethyl-β-CD. In the final step, the surface of the silica-coated magnetic nanoparticles was functionalized with the carboxymethyl-β-CD in the presence of cyanamide to provide adsorption sites. The product was purified and concentrated by washing with the HGMS to remove the reaction by-products and then releasing the captured particles into MQ water. The concentration of the wet particles was determined by the dry weight of the particles and the density of the solution as determined by measuring the mass of 50 ml of the particle solution and dividing the mass of the solution by the volume of the solution [45].

The characterization of the β-CD functionalized magnetic nano adsorbent was previously reported in the literature [45]. The morphology and size of the nanogel, the magnetic nanoparticle and the silica-coated magnetic nanoparticle were examined by TEM (transmission electron microscopy). The magnetic properties of the particles were characterized by VSM (vibrating sample magnetometer). The presence of the silica shell was confirmed by XRD (X-ray diffraction) and the grafting of β-CD onto the silica surface was confirmed by FTIR (Fourier transform infrared spectroscopy) and TGA (thermogravimetric analysis). The particle size distribution (average size of 400nm) and Z-potential (-38 mV) were consistent with that reported in the literature. Hence, it was concluded that the particles synthesized in the current study were similar to those of the particles that had been previously characterized in detail [45].

Table 5: Method detection limit of turbidity method

Replicates	LOW (2.5 mg/L)	HIGH (30 mg/L)
1	5.92	55.8
2	5.81	58.9
3	5.76	57.1
4	5.81	55.2
5	5.88	56.1
6	5.82	55.8
7	5.81	58.2
mean	5.83	56.73
std	0.05	1.28
LOD	0.49	12.80

Table 6: Gravimetric analysis versus turbidity measurements

column configuration (mass (g)/piece)	sample	Dish (g)	Dish+sample (g)	Final (g)	Concentration from gravimetric analysis (mg/L)	Mean	standard deviation	RSD %		Concentration from Turbidity (mg/L)
0.6/1	1	1.2235	10.1425	1.224	56.1	55.7	0.9	1.6	56.3	57.1
	2	1.2287	10.375	1.2292	54.7				58.1	
	3	1.232	10.266	1.2323	56.4				56.8	

Table 7: Statistical analysis for comparison of gravimetric method and turbidity method

t-Test: Two-Sample Assuming Unequal Variances			
	Variable 1	*Variable 2*	
Mean	55.70900364	57.06666667	
Variance	0.843345954	0.863333333	
Observations	3	3	
Hypothesized M	0		
df	4		
t Stat	-1.800017221		
P(T<=t) one-tai	0.073117725		
t Critical one-ta	2.131846786		
P(T<=t) two-tai	0.146235451		
t Critical two-ta	2.776445105		